2021

Use and Improvement of Remote Sensing and Geospatial Technologies in Support of Crop Area and Yield Estimations in the West African Sahel

Kaboro Samasse
South Dakota State University

USE AND IMPROVEMENT OF REMOTE SENSING AND GEOSPATIAL TECHNOLOGIES IN SUPPORT OF CROP AREA AND YIELD ESTIMATIONS IN THE WEST AFRICAN SAHEL

BY

KABORO SAMASSE

A dissertation submitted in partial fulfillment of the requirements for the

Doctor of Philosophy

Major in Geospatial Science and Engineering

Specialization in Remote Sensing Geography

South Dakota State University

2021

DISSERTATION ACCEPTANCE PAGE

Kaboro Samasse

This dissertation is approved as a creditable and independent investigation by a candidate for the Doctor of Philosophy degree and is acceptable for meeting the dissertation requirements for this degree. Acceptance of this does not imply that the conclusions reached by the candidate are necessarily the conclusions of the major department.

Niall Hanan
Advisor Date

Robert Watrel
Department Head Date

Nicole Lounsbery, PhD
Director, Graduate School Date

This dissertation is dedicated to my parents, my beloved wife Aminata Nientao, and our children Oumou, Ousmane, and Fatoumata.

ACKNOWLEDGEMENTS

First, I would like to thank Allah almighty for His guidance during this thesis period.

Second, I would like to acknowledge my main advisor, Dr. Niall Hanan, for being available for me all time, and providing me the “right” advices at the right time. Thank you, Dr., for helping me help myself.

I have been lucky to have two more chairs of my advisory committee, I would like to thank Drs. Evert Van der Sluis (currently chair of my advisory committee) and Geoffrey Henebry (former chair and former Co-Director of the GSCE center), particularly for all the advice and administrative work at SDSU allowing me to keep my status at South Dakota State University. Also, I would like to thank Dr. Emmanuel Byamukama the graduate school representative in my advisory committee for his availability.

My acknowledgments also toward Dr. Yacouba Diallo from IPR/IFRA, my institution in Mali, for his support during my research fieldwork. Also, I would like to show my gratitude to the Malian Government through the IPR/IFRA General Direction for providing me with all administrative support this PhD program required.

This thesis could not work without financial support, I would like to thank USAID mission in Mali through BHEARD for making possible to study and doing research in this important area of geospatial sciences and their applications in agriculture.

As very good lecturers, collaborators, and friends, I would like to acknowledge all professors and graduate students of GSCE center at South Dakota State University, for their support and availability.

Finally, I would like to thank my family members and all my hometown (Djenne) friends for their valuable support and advice.

CONTENTS

ABBREVIATIONS

AGRHYMET	Agriculture Hydrology and Meteorology
APSIM	Agricultural Production Systems sIMulator
ASI	Agricultural Stress Index
BRT	Boosted Regression Trees
CHIRPS	Climate Hazard group InfraRed Precipitation with Stations
CILSS	Permanent Interstate Committee for drought control in the Sahel
CM4EW	Crop Monitor for Early Warning
DSSAT	Decision-Support System for Agrotechnology Transfer
EPIC	Environmental Policy Integrated Climate
EVI	Enhanced Vegetation Index
FAO	Food and Agricultural Organization
FEWS NET	Famine and Early Warning System Network
FLDAS	FEWS NET Land Data Assimilation System
GEE	Google Earth Engine
GIEWS	Global Information and Early Warning System
GIS	Geographical Information System
MAP	Mean Annual Precipitation
ML	Machine Learning
MSAVI	Modified Soil Adjusted Vegetation Index
NASA	National Aeronautics and Space Administration
NDVI	Normalized Vegetation Index
NDWI	Normalized Difference Water Index
OLI	Operational Land Imager
RF	Random Forest
RMSE	Root Mean Square Error
SARRA-H	Système d'Analyse Régionale des Risques Agroclimatologiques Version H
SAVI	Soil Adjusted Vegetation Index
TIRS	Thermal Infrared Sensor
USGS	United States Geological Survey
WASC30	West Africa Sahel Cropland at 30 m
WFP	World Food Programme
WRSI	Water Requirements Satisfaction Indices

LIST OF FIGURES

LIST OF TABLES

ABSTRACT

USE AND IMPROVEMENT OF REMOTE SENSING AND GEOSPATIAL TECHNOLOGIES IN SUPPORT OF CROP AREA AND YIELD ESTIMATIONS IN THE WEST AFRICAN SAHEL

KABORO SAMASSE

2021

In arid and semi-arid West Africa, agricultural production and regional food security depend largely on small-scale subsistence farming and rainfed crops, both of which are vulnerable to climate variability and drought. Efforts made to improve crop monitoring and our ability to estimate crop production (areas planted and yield estimations by crop type) in the major agricultural zones of the region are critical paths for minimizing climate risks and to support food security planning. The main objective of this dissertation research was to contribute to these efforts using remote sensing technologies. In this regard, the first analysis documented the low reliability of existing land cover products for cropland area estimation (Chapter 2). Then two satellite remote sensing-based datasets were developed that 1) accurately map cropland areas in the five countries of Sahelian West Africa (Senegal, Mauritania, Mali, Burkina Faso and Niger; Chapter 3), and 2) focus on the country of Mali to identify the location and prevalence of the major subsistence crops (millet, sorghum, maize and non-irrigated rice; Chapter 4).

The regional cropland area product is distributed as the West African Sahel Cropland area at 30 m (WASC30). The development of the new dataset involved high density training data (380,000 samples) developed by USGS in collaboration with CILSS for training about 200 locally optimized random forest (RF) classifiers using Landsat 8 surface reflectances and vegetation indices and the Google Earth Engine platform. WASC30 greatly improves earlier estimates through inclusion of cropland information for both rainfed and irrigated areas mapped with a class-specific accuracy of 79% across the West Africa Sahel. Used as a mask in crop monitoring systems, the new cropland area data could bring critical insights by reducing uncertainties in

identification of croplands as crop growth condition metrics are extracted. WASC30 allowed us to derive detailed statistics on cultivated areas in the Sahel, at country and agroclimatic scales. Intensive agricultural zones were highlighted as well. The second dataset, mapping crop types for the country of Mali, is meant to separate signals of different crop types for improved crop yield estimation. The crop type map was used to derive detailed agricultural statistics (e.g. acreage by crop types, spatial distribution) at finer administrative scales than has previously been possible. The crop fraction information by crop type extracted from the map, gives additional details on farmers preferences by regions, and the natural adaptability of different crop types.

The final analysis of this dissertation explores the use of ensemble machine learning techniques to predict maize yield in Mali (Chapter 5). Climate data (precipitation and temperature), and vegetation indices (Normalized Difference Vegetation Index, NDVI, the Enhanced Vegetation Index, EVI, and the Normalized Difference Water Index, NDWI) are used as predictors, while actual yields collected in 2017 by the Malian Ministry of Agriculture are the reference data. Random forest presented better predictive performance as compared to boosted regression trees (BRT). Results showed that climate variables have more predictive power for maize yield compared to vegetation indices. Among vegetation indices, the NDWI appeared to be the most influential predictor, maybe because of water requirement of maize and the sensitivity of this index to water in semi-arid regions. Tested with two different independent datasets, one constituted by 20% of the reference information, and another including observed yields for year 2018 (a one-year-left analysis), maize yield predictions were promising for year 2017 (RMSE = 362 kg/ha), but showed higher error for 2018 (RMSE = 707 kg/ha). That is, the fitted model may not capture accurately year to year variabilities in predicted maize yield. In this analysis, predictions were limited to field samples (~600 fields) across the country of Mali. It would be valuable in the future to predict maize yield for each pixel of the new developed crop type map. That will lead to a detailed spatial analysis of maize yield, allowing identification of low yielding regions for targeted interventions which could improve food security.

Keywords: Agricultural land area, crop type mapping, Sahel, West Africa, Machine Learning, Earth Engine, food security, famine early warning

CHAPTER 1

Introduction

1.1. Background

Food security is defined as "when all people at all times have physical, social and economic access to sufficient, safe and nutritious food to meet their dietary needs and food preferences for an active and healthy life" (Committee on World Food Security, 2011). The four pillars of food security are: food availability, access to food, utilization, and stability. Availability refers to the physical existence of food, whether it is produced locally or imported. The three other pillars of food security depend on food availability. Regarding food production, the Sahel region of Africa is particularly food insecure for a variety of geographic, demographic, and economic reasons that have resulted in food shortages and famines affecting millions of people living in the region (Lifland, 2012).

The Sahel of Africa is a region of transition between the Sahara and the tropical savannas. It extends from the Atlantic Ocean in the west to the Red Sea in the east, roughly from 12° N to 18° N (Anyamba & Tucker, 2005). The Western Africa Sahel, which is the focus of this dissertation research, includes parts of Mauritania, Senegal, Mali, Niger, and Burkina Faso. Strong climatic variations and fluctuations in rainfall have long time characterized the Sahel (Hiernaux et al., 2016). Since 1980s severe droughts the Sahel has experienced (Zeng, 2003) have caused periodic food shortages, as agricultural production is primarily rainfed in the region. This situation is worsened by the rapid population growth leading to pressure on land and water resources required for food production.

In addition to rapid population growth, other socioeconomics factors may contribute creating food insecurity situations in a region. For example, according to the Ministry of Rural Development of Mali, despite the agricultural potential of the country in terms of arable land (43.7 million hectares) for croplands and pastures, and water resources (70 billion cubic meters of water per year for irrigation), multiple structural challenges limit the degree of agricultural production (Cellule de Planification et de Statistique du Secteur Développement Rural (CPS/SDR), 2013). These challenges include limited private and/or public investments in the agricultural sector and limited access of farmers to credit, farmers' low level of education, fluctuations of cereal price, and limited trade opportunities for farm produce, both within countries and with

neighboring countries. These underlie the agronomic causes of low yields, even in years of good rainfall, caused by limited access to fertilizers, improved seeds, and mechanization tools like tractors (Cellule de Planification et de Statistique du Secteur Développement Rural (CPS/SDR), 2013).

In this context, it is important to develop tools and policies that can monitor agricultural production, and improve our understanding of these climatological, biophysical, technological, and economic factors causing the spatial and temporal variability of crop yields. Remote sensing based accurate estimates of cultivated area and crop yields modelling are some of those tools which are critical to our understanding of agricultural production, food security in rural West Africa.

1.1.1. Modeling in Agriculture

Modeling in agriculture is an essential tool to support decisions making. Typically, two broad categories of models are used to estimate crop yield in agriculture. They are mechanistic or process-based models, and statistical or empirical models (Thornley & France, 2007). Mechanistic modeling is a process-based method, built from our knowledge of the physical, chemical and biological processes governing the phenomenon under study (e.g. yield). Thus, mechanistic modeling is sometimes known as an explanatory modeling because it represents the cause and effect relationships among the variables involved. Process-based models are more difficult to deploy because they require knowledge about the underlying mechanism that determine how the various variables are related to each other.

Most Decision Support Systems (DSS) for agriculture use mechanistically based crop growth simulations to predict yield. Examples include APSIM (Agricultural Production Systems sIMulator, Keating et al., 2003), DSSAT (The Decision Support System for Agrotechnology Transfer, Jones et al., 2003), *Système d'Analyse Régionale des Risques Agroclimatologiques Version H* (SARRA-H; System of Agroclimatological Regional Risk Analysis), and EPIC (Environmental Policy Integrated Climate, Williams et al., 1989). Crop growth simulation tools can support agricultural decision making in two major levels. First, they help to understand the functioning of soil-plant-climate systems. Second, they are useful for design and assessment of new crop systems that would be difficult to develop through field experimentation. Of course, field experimentations will continue to be necessary for

calibration and assessing the robustness and relevance of simulation models. For example, DSS platforms have been used in numerous studies to understand cereals behavior in different climate and management scenarios across the West African region (Amouzou et al., 2019; Guan et al., 2017; Sultan et al., 2013).

In general, process-based models make predictions based on site-specific data. Application of these models at coarser scales (e.g. regional or national), is achieved using either (i) sample simulations: identification of climate, soil and management clusters representative of large areas, so that computational load is reduced but results may be applied to the larger domain of interest (Hoffman et al., 2018), or (ii) fully spatially distributed models parameterized using spatially varying soils, climate and management using Geographical Information Systems (GIS) and spatial analysis tools (Thorp et al., 2008; Venkatesan & Pazhanivelan, 2018; Yin et al., 2014). Spatially distributed models, however, are computationally demanding and require spatially contiguous data (soil, weather, genotype, and management) adding to parameterization uncertainty and difficulties defining initial conditions, making these models challenging to use in data-deficient regions like the West African Sahel.

Statistical modeling, as opposed to process-based modeling, is based on empirical relationships between response and explanatory variables. Historically, statistical crop models have used linear regression techniques, making them easy to be implemented (Thornley & France, 2007). They have been used to predict crop growth at large scales which are compatible with nation-scale statistics on seasonal yields (Kern et al., 2018). In general, statistical models offer the possibility to select variables based on their relationships (through mathematical equations) with the underlying yield analysis. However, statistical models are limited in their ability to predict outside the calibration data, and future scenario analysis (prediction) is impossible (Lambin et al., 2000). Statistical models also offer little or no insight into the underlying process that govern the phenomenon under study. Statistical models has been widely used to explore actual yield relationships with climate variables (Lobell & Burke, 2010; Lobell & Field, 2007). Sometimes climate variables are combined with satellites remote sensing derived information (Kern et al., 2018; Y. Li et al., 2019) or socioeconomics data (Iizumi et al., 2017) for improved yield predictions.

As satellite remote sensing is increasingly improving in spatial, spectral, and temporal resolution, it can contribute significantly to a system that collects information on crops conditions and other environmental variables at larger geographical scale (Lambin et al., 1993). Free online access to time series of medium-resolution satellite remote sensing data (e.g. Landsat, Sentinel systems; (Claverie et al., 2018; Roy et al., 2014; Woodcock et al., 2008)), coupled with the availability of new computational resources (e.g. cloud and parallel computations; (Gorelick et al., 2017; Huang et al., 2018; Wolfert et al., 2017)) has made large scale and long-term analysis of crop growth and productivity a reality (Johnson, 2019a; P. Kumar et al., 2018; Rufin et al., 2019).

That creates opportunities in using data-driven techniques such as Machine Learning (ML) in agricultural modeling. ML techniques have been used in agriculture for multi-classes land cover classification, cropland and crop type mapping, and crop yield modeling (Samasse et al., 2020; Zhang et al., 2019; Zwart & Leclert, 2010). Main agricultural applications using ML have been recently reviewed by Liakos et al. (2018). Compared to more traditional statistical and process-based crop monitoring methods, ML is a method apart, based on intelligent predictive algorithms that are capable to "learn" from the data without any rules defined in advance by explicit programming (Liakos et al., 2018). However, machine learning is a complex process necessitating large amounts of data ("data-driven approach"; (Bzdok et al., 2018)) for better learning results. That is, as we provide ML algorithms more training data, it becomes possible to create more accurate models based on that data (Liakos et al., 2018). For practical considerations, and to compensate weaknesses that might occur with a single ML model instance, ensemble approaches are used (Dietterich, 2000; Zhou, 2009). Ensemble learning techniques can be applied for both classification and regression problems. The final prediction is determined by major voting (classification), or by averaging model outputs (regression). Sample data selection and methods to integrate multiple ensemble members are two significant characteristics of ensemble models. Bagging (Breiman, 1996) and boosting (Freund, 1995) are two widely used ensemble learning techniques. Random Forests (RF; Breiman, 2001) and Boosted Regression Trees (BRT; Elith et al., 2008) are examples of Ensemble Learning models, implementing bagging and boosting methods, respectively. They have been widely used in satellite remote sensing data processing (classification and regression) for agricultural applications (Aghighi et al.,

2018; Charoen-Ung & Mittrapiyanuruk, 2018; Jeong et al., 2016; Xu et al., 2020; Zhang et al., 2019).

1.1.2. Satellite remote sensing-based crop monitoring

Satellites remote sensing-based tools and models have been used for decades in the Sahelian region through different regional and national initiatives, and in collaboration with international institutions, to allow near-real-time monitoring of the cropping season.

At global scale, the Global Information and Early Warning System (GIEWS; http://www.fao.org/giews), established by the Food and Agriculture Organization of the United Nations (FAO), monitors the condition of major crops to assess production prospects using a variety of data sources including earth observation products. The major remote sensing-based product used in GIEWS for water stress and cop condition monitoring is the Agricultural Stress Index (ASI). ASI is computed in the Agricultural Stress Index System (ASIS), which is integrated in the GIEWS platform, based on NDVI, and BT4 (Brightness Temperature in AVHRR band 4) derived from NOAA/METOP-AVHR. It integrates also NDVI from SPOT-VEGETATION series (Van Hoolst et al., 2016). GIEWS provides information on countries facing food insecurity through monthly briefing reports, which includes areas that might have anomalies caused by dry spells during crop growing seasons.

At regional scale, the USAID's Famine Early Warning System Network (FEWS NET) combines biophysical remote sensing applications through its collaboration with NASA, NOAA, USGS and USDA, and socio-economic methodologies through its involvement with UN WFP and numerous international non-governmental organizations such as Save the Children, Oxfam and others (Brown, 2008; Ross et al., 2009). FEWS NET provides monitoring and early warning support to decision makers responsible for responding to humanitarian crises including famine and food insecurity. The primary FEWS NET satellite remote sensing-based inputs include rainfall and vegetation information (Ross et al., 2009). An example of an analysis tool promoted by FEWS NET is the Early Warning eXplorer (EWX; https://earlywarning.usgs.gov/fews/ewx/index.html) interactive web-based mapping tool, which allows users to visualize continental-scale rainfall estimates (RFE; Xie, 2001), rainfall estimates from the Climate Hazard group InfraRed Precipitation with

Stations (CHIRPS; Funk et al., 2015), land surface temperature (LST) and normalized difference vegetation index (NDVI) data and anomalies at varied time steps (covering crop growing season; FEWS NET, 2020). The FLDAS (FEWS NET Land Data Assimilation System; https://ldas.gsfc.nasa.gov/fldas) provides additional hydroclimatic variables (e.g. Soil moisture, Evapotranspiration, Wind speed) to support agricultural monitoring and modeling. Through regular reports, FEWS NET provides crop condition monitoring support to most of the developing world, including Sahelian countries in West Africa.

In West Africa, the AGRHYMET (Agriculture, Hydrology and Meteorology) Regional Center in Niamey, Niger, is a specialized institution which promotes integration of Earth observations data and crop growth models to build improved drought assessment across member countries. This system includes crop monitoring during the growing season and yield predictions. AGRHYMET uses the crop growth simulation model named *Système d'Analyse Régional des Risques Agroclimatiques, version H* (SARRA-H; http://sarra-h.teledetection.fr/SARRAH_Home.html), which has been adapted to the operational needs of agrometeorological monitoring in West Africa (Traore et al., 2014). Major spatialized outputs of SARRA-H to monitor crop are onset dates of the season, water requirements satisfaction indices (WRSI), and potential yields. In addition to these outputs, the normalized difference vegetation index (NDVI; Tucker, 1979), and other NDVI-based indices like the vegetation condition index (VCI), are also used at AGRHYMET for crop condition and anomaly analysis during the growing season (Traore et al., 2014). The AGRHYMET regional center also implemented the "Water Management for Cropland and Rangeland Management" thematic application of the African Monitoring of the Environment for Sustainable Development (AMESD) project coordinated by ECOWAS and AUC. This project aimed to use EUMETSAT satellite data and products to develop indicators for 1) Monitoring vegetation growth to evaluate cropland and rangeland productivity, 2) Determination of areas affected by droughts, 3) Localization and monitoring of small surface water bodies, and 4) Localization of bush fires and estimation of size of burned areas (EUTELSAT, 2009). Through monthly and special environmental monitoring reports, AGRHYMET provides critical agrometeorological information to member countries for decision making related to areas as risk of drought.

GEOGLAM Crop Monitoring system (https://cropmonitor.org/) was initiated by the Group of Twenty (G20) countries in 2011 to reinforce international community capacity in crop condition monitoring using satellite remote sensing products for the promotion of food security. These products include NDVI and NDVI anomalies derived from NASA MODIS vegetation index products, CHIRPS precipitation, temperature and temperature anomalies, soil moisture, evapotranspiration, and runoff extracted from diverse sources including FEWS NET Land Data Assimilation System (FLDAS; (Loeser et al., 2020; McNally et al., 2017; Pervez et al., 2016)). Overall, the Crop Monitor for Early Warning (CM4EW) provides, based on the best available information, transparent, multi-sourced, consensus assessments of the crop growing conditions, status, and agroclimatic conditions that are likely to impact production in countries vulnerable to food insecurity in order to strengthen agricultural, humanitarian intervention, food security decision making and policy implementations (Becker-Reshef et al., 2020). CM4EW reports include most of the sub-Saharan countries.

To become effective and accurate in crop condition monitoring, the above-mentioned systems integrate remote sensing indices (e.g. ASI, VCI, WRSI, and NDVI) based on cultivated areas, whenever it is available. Thus, cropland and crop specific mapping is of first level importance for all operational crop monitoring system. Several previous studies have examined mapping cultivated areas using remotely sensed data at different scales (Fritz et al., 2011; Lambert et al., 2016; Ramankutty, 2004; Thenkabail et al., 2009; Tong et al., 2020; Xiong et al., 2017). However, none of these studies were focused on crop specific mapping at regional scale across the Sahel. Furthermore, the coarse to moderate spatial resolution of most earlier efforts (~1 km to 100 m) are limited in their ability to resolve individual farmer fields or specific crops (Y. Shao et al., 2015), particularly in spatially fragmented rural Sahelian landscapes.

1.2. Research Objectives

This dissertation research aims to explore the use and improvement of remote sensing and geospatial technologies in support of regional and national-level famine early warning and food security institutions in West Africa, with a focus on Mali. The research aims to investigate the current technologies used for national and regional-scale agricultural monitoring, and develop new approaches using remote sensing and modeling that will improve our ability to monitor and understand current patterns and

major processes. Specifically, the research is structured to use earth observation technologies to contribute in four critical respects to our understanding of agricultural production in rural West Africa:

1. assess the accuracy of existing maps of cropland area in the West African Sahel
2. use new training data with new geospatial tools and machine learning to develop an improved 30-m cropland database for West Africa,
3. develop a crop type map for major subsistence cereals crops of Mali and analyze their spatial distribution for yield modelling purposes,
4. explore ensemble machine learning and data-driven based models to predict yields for maize production in Mali.

1.3. Structure of the Dissertation

This thesis is organized in six (6) chapters with four (4) of them leading to scientific articles.

1.3.1. Chapter 1: Introduction (this Chapter)

Introduces agricultural production and the food security situation in the West African Sahel, techniques of agricultural production modeling and crop condition monitoring using satellite remote sensing data.

1.3.2. Chapter 2: Existing cropland datasets accuracy assessment (Paper #1)

Identification of agricultural land areas, as distinct from pasture, fallow, and other land uses, is a critical first step in developing remote sensing technologies for agricultural applications. Several coarse-resolution (~1 km) satellite-based global land cover (GLC) products are available and freely downloadable. However, their accuracy at fine spatial scales is unknown. Chapter 2 of this thesis deals with an assessment of common GLCs accuracy in terms of spatial distribution of cropland in the West African Sahel, using a newly available reference dataset. Assessment results have been published as the first scientific paper from this dissertation.

1.3.3. Chapter 3: Development of a new cropland map for West Africa Sahel (Paper #2)

The relatively high uncertainty associated with existing data on cropland location in West Africa identified in Chapter 2 motivated this Chapter. The reference cropland

dataset is used to train Random Forest (an ensemble learning classifier) with 30-m resolution satellite data from the Landsat 7,8 time series, and geospatial datasets (climate, soils, and terrain) for the development of an improved Cropland product for West African Sahel. The resulting cropland dataset named WASC30 (West African Sahel Cropland 30 m) and related main findings have constituted the second published article (Paper #2) of this research.

1.3.4. Chapter 4: National scale crop type mapping for the major rainfed cereal crops of Mali, West Africa (Paper #3)

By using extensive sample data on crop types provided by the Malian Department of Agriculture, a 30 m crop type map is developed describing the spatial distribution of the major cereal crops (maize, millet, and sorghum) for the country of Mali. The WASC30 cropland areas database (Chapter 3) was used to mask non crop and irrigated areas from the new crop type map. Crop type mapping used climate averages (CHIRPS precipitation data) with terrain (elevation and slope) and four vegetation indices (NDVI, EVI, SAVI, and MSAVI) as predictors for Random Forest models to map major subsistence cereal crops of Mali (maize, pearl millet, rice, and sorghum). Area and spatial distribution of crop fractions by crop types are also analyzed in this Chapter. A manuscript, including the main findings of this Chapter are under preparation for publication as Paper #3.

1.3.5. Chapter 5: Preliminary analysis of crop yield predictions using satellite and environmental data for maize production in Mali, West Africa (Paper #4)

The spatially explicit crop type map of the most important cereal crops across the country of Mali, developed in Chapter 4, is a critical step toward crop yield modeling. As separating crop specific locations from non-crop, fallow, and other vegetation contributes to reduce mixture in extracting information from other necessary variables (e.g. weather, soil, management) in crop yield predictions. Here I use Malian Department of Agriculture data on yield, with ensemble machine learning and satellite data to predict crop yields for maize production in Mali. This Chapter 5 of my dissertation gathers method, data, and preliminary results of such maize yield analysis for submission as Paper #4.

1.3.6. Chapter 6: Conclusions and Perspectives

This Chapter provides a summary and synthesis of the main findings of Chapters 2-5 and their implications in terms of agricultural monitoring, food security and policy making for West African Sahel countries. Recommendations for future directions in remote sensing-based crop monitoring and yield predictions are also highlighted.

1.4. References

Aghighi, H., Azadbakht, M., Ashourloo, D., Shahrabi, H. S., & Radiom, S. (2018). Machine learning regression techniques for the silage maize yield prediction using time-series images of landsat 8 OLI. IEEE Journal of Selected Topics in Applied Earth Observations and Remote Sensing, 11(12), 4563–4577.

Amouzou, K. A., Lamers, J. P. A., Naab, J. B., Borgemeister, C., Vlek, P. L. G., & Becker, M. (2019). Climate change impact on water-and nitrogen-use efficiencies and yields of maize and sorghum in the northern Benin dry savanna, West Africa. Field Crops Research, 235, 104–117.

Anyamba, A., & Tucker, C. J. (2005). Analysis of Sahelian vegetation dynamics using NOAA-AVHRR NDVI data from 1981--2003. Journal of Arid Environments, 63(3), 596–614.

Becker-Reshef, I., Justice, C., Barker, B., Humber, M., Rembold, F., Bonifacio, R., Zappacosta, M., Budde, M., Magadzire, T., Shitote, C., & others. (2020). Strengthening agricultural decisions in countries at risk of food insecurity: The GEOGLAM Crop Monitor for Early Warning. RSEnv, 237, 111553.

Breiman, L. (1996). Bagging predictors. Machine Learning. https://doi.org/10.1007/bf00058655

Breiman, L. (2001). Random forests. Machine Learning, 45(1), 5–32.

Brown, M. E. (2008). Famine early warning systems and remote sensing data. In Famine Early Warning Systems and Remote Sensing Data. https://doi.org/10.1007/978-3-540-75369-8

Bzdok, D., Altman, N., & Krzywinski, M. (2018). Points of significance: statistics versus machine learning. Nature Publishing Group.

Cellule de Planification et de Statistique du Secteur Développement Rural (CPS/SDR). (2013). Politique de Développement Agricole. iv+ 68 pages.

Charoen-Ung, P., & Mittrapiyanuruk, P. (2018). Sugarcane yield grade prediction using random forest and gradient boosting tree techniques. 2018 15th International Joint Conference on Computer Science and Software Engineering (JCSSE), 1–6.

Claverie, M., Ju, J., Masek, J. G., Dungan, J. L., Vermote, E. F., Roger, J.-C., Skakun, S. V, & Justice, C. (2018). The Harmonized Landsat and Sentinel-2 surface reflectance data set. Remote Sensing of Environment, 219, 145–161.

Committee on World Food Security. (2011). Global Strategic Framework for Food Security and Nutrition. United Nations Food and Agricultural Organization Rome.

Dietterich, T. G. (2000). Ensemble methods in machine learning. International Workshop on Multiple Classifier Systems, 1–15.

Elith, J., Leathwick, J. R., & Hastie, T. (2008). A working guide to boosted regression trees. In Journal of Animal Ecology. https://doi.org/10.1111/j.1365-2656.2008.01390.x

EUTELSAT. (2009). AMESD in the ECOWAS region: Water management for cropland and rangeland management.

Freund, Y. (1995). Boosting a weak learning algorithm by majority. Information and Computation. https://doi.org/10.1006/inco.1995.1136

Fritz, S., You, L., Bun, A., See, L., McCallum, I., Schill, C., Perger, C., Liu, J., Hansen, M., & Obersteiner, M. (2011). Cropland for sub-Saharan Africa: A synergistic approach using five land cover data sets. Geophysical Research Letters, 38(4).

Funk, C., Peterson, P., Landsfeld, M., Pedreros, D., Verdin, J., Shukla, S., Husak, G., Rowland, J., Harrison, L., Hoell, A., & Michaelsen, J. (2015). The climate hazards infrared precipitation with stations - A new environmental record for monitoring extremes. Scientific Data. https://doi.org/10.1038/sdata.2015.66

Gorelick, N., Hancher, M., Dixon, M., Ilyushchenko, S., Thau, D., & Moore, R. (2017). Google Earth Engine: Planetary-scale geospatial analysis for everyone. Remote Sensing of Environment, 202, 18–27. https://doi.org/10.1016/j.rse.2017.06.031

Guan, K., Sultan, B., Biasutti, M., Baron, C., & Lobell, D. B. (2017). Assessing climate adaptation options and uncertainties for cereal systems in West Africa. Agricultural and Forest Meteorology, 232, 291–305.

Hiernaux, P., Dardel, C., Kergoat, L., & Mougin, E. (2016). Desertification, adaptation and resilience in the Sahel: Lessons from long term monitoring of agro-ecosystems. In The end of desertification? (pp. 147–178). Springer.

Hoffman, A. L., Kemanian, A. R., & Forest, C. E. (2018). Analysis of climate signals in the crop yield record of sub-Saharan Africa. Global Change Biology, 24(1), 143–157.

Huang, Y., Chen, Z., Tao, Y. U., Huang, X., & Gu, X. (2018). Agricultural remote sensing big data: Management and applications. Journal of Integrative Agriculture, 17(9), 1915–1931.

Iizumi, T., Furuya, J., Shen, Z., Kim, W., Okada, M., Fujimori, S., Hasegawa, T., & Nishimori, M. (2017). Responses of crop yield growth to global temperature and socioeconomic changes. Scientific Reports, 7(1), 1–10.

Jeong, J. H., Resop, J. P., Mueller, N. D., Fleisher, D. H., Yun, K., Butler, E. E., Timlin, D. J., Shim, K.-M., Gerber, J. S., Reddy, V. R., & others. (2016). Random forests for global and regional crop yield predictions. PLoS One, 11(6), e0156571.

Johnson, D. M. (2019). Using the Landsat archive to map crop cover history across the United States. Remote Sensing of Environment, 232(October 2018), 111286. https://doi.org/10.1016/j.rse.2019.111286

Jones, J. W., Hoogenboom, G., Porter, C. H., Boote, K. J., Batchelor, W. D., Hunt, L. A., Wilkens, P. W., Singh, U., Gijsman, A. J., & Ritchie, J. T. (2003). The DSSAT cropping system model. European Journal of Agronomy. https://doi.org/10.1016/S1161-0301(02)00107-7

Keating, B. A., Carberry, P. S., Hammer, G. L., Probert, M. E., Robertson, M. J., Holzworth, D., Huth, N. I., Hargreaves, J. N. G., Meinke, H., Hochman, Z., McLean, G., Verburg, K., Snow, V., Dimes, J. P., Silburn, M., Wang, E., Brown, S., Bristow, K. L., Asseng, S., … Smith, C. J. (2003). An overview of APSIM, a model designed for farming systems simulation. European Journal of Agronomy. https://doi.org/10.1016/S1161-0301(02)00108-9

Kern, A., Barcza, Z., Marjanović, H., Árendás, T., Fodor, N., Bónis, P., Bognár, P., & Lichtenberger, J. (2018). Statistical modelling of crop yield in Central Europe using climate data and remote sensing vegetation indices. Agricultural and Forest Meteorology, 260–261, 300–320. https://doi.org/10.1016/j.agrformet.2018.06.009

Kumar, P., Prasad, R., Gupta, D. K., Mishra, V. N., Vishwakarma, A. K., Yadav, V. P., Bala, R., Choudhary, A., & Avtar, R. (2018). Estimation of winter wheat crop growth parameters using time series Sentinel-1A SAR data. Geocarto International, 33(9), 942–956.

Lambert, M. J., Waldner, F., & Defourny, P. (2016). Cropland mapping over Sahelian and Sudanian agrosystems: A Knowledge-based approach using PROBA-V time series at 100-m. Remote Sensing, 8(3). https://doi.org/10.3390/rs8030232

Lambin, Eric F., Cashman, P., Moody, A., Parkhurst, B. H., Pax, M. H., & Schaaf, C. B. (1993). Agricultural Production Monitoring in the Sahel Using Remote Sensing: Present Possibilities and Research Needs. Journal of Environmental Management. https://doi.org/10.1006/jema.1993.1047

Lambin, Eric FMDA, Rounsevell, M. D. A., & Geist, H. J. (2000). Are agricultural land-use models able to predict changes in land-use intensity? Agriculture, Ecosystems & Environment, 82(1–3), 321–331.

Li, Y., Guan, K., Yu, A., Peng, B., Zhao, L., Li, B., & Peng, J. (2019). Toward building a transparent statistical model for improving crop yield prediction: Modeling rainfed corn in the US. Field Crops Research, 234, 55–65.

Liakos, K. G., Busato, P., Moshou, D., Pearson, S., & Bochtis, D. (2018). Machine learning in agriculture: A review. Sensors, 18(8), 2674.

Lifland, A. (2012). Starvation in the Sahel: food security in Africa. Harvard International Review, 34(1), 6.

Lobell, D. B., & Burke, M. B. (2010). On the use of statistical models to predict crop yield responses to climate change. Agricultural and Forest Meteorology, 150(11), 1443–1452.

Lobell, D. B., & Field, C. B. (2007). Global scale climate--crop yield relationships and the impacts of recent warming. Environmental Research Letters, 2(1), 14002.

Loeser, C., Rui, H., Teng, W. L., Ostrenga, D. M., Wei, J. C., Mcnally, A. L., Jacob, J. P., & Meyer, D. J. (2020). Famine Early Warning Systems Network (FEWS NET) Land Data Assimilation System (LDAS) and Other Assimilated Hydrological Data at NASA GES DISC.

McNally, A., Arsenault, K., Kumar, S., Shukla, S., Peterson, P., Wang, S., Funk, C., Peters-Lidard, C. D., & Verdin, J. P. (2017). A land data assimilation system for sub-Saharan Africa food and water security applications. Scientific Data. https://doi.org/10.1038/sdata.2017.12

Pervez, M. S., McNally, A., & Shukla, S. (2016). Evaluation of Famine Early Warning Systems Network (FEWS NET) Land Data Assimilation System (FLDAS) and application in East Africa. AGUFM, 2016, H51I--1639.

Ramankutty, N. (2004). Croplands in West Africa: A Geographically Explicit Dataset for Use in Models. Earth Interactions. https://doi.org/10.1175/1087-3562(2004)8<1:ciwaag>2.0.co;2

Ross, K. W., Brown, M. E., Verdin, J. P., & Underwood, L. W. (2009). Review of FEWS NET biophysical monitoring requirements. In Environmental Research Letters. https://doi.org/10.1088/1748-9326/4/2/024009

Roy, D. P., Wulder, M. A., Loveland, T. R., Woodcock, C. E., Allen, R. G., Anderson, M. C., Helder, D., Irons, J. R., Johnson, D. M., Kennedy, R., & others. (2014). Landsat-8: Science and product vision for terrestrial global change research. Remote Sensing of Environment, 145, 154–172.

Rufin, P., Frantz, D., Ernst, S., Rabe, A., Griffiths, P., Özdo\ugan, M., & Hostert, P. (2019). Mapping cropping practices on a national scale using intra-annual Landsat time series binning. Remote Sensing, 11(3), 232.

Samasse, K., Hanan, N. P., Anchang, J. Y., & Diallo, Y. (2020). A high-resolution cropland map for the West African Sahel based on high-density training data, google earth engine, and locally optimized machine learning. Remote Sensing. https://doi.org/10.3390/RS12091436

Shao, Y., Campbell, J. B., Taff, G. N., & Zheng, B. (2015). An analysis of cropland mask choice and ancillary data for annual corn yield forecasting using MODIS data. International Journal of Applied Earth Observation and Geoinformation, 38, 78–87.

Sultan, B., Roudier, P., Quirion, P., Alhassane, A., Muller, B., Dingkuhn, M., Ciais, P., Guimberteau, M., Traore, S., & Baron, C. (2013). Assessing climate change impacts on sorghum and millet yields in the Sudanian and Sahelian savannas of West Africa. Environmental Research Letters, 8(1), 14040. https://doi.org/10.1088/1748-9326/8/1/014040

Thenkabail, P., Lyon, J. G., Turral, H., & Biradar, C. (2009). Remote sensing of global croplands for food security. CRC Press.

Thornley, J. H. M., & France, J. (2007). Mathematical models in agriculture: quantitative methods for the plant, animal and ecological sciences. Cabi.

Thorp, K. R., DeJonge, K. C., Kaleita, A. L., Batchelor, W. D., & Paz, J. O. (2008). Methodology for the use of DSSAT models for precision agriculture decision support. Computers and Electronics in Agriculture, 64(2), 276–285.

Tong, X., Brandt, M., Hiernaux, P., Herrmann, S., Rasmussen, L. V., Rasmussen, K., Tian, F., Tagesson, T., Zhang, W., & Fensholt, R. (2020). The forgotten land use class: Mapping of fallow fields across the Sahel using Sentinel-2. Remote Sensing of Environment, 239, 111598.

Traore, S. B., Ali, A., Tinni, S. H., Samake, M., Garba, I., Maigari, I., Alhassane, A., Samba, A., Diao, M. B., Atta, S., Dieye, P. O., Nacro, H. B., & Bouafou, K. G. M.

(2014). AGRHYMET: A drought monitoring and capacity building center in the West Africa Region. Weather and Climate Extremes. https://doi.org/10.1016/j.wace.2014.03.008

Tucker, C. J. (1979). Red and photographic infrared linear combinations for monitoring vegetation. Remote Sensing of Environment, 8(2), 127–150.

Van Hoolst, R., Eerens, H., Haesen, D., Royer, A., Bydekerke, L., Rojas, O., Li, Y., & Racionzer, P. (2016). FAO's AVHRR-based Agricultural Stress Index System (ASIS) for global drought monitoring. International Journal of Remote Sensing, 37(2), 418–439.

Venkatesan, M., & Pazhanivelan, S. (2018). Estimation of Maize Yield at Spatial Level Using DSSAT Crop Simulation Model. Madras Agricultural Journal, 105.

Williams, J. R., Jones, C. A., Kiniry, J. R., & Spanel, D. A. (1989). EPIC crop growth model. Transactions of the American Society of Agricultural Engineers. https://doi.org/10.13031/2013.31032

Wolfert, S., Ge, L., Verdouw, C., & Bogaardt, M.-J. (2017). Big data in smart farming--a review. Agricultural Systems, 153, 69–80.

Woodcock, C. E., Allen, R., Anderson, M., Belward, A., Bindschadler, R., Cohen, W., Gao, F., Goward, S. N., Helder, D., Helmer, E., & others. (2008). Free access to Landsat imagery. SCIENCE VOL 320: 1011.

Xie, P. (2001). CPC RFE Version 2.0. NOAA/CPC Training Guide.

Xiong, J., Thenkabail, P. S., Tilton, J. C., Gumma, M. K., Teluguntla, P., Oliphant, A., Congalton, R. G., Yadav, K., & Gorelick, N. (2017). Nominal 30-m cropland extent map of continental Africa by integrating pixel-based and object-based algorithms using Sentinel-2 and Landsat-8 data on google earth engine. Remote Sensing, 9(10), 1–27. https://doi.org/10.3390/rs9101065

Xu, J.-X., Ma, J., Tang, Y.-N., Wu, W.-X., Shao, J.-H., Wu, W.-B., Wei, S.-Y., Liu, Y.-F., Wang, Y.-C., & Guo, H.-Q. (2020). Estimation of Sugarcane Yield Using a Machine Learning Approach Based on UAV-LiDAR Data. Remote Sensing, 12(17), 2823.

Yin, Y., Zhang, X., Lin, D., Yu, H., Shi, P., & others. (2014). GEPIC-VR model: a GIS-based tool for regional crop drought risk assessment. Agricultural Water Management, 144, 107–119.

Zeng, N. (2003). Drought in the Sahel. Science, 302(5647), 999–1000.

Zhang, L., Traore, S., Ge, J., Li, Y., Wang, S., Zhu, G., Cui, Y., & Fipps, G. (2019). Using boosted tree regression and artificial neural networks to forecast upland rice yield under climate change in Sahel. Computers and Electronics in Agriculture, 166, 105031.

Zhou, Z.-H. (2009). Ensemble Learning. Encyclopedia of Biometrics, 1, 270–273.

Zwart, S. J., & Leclert, L. M. C. (2010). A remote sensing-based irrigation performance assessment: A case study of the Office du Niger in Mali. Irrigation Science, 28(5), 371–385. https://doi.org/10.1007/s00271-009-0199-3

CHAPTER 2

Assessing Cropland Area in West Africa for Agricultural Yield Analysis

Paper # 1

Samasse, K.; Hanan, N.P.; Tappan, G.; Diallo, Y. Assessing Cropland Area in West Africa for Agricultural Yield Analysis. *Remote Sens.* 2018, *10*, 1785.

Abstract

Accurate estimates of cultivated area and crop yield are critical to our understanding of agricultural production and food security, particularly for semi-arid regions like the Sahel of West Africa, where crop production is mainly rainfed and food security is closely correlated with the inter-annual variations in rainfall. Several global and regional land cover products, based on satellite remotely-sensed data, provide estimates of the agricultural land use intensity, but the initial comparisons indicate considerable differences among them, relating to differences in the satellite data quality, classification approaches, and spatial and temporal resolutions. Here, we quantify the accuracy of available cropland products across Sahelian West Africa using an independent, high-resolution, visually interpreted sample dataset that classifies all points across West Africa using a 2-km sample grid (~500,000 points for the study area). We estimate the "quantity" and "allocation" disagreements for the cropland class of eight land cover products in five Western Sahel countries (Burkina Faso, Mali, Mauritania, Niger, and Senegal). The results confirm that coarse spatial resolution (300 m, 500 m, and 1000 m) land cover products have higher disagreements in mapping the fragmented agricultural landscape of the Western Sahel. Earlier products (e.g., GLC2000) are less accurate than recent products (e.g., ESA CCI 2013, MODIS 2013 and GlobCover 2009). We also show that two of the finer spatial resolution maps (GFSAD30, and GlobeLand30) using advanced classification approaches (random forest, decision trees, and pixel-object combined) are currently the best available products for cropland identification. However, none of the eight land cover databases examined is consistent in reaching the targeted 75% accuracy threshold in the five Sahelian countries. The majority of currently available land cover products overestimate cultivated areas by an average of 170% relative to the cropland area in the reference data.

2.1. Introduction

Inter-annual variability in crop production associated with climate variability, pests, and diseases is a global concern, particularly for developing countries, where rural communities often lack the capital to help them cope with crop failures and food shortages (Conceição et al., 2011). Food security is therefore one of the major challenges faced by rural communities in developing countries. In this context, accurate estimates of the cultivated area, as part of crop yield and monitoring programs, are critical to our understanding of agricultural production, food security, and the associated social and economic issues (Zhong et al., 2014). Remote sensing-based land cover products constitute an important source of information for analyzing the dynamics of natural and anthropogenic terrestrial ecosystems, particularly for planning food security policies (Hüttich et al., 2011). At national, regional, and global scales, satellite-based systems are necessary, because of their ability to measure large areas, providing timely and consistent data.

Several freely accessible global land cover products, including agricultural land cover classes, are available at varying spatial resolutions. These products utilize different sources of satellite data and implement different classification approaches, with varying accuracy and spatial resolution (Herold et al., 2008). Previous analyses have reported overall and class-specific accuracies at a global scale for some of these land cover products (Olivier Arino et al., 2008; ESA-CCI, 2013; Friedl et al., 2010; Mayaux et al., 2006). However, a more detailed regional assessment, particularly for the West African Sahel, of these global products has so far not been published.

The class-specific accuracy of GLC2000 (Mayaux et al., 2006), MODIS collection 5 land cover (Friedl et al., 2010), GlobCover (Olivier Arino et al., 2007), and ESA CCI Land Cover (ESA-CCI, 2013) have been reported only at global or continent scales, with important disparities among them, particularly for the cropland classes. At a continent scale, Fritz et al. (2011) developed a synergy cropland map (IIASA Cropland) for sub-Saharan Africa, using five global land cover datasets (GLC2000, MODIS Land Cover, GlobCover, MODIS Crop Likelihood, and AfriCover). The combined product has been validated using a Geo-Wiki crowdsourcing application, with reported improvements over the individual datasets for the cropland class (Fritz et al., 2011). A similar cropland intensity map has been initiated by the Food and Agriculture Organization of the United Nations (FAO) as part of the GLC-SHARE global land

cover data. GLC-SHARE aims to provide the global climate modeling community with a baseline product (Latham et al., 2014).

The overall accuracy or cropland class accuracy may change among regions and continents, because the classification approaches may be more or less successful, and because the availability and quality of the training and reference datasets may vary. For example, at an Africa continent scale, Wei et al. (2018) compared the cropland class of five land cover products using Google Earth imagery and the FROM-GLC dataset for validation information. The results showed different accuracies for the different climate zones in Africa. However, the FROM-GLC product itself is found to underestimate the cropland area for African countries (Laso Bayas et al., 2017), and the overall accuracy reported by Wei et al. (2018) includes both crop and non-crop classes, without a crop class-specific accuracy assessment. In general, accuracy assessments of land cover products have been done with a less detailed evaluation of the cropland classes at national or regional levels. By using a more accurate reference dataset (the result of manual interpretation of higher spatial resolution images and USGS expert validation; (Tappan et al., 2016)), this paper aims to conduct a detailed performance assessment of the various global land cover datasets so as to accurately map the cultivated area in five Sahelian West Africa countries (Burkina Faso, Mali, Mauritania, Niger, and Senegal). Specifically, we focus on reporting the cropland class user's accuracy (i.e., number correctly identified in a given map class divided by number claimed to be in that map class, related to commission error), the quantity and allocation disagreements based on Pontius and Millones (Pontius Jr & Millones, 2011), and the good practices of map accuracy assessment suggested in Olofsson et al. (2014). We also report the "area ratio", which is the area of cropland estimated in each global land cover (GLC) product for each country, divided by the area in the reference dataset, as a metric of how well each product defines cropland area.

2.2. Materials and Methods

Figure 2.1 describes the different steps for assessing the accuracy of the land cover products for each of the five Sahelian countries, including the eight global datasets included in the analysis, preprocessing, and extraction of the sample points derived from the reference data (details below). For each global land cover product, we created

a confusion matrix with error metrics. The final assessment is the comparison of crop areas as identified by the land cover products and the reference data.

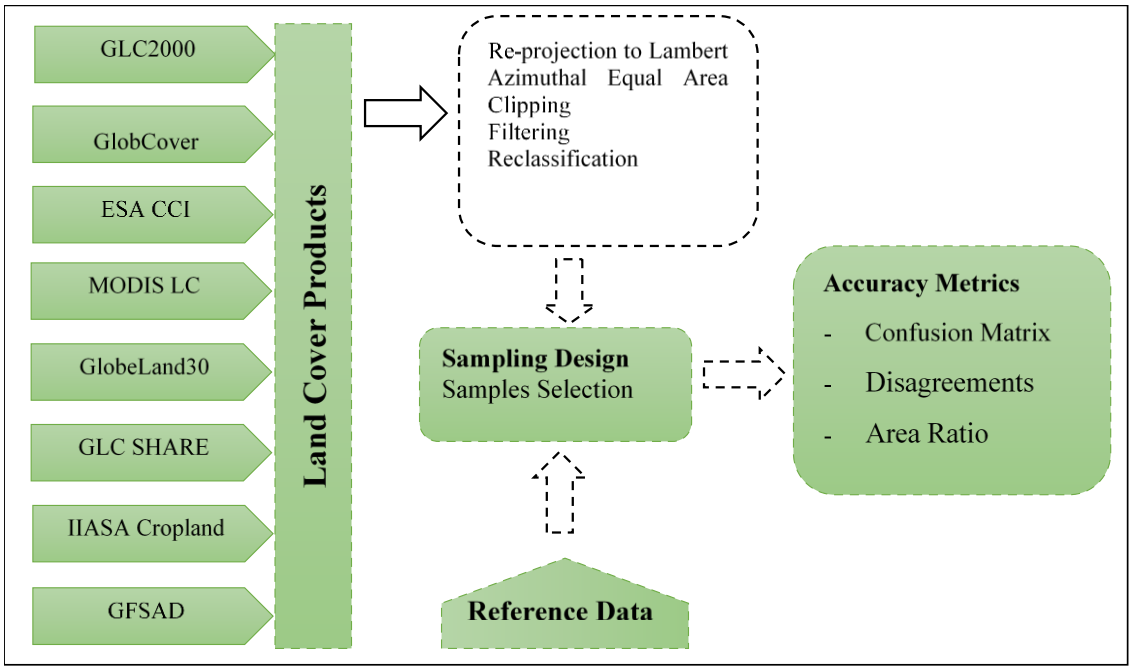

Figure 2. 1. Major steps of the accuracy assessment of different land cover products.

2.2.1. Reference Data

The West Africa Land Use Dynamics Project (WALUDP) has developed a three-period dataset (1975, 2000, and 2013) to map land use and land cover change across West Africa (CILSS, 2016; Cotillon, 2017b; Tappan et al., 2016). Hundreds of Landsat images with a 30 m spatial resolution (Landsat TM, ETM+, and OLI) and 80 m spatial resolution (Landsat MSS) were sampled at 2 km intervals using the Rapid Land Cover Mapper (RLCM) tool. RLCM was developed by the U.S. Geological Survey (USGS) to facilitate manual image interpretation over large areas and for different periods of time (Cotillon & Mathis, 2017). The sampling consisted of superimposing a grid of dots over the imagery. Each dot of the 2 km by 2 km grid was visually interpreted by experts with local experience in each country. The interpretations were based on Landsat data, with high resolution satellite and aerial photography used to supplement or validate the Landsat classifications. The final dataset provides a classification into one of the 25 land cover types for each centroid of the 2 km grid, with possible land cover classes, including multiple non-agricultural classes, and agricultural classes, including rainfed and irrigated cropland. The approach, based on expert visual interpretation, with specific local knowledge of the environments being classified, is expected to show better results than semi- or fully-automated classifiers, particularly for the cropland land

cover type across West Africa (CILSS, 2016). In this study, we used 50% of the 2 km by 2 km data points (selecting data from 2000 or 2013 so as to be closest to the nominal date of the global datasets) as the reference information for assessing the independent land cover products.

Quality control for the reference data was carried out using multiple sources of ancillary data, including thousands of aerial photographs taken by the WALUDP team, high-resolution verification using Google Earth satellite imagery, and field validation in each country, facilitating the systematic verification of land cover assessments (Cotillon, 2017a). In addition, image interpretation and land cover assessments carried out by national experts were reviewed and revised during regular collaborative workshops in West Africa, in order to ensure consistent practice between country teams and USGS partners.

2.2.2. Land Cover Products

The land cover products assessed in this analysis are shown in Table 2.1. In this paper, we focus on the accuracy assessment of crop classes rather than on assessing the performance of non-crop land cover classes.

2.2.2.1. GLC2000

The global land cover database for the year 2000 (GLC2000) has been coordinated by the European Commission's Joint Research Center (JRC) in collaboration with 30 research partners (http://forobs.jrc.ec.europa.eu/products/glc2000/products.php). The global product is generated based on regional products defined by national and regional experts across the world, using the SPOT-Vegetation data [4]. In total, the global product has 22 land cover types at a 1 km spatial resolution. The land cover classes are compatible with the United Nations Land Cover Classification System (UN-LCCS) (Bartholome & Belward, 2005).

2.2.2.2. GlobCover

GlobCover is an initiative of the European Space Agency (ESA) to produce a global land cover product at a finer spatial resolution than the GLC2000 (http://due.esrin.esa.int/page_globcover.php). The first product (GlobCover V2.2) is centered on years 2005–2006 (Olivier Arino et al., 2007) and the second (GlobCover V2.3) is on year 2009 (O. Arino, 2009). The ENVISAT MERIS sensor data at a 300 m spatial resolution is the main input data for the GlobCover product. Given the improvements in the underlying data and the classification technique in V2.3 (O. Arino, 2009), we have focussed more on the performance of the more recent product.

2.2.2.3. ESA LC CCI

The European Space Agency Land Cover of the Climate Change Initiative project (ESA LC CCI) is a set of multi-sensor global land cover databases (https://www.esa-landcover-cci.org/). Recently, the ESA has released a time series of land cover maps, from 1992 to 2015, at a 300 m pixel size (UCL-Geomatics, n.d.). A combination of ENVISAT MERIS, SPOT-Vegetation, and ASAR instruments are used to develop a consistent global land cover product, as a European contribution to the Essential Climate Variables (ECV) list required by the United Nations Framework Convention on Climate Change (UNFCCC). The availability of Sentinel-2 time-series data has also contributed to the development of a prototype for the existing finest spatial resolution

(20 m) land cover database of Africa for the year 2016. Both the 300 m (CCI) and 20 m (CCI-20) land cover maps are assessed in this study.

2.2.2.4. GlobeLand30

A 30-m global land cover product was recently developed by Chinese National Geomatics Center for two periods, 2000 and 2010 (http://www.globeland30.org/GLC30Download/index.aspx). An ensemble of classifiers based on the integration of pixel- and object-based land cover classification were used, with expert knowledge for better handling of spectral confusion and diversity of complex landscapes across the globe (J. Chen et al., 2015). Thousands of Landsat images, together with the Chinese HJ-1 satellite images, served in the development of GlobeLand30 maps.

2.2.2.5. MODIS Land Cover

The Moderate Resolution Imaging Spectroradiometer (MODIS) collection 5.1 Land Cover product (MCD12Q1 at 500 m) was also assessed in this study (https://lpdaac.usgs.gov/dataset_discovery/modis/modis_products_table/mcd12q1). MCD12Q1 is a yearly global land cover dataset, covering years 2001 to 2013, derived from both Terra and Aqua observations, using five global land cover classification systems (Friedl et al., 2010). We used the International Geosphere Biosphere Programme (IGBP) classification scheme with 17 land cover classes developed using an ensemble of decision trees based on training data and ancillary data layers, with noise reduction and quality assessments (as described by the authors of (Friedl et al., 2010)).

2.2.2.6. Global Land Cover SHARE

The Global Land Cover SHARE (GLC-SHARE; http://www.fao.org/geonetwork/srv/en/main.home) was developed by the Food and Agriculture Organization of the United Nations (FAO) as a merger of national, regional, and global databases, with a high and medium spatial resolution (30 m or less) and ~66% global coverage. In the absence of high resolution national and regional data, coarser-scale land cover estimates were used. The multi-temporal and multi-source data were then harmonized and standardized using a data fusion approach based on the Land Cover Classification System (LCCS) and the Land Cover Meta Language (LCML) elements. The final product has a spatial resolution of ~1 km, with 11 aggregated land

cover types represented with 0 to 100% of the area covered in each pixel (Latham et al., 2014).

2.2.2.7. IIASA IFPRI Cropland Map

By adopting a hybrid data integration approach, the authors of (Fritz et al., 2015) developed a global cropland percentage map at a 1 km spatial resolution, referred to as the International Institute for Applied Systems Analysis-International Food Policy Research Institute (IIASA IFPRI) cropland product (http://www.iiasa.ac.at/web/home/about/news/150116-Cropland-Maps.html). Several global land cover products combined, with regional and national datasets used as the inputs to create this cropland intensity map, which were validated using FAO agricultural statistics data.

2.2.2.8. GFSAD Crop Extent for Africa

This product was developed by the NASA Global Food Security Support Analysis Data (GFSAD) combining Landsat 8 and Sentinel-2 data. A combination of pixel- and object-based classification approaches has been used to develop the dataset. Specifically, random forest, support vector machine, and the recursive hierarchical segmentation (RHSeg) algorithms were used to improve the performance of the data classification for cropland mapping. The product has a 30 m spatial resolution with 2015 as the nominal assessment year (Xiong et al., 2017).

2.2.3. Accuracy Assessment

2.2.3.1. Sampling Design

The global land cover datasets were separated into two groups so as to differentiate those with multiple land cover classes from those with only crop intensity information (Table 2.1). The land cover classes for class-based products were redefined as “cropland”, “mixed cropland”, and “non-cropland”, based on the class descriptions associated with each product. For the second group, we reclassified the crop intensity according to the percentage cropland, with 50–100% of the crops defined as “cropland”, and less than 50% defined as “mixed crop” (Table 2.1). We then sampled the reclassified (crop, mixed crop, and non-crop) land cover datasets using the coordinates of the reference data (described above), providing systematic (regular) reference land cover assessments every 4 km across the entire region (257,724 sample points; Figure

2.2). That is, for each reclassified land cover, at each of these 257,724 points, we extracted the pixel value (equivalent to the category or land cover class). An error matrix is then created using the extracted pixel values.

Table 2. 1. Characteristics of the different Land Cover Products Crop classes. The numbers in brackets (e.g., in Cropland (4)), are the class numbers, as reported by the producers.

	Product	Crop Classes	Mixed Crop Classes	Year	Resolution (m)
Group I	GLC2000	Croplands (>50%) (18); tree crops (21); irrigated croplands (20)	Mosaic Forest/Croplands (7); Croplands with open woody vegetation (19)	2000	1000
	GlobCover	Post-flooding or irrigated croplands (11); rainfed croplands (14)	Mosaic cropland (50–70%)/vegetation (grassland, shrubland, and forest) (20–50%) (20); mosaic vegetation (grassland, shrubland, and forest) (50–70%)/cropland (20–50%) (30)	2005;2009	300
	ESA CCI LC series	Cropland rainfed (10); cropland irrigated (20)	Mosaic cropland (30)	1992–2015	300
	ESA CCI 20 m	Cropland (4)		2016	20
	GlobeLand30	Cultivated land (10)		2010	30
	GFSAD 30 m Crop Extent	Croplands (2)		2015	30
	MODIS Land Cover (MCD12Q1)	Croplands (12)	Cropland/natural vegetation mosaic (14)	2001–2013	500
Group II	IIASA IFPRI Cropland	Crop intensity greater than 50%	Crop intensity less than 50%	2005	1000
	GLC SHARE	Crop intensity greater than 50%	Crop intensity less than 50%	2014	1000

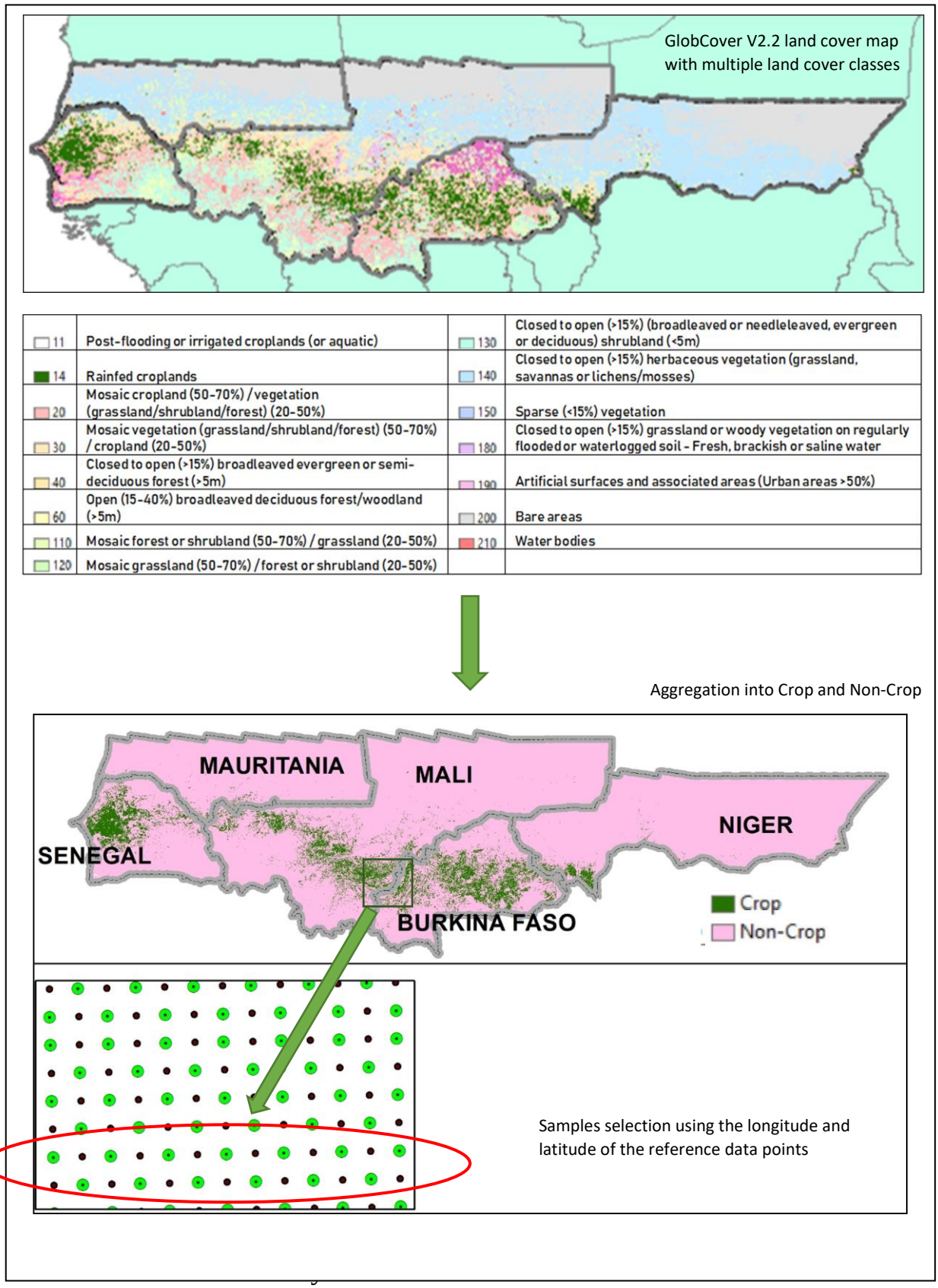

Pontius Jr & Millones (2011) suggested a method to assess the accuracy of classified maps derived from the remote sensed data. The method is based on two simple concepts, quantity disagreement (Q) and allocation disagreement (A). Q is

defined as the difference between the reference classes and the map classes, which is due to the mismatch in the proportions of the different classes. For our study, the Q can be considered to be a measure of error in "how much cropland" there is. A is the difference between the reference classes and the map classes, which is due to a mismatch in the spatial location of the categories. For our study, A translates as error in "where the cropland is". The total disagreement is the sum of Q and A (Pontius Jr & Millones, 2011). The calculation is based on a stratified sampling method. Each land cover class (in our case, crop, mixed crop, and non-crop) is considered as a stratum with a number of pixels, N. The sample confusion matrix (Table 2.2) is created by extracting the pixel values corresponding to the reference data points within each country. From this sample table, we then estimated the population confusion matrix (Table 2.3) for a random or systematic stratified sampling, using equation (1).

Table 2. 2. Sample confusion matrix for two aggregated land cover types (i.e., GLC group 2).

GLC \ Ref.	1. Crop/Mixed Crop	2. Non-Crop
1. Crop/Mixed Crop	n_{11}	n_{12}
2. Non-Crop	n_{21}	n_{22}

The p_{ij} represents the estimate of the area proportion of the population that has class i of the global land cover product and class j for the reference data (Olofsson et al., 2014).

$$p_{ij} = \left(\frac{n_{ij}}{\sum_{j=1}^{J} n_{ij}}\right)\left(\frac{N_i}{\sum_{i=1}^{J} N_i}\right) \quad (1)$$

Where

j=1 … J is the number of classes in the reference data,

i=1 … J is the number of classes in the global land cover product,

$\sum_{j=1}^{J} n_{ij}$ is the sample total for class i,

N_i is the population total for class i

Table 2. 3. Population confusion matrix for two aggregated land cover types (i.e., global land cover (GLC) group 2).

Ref. / GLC	1. Crop/Mixed Crop	2. Non-Crop
1. Crop/Mixed Crop	p_{11}	p_{12}
2. Non-Crop	p_{21}	p_{22}

Summary of the confusion matrix

The quantity disagreement (Q) and allocation disagreement (A) are estimated using the population table [23], expressed by Equations (2) to (5).

$$q_k = \left|\left(\sum_{i=1}^{J} p_{ik}\right) - \left(\sum_{j=1}^{J} p_{kj}\right)\right| \tag{2}$$

$$q_k: quantity\ disagreement\ for\ class\ k$$

$$Q = \frac{\sum_{k=1}^{J} q_k}{2} \tag{3}$$

$$a_k = 2 \times min\left[\left|\left(\sum_{i=1}^{J} p_{ik}\right) - p_{kk}\right|, \left|\left(\sum_{j=1}^{J} p_{kj}\right) - p_{kk}\right|\right] \tag{4}$$

$$a_k: allocation\ disagreement\ for\ class\ k$$

$$A = \frac{\sum_{k=1}^{J} a_k}{2} \tag{5}$$

The overall accuracy (OA) or proportion correct is estimated using Equation (6), and the user's accuracy (UA) for a specified class is given by Equation (7).

$$OA = \sum_{i=1}^{J} p_{ii} \tag{6}$$

$$UA_k = \frac{p_{kk}}{\sum_{i=1}^{J} p_{ki}} \tag{7}$$

2.3. Results

2.3.1. All Crop (Crop and Mixed Crop) Quantity and Allocation Disagreements

Here, we focused on the overall accuracy of the cropland designations in the global land cover products, defining "all crop" to be the sum of the "crop" and "mixed crop" classes. Figure 2.3 shows the results obtained in terms of the disagreements in the crop class, organized by country. The proportions are expressed in terms of quantity disagreement and allocation disagreement. In the majority of cases, the most important part in the total disagreement is as a result of the quantity disagreement. This is

particularly the case in Mauritania, where the disagreement due to allocation is negligible compared with the quantity disagreement, resulting in a large overestimation in the total number of pixels identified as crop in the land cover products, relative to the reference data. The maximum total disagreement occurs with the GLC2000 product in Burkina Faso (50%), Mali (28%), and Senegal (66%). The maximum disagreement in Niger is observed with GLOBCOVER2009 (26%), and in Mauritania with ESACCI20.2016 (30%). The 20 m spatial resolution land cover product of ESA CCI (for 2016) is significantly less accurate among the databases for cropland mapping in Mauritania, as compared to the other countries in the study area. Qualitatively and quantitatively, the most accurate crop predictions are from GlobeLand30 and GFSAD30. These products both have a 30 m spatial resolution, using Landsat images as the main inputs for the classification. This finding regarding GlobeLand30 is in line with previous studies at the Africa continent level (Wei et al., 2018).

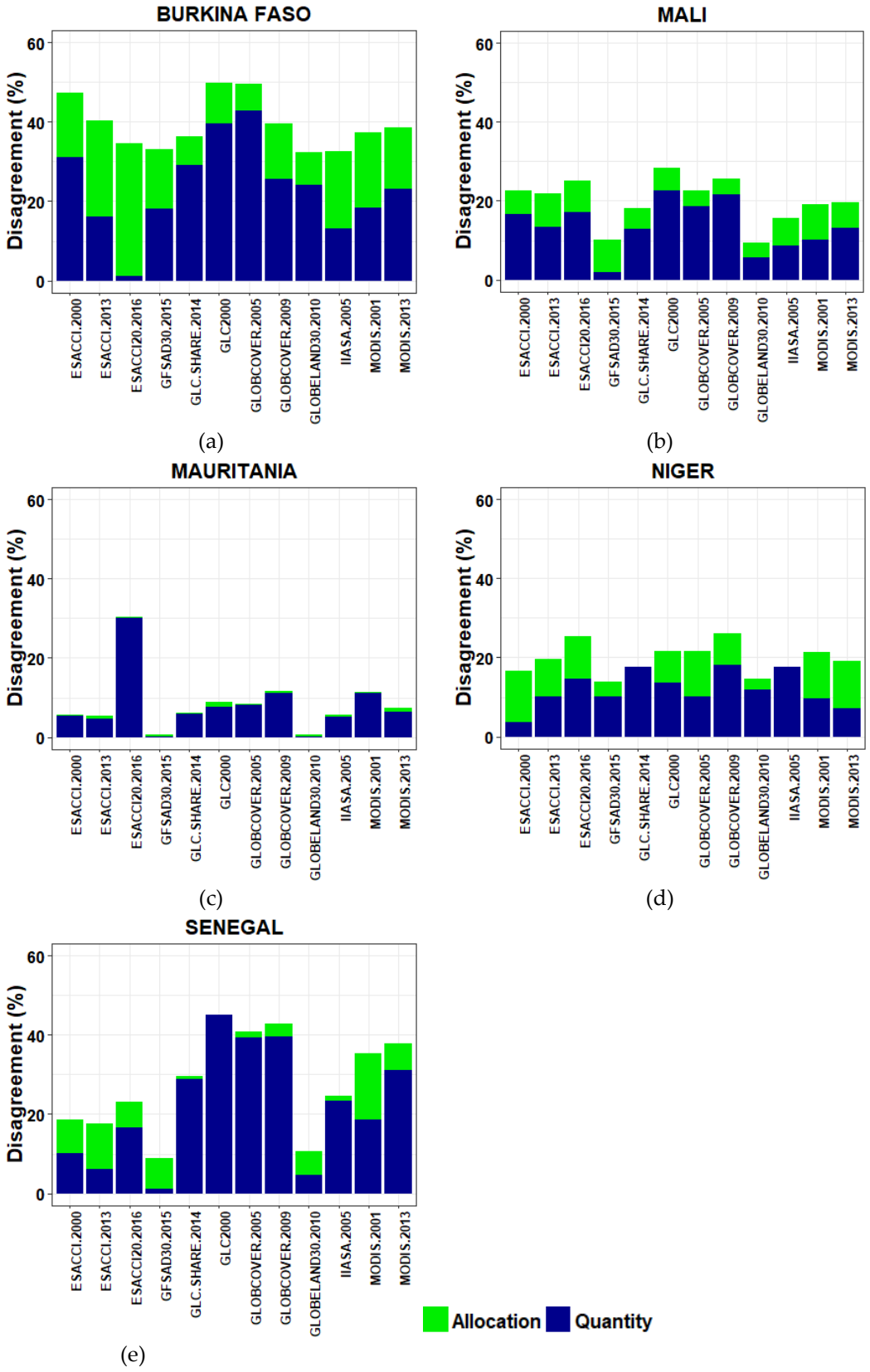

Figure 2. 3. All cropland (sum of crop and mixed-crop classes) quantity disagreement (quantity = how much cropland) and allocation disagreement (allocation = where the cropland is) in five Sahelian West African countries: Burkina Faso (a), Mali (b), Mauritania (c), Niger (d) and Senegal (e). Twelve independent land cover assessments (eight "products", some with multiple years) are used.

2.3.2. Cropland User's Accuracy

2.3.2.1. All Crop (Crop and Mixed Crop) User's Accuracy

Metrics like the user's and producer's accuracy are often reported to bring additional class-specific information to remote sensing-based classifications. In this study, we are interested in assessing how well land cover products classify crop classes (i.e., the user's accuracy). Based on Figure 2.4, it is evident that GlobeLand30 and GFSAD30 present the best accuracy for cropland mapping. GLC2000 has the greatest misclassification proportion. Mauritania is the country among the five involved that are in this research where the land cover products did not perform well in locating crop areas. Half of the land cover products completely failed (accuracy ~0%) to identify cropland correctly. Maybe because of the particularly small size of farms in this country. Mauritania also has the least agricultural land area in West Africa, mostly localized along the Senegal River. It is also worth mentioning that the 20 m land cover product of Africa (ESACC20) has a similar or worse accuracy than the 300 m ESA land cover products.

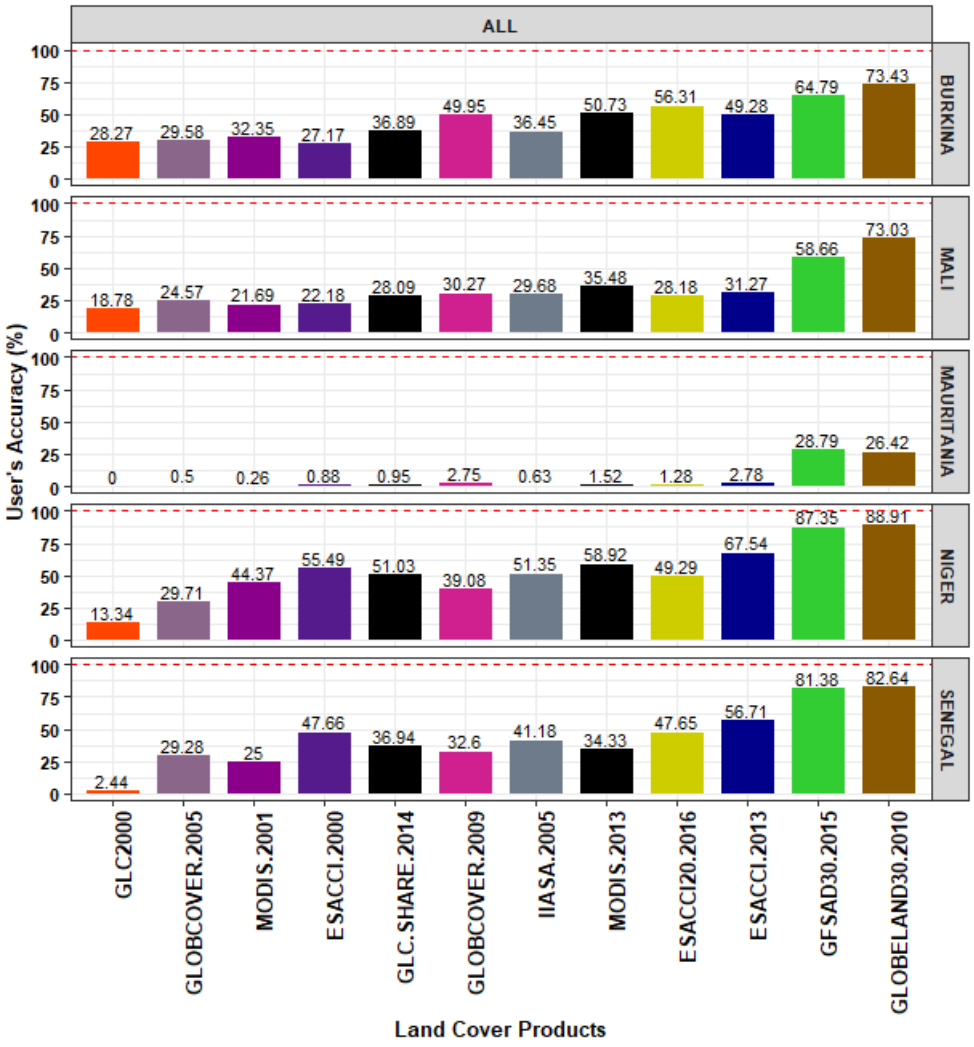

Figure 2. 4. User's accuracy of the "all crop" class by country and land cover product.

On average, for all countries and land cover products, the user accuracy is 35.97% (Figure 2.5a). Figure 2.5b shows that the low accuracy in Mauritania reduces the overall average user's accuracy. Averaging the user's accuracy without Mauritania increases the metric to 43.57% (Figure 2.5c). Cropland mapping accuracy among land cover products shows that GFSAD30 and GlobeLand30 present the best accuracies (with and without the inclusion of Mauritania). In the majority of cases, land cover products have less than 50% of the cropland pixels identified, based on the reference information. Most of the more recent land cover datasets (those developed after 2010, except for the FAO GLC SHARE) present accuracies above the average, indicating gradual improvements related to the availability of more recent remote sensing datasets, calibration data, and analytics. Those datasets are the 2013 ESACCI with a 300 m pixel size (51.2%), ESACCI prototype with a 20 m for 2016 (45.4%), GFSAD with a 30 m

for 2015 (73.1%), GlobeLand30 with a 30 m for 2010 (79.5%), and MODIS with a 500 m for 2013 (44.9%).

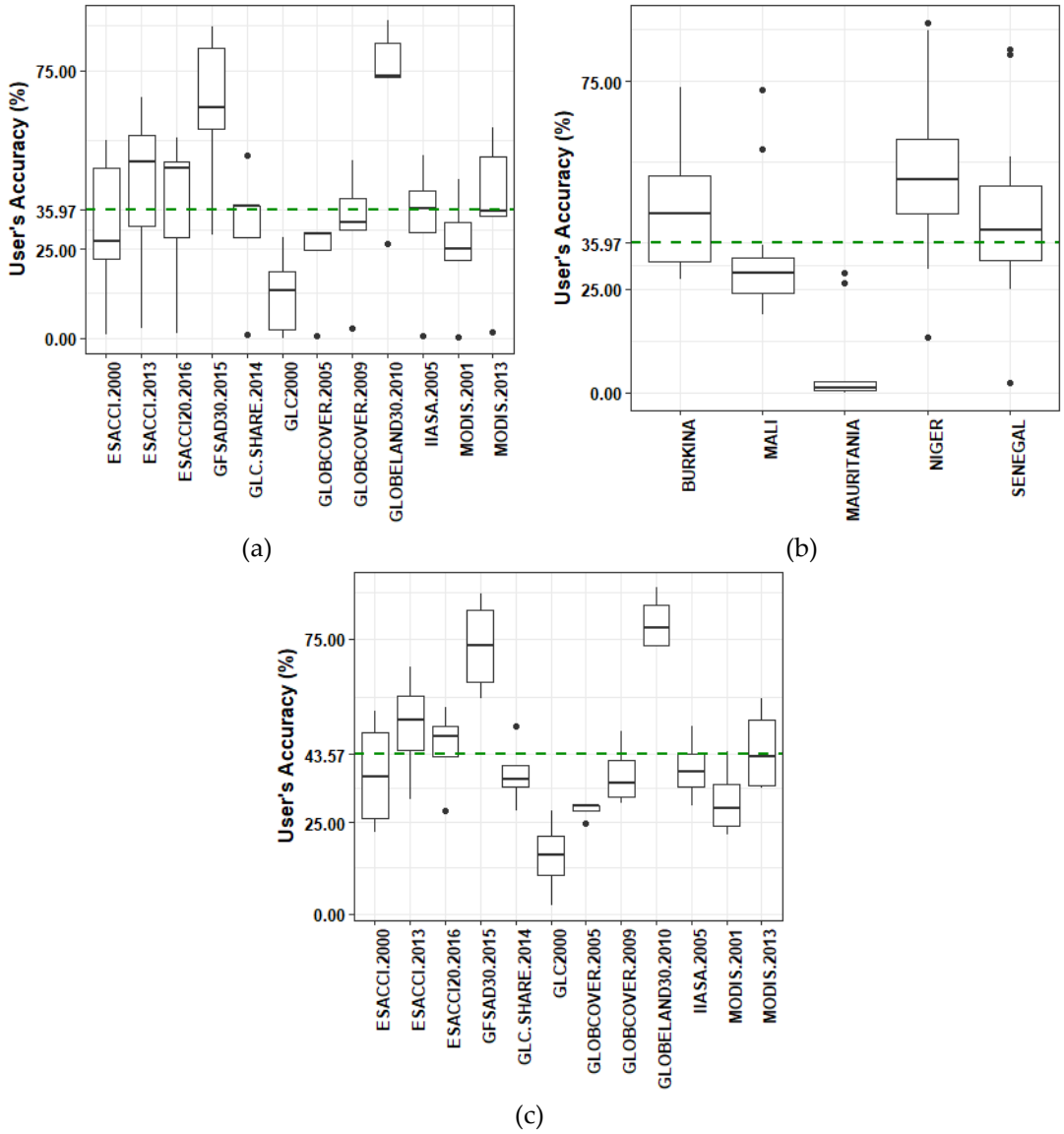

Figure 2. 5. User's accuracy of crop class for all countries (a), all GLC products (b), and all GLC products, with Mauritania removed (c).

2.3.2.2. User's Accuracy for Separate Crop and Mixed Crop Classes

The two land cover classes ("crop" and "mixed-crop"; Table 2.1) are analyzed separately in this section. Land cover products with a unique agricultural class, like ESA CCI at 20 m, GFSAD30, and GlobeLand30, are analyzed in the category of crop class without a mixed crop (Table 2.1). The products with the crop intensity in a percentage, like GLC SHARE and the IIASA crop intensity, are analyzed with separate crop and mixed crop classes. A striking illustration of user's accuracy through the two

above-mentioned crop classes can be seen in Figure 2.6. Each of the five countries (Burkina Faso, Mali, Mauritania, Niger, and Senegal) are presented by crop class and land cover product. The two thresholds (see Figure 2.5), one at 75% and another at 25%, are taken as the targeted values for crop and mixed crop classes, respectively. The assumptions being that the crop class pixels with a 50–100% crop cover are identified as cropland (hence an average value of 75%), while pixels with a 0–50% crop cover are identified as the mixed crop (hence an average value of 25%). For the crop and mixed crop categories, land cover products with explicit details on the fraction of cropland in pixels are considered in the analysis. Those products are ESA CCI, GLC2000, GlobCover, GLC SHARE, IIASA Cropland, and MODIS land cover datasets (Table 2.1). None of the land cover products reach the accuracy of 75% for crop class for all of the five countries. GFSAD30 and GlobeLand30 have the most accurately mapped cropland in this category, with accuracies exceeding 80% in some countries. For example, in Niger and Senegal, these accuracies are 87.35% and 81.38%, respectively, for GFSAD30, and 88.91% and 82.64%, respectively, for GlobeLand30. They are followed by the ESA CCI land cover of year 2013, GLC SHARE, and IIASA crop intensity map. GlobCover and MODIS have a similar crop accuracy in Burkina Faso and Senegal. GLC2000 remains the least accurate in this category of crop class in terms of user's accuracy. Contrary to the crop class, the mixed crop class has been relatively well identified, as the majority of land cover products have more than 25% of mixed crop user's accuracy. On average, the MODIS and ESA CCI land cover products for 2013 have the best accuracies in locating pixels with mixed cropland. They both have a coarse resolution, of 500 m and 300 m, respectively. At the country level, Mauritania is shown as being exceptionally poorly mapped in terms of cropland for both of the two categories of the crop classes.

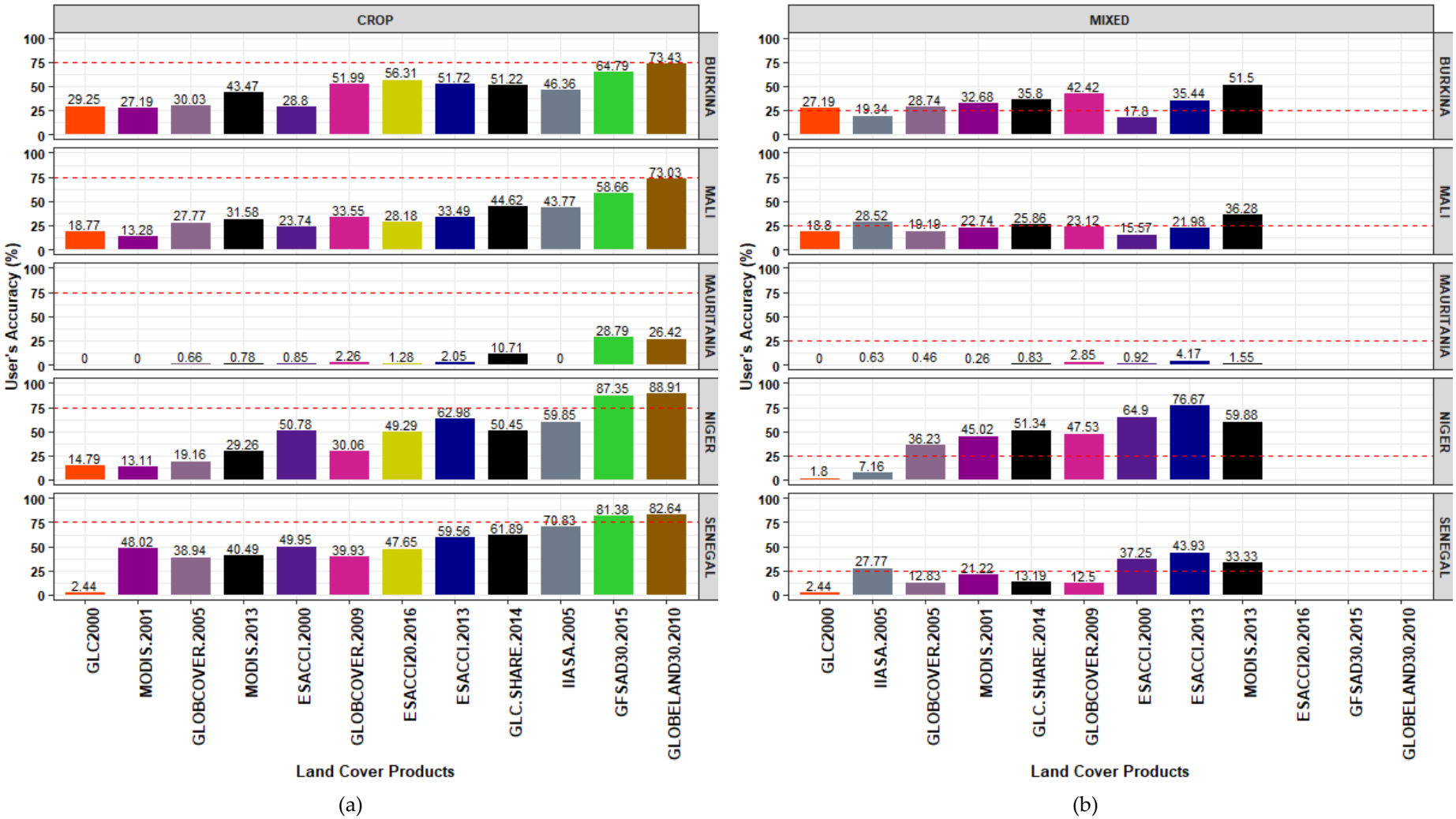

Figure 2. 6. User's accuracy for crop (a) and mixed crop (b) classes. ESACCI 20 m, GFSAD30, and GlobeLand30 do not have mixed crop class (b).

2.3.3. Cropland Area Assessment

2.3.3.1. All Crop Commission and Omission Disagreements

The reported omission disagreement and commission disagreement in Figure 2.7 correspond to false negative and the false positive outcomes [or cases], respectively. They are equivalent to the off-diagonal terms of the crop/mixed crop class p12 (commission) and p21 (omission), as defined in Table 2.3. The agreement value is the diagonal term p11 for the crop/mixed crop class. A higher value of commission disagreement compared to omission disagreement is similar to an overestimation cropland. On the other hand, if the omission disagreement is greater than the commission disagreement, the cropland is underestimated by the land cover product. Any difference between these two metrics of disagreement means a non-zero quantity disagreement from the crop class. Based on this analysis, the GLC2000, GlobCover 2005, GLC SHARE, ESACCCI 2000, and MODIS 2013 products visibly present the most important difference between omission and commission disagreements. Therefore, they are expected to have a greater overestimation of crop area. GlobeLand30 and GFSAD30 have omission disagreements greater than commission disagreements, leading to an underestimation of crop area. This underestimation is expected to be more important in the GlobeLand30 compared to GFSAD30.

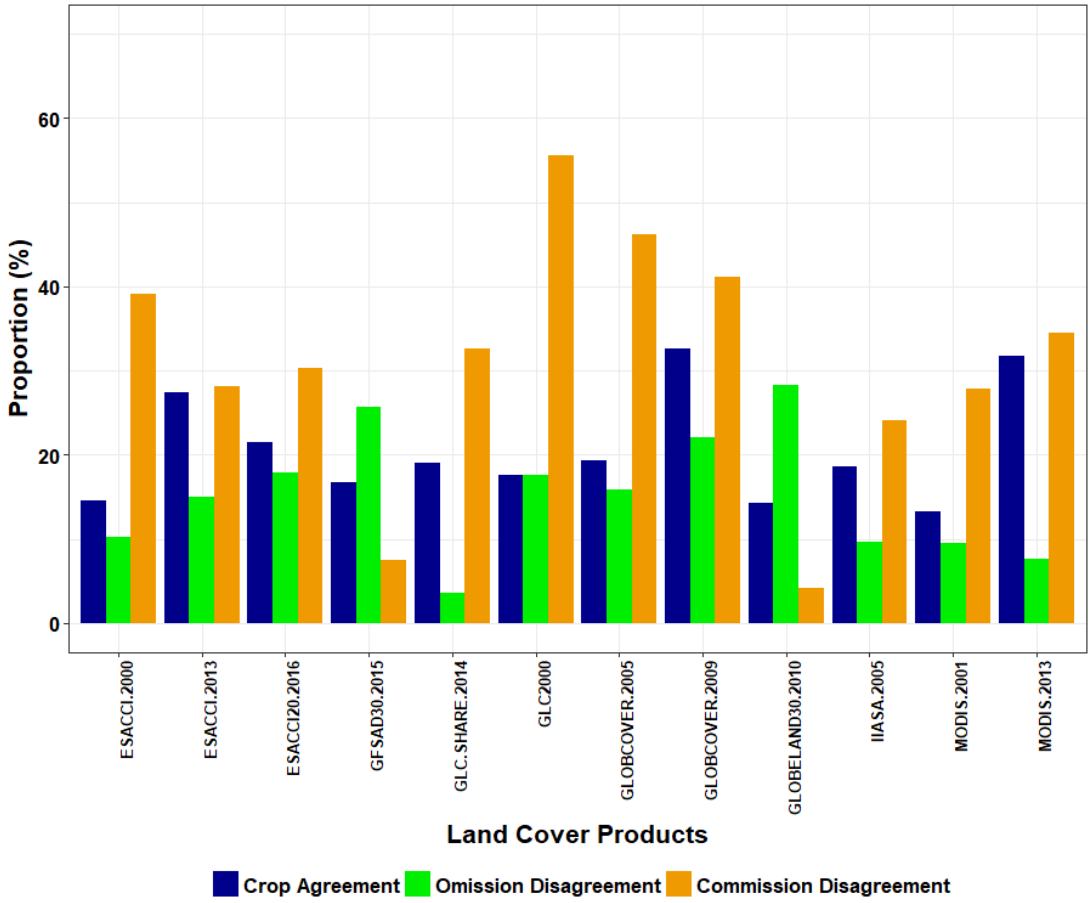

Figure 2. 7. Crop proportion correct with the relative omission and commission misclassifications. Higher commission to omission disagreement = overestimation of cropland, while higher omission to commission disagreement = underestimation of cropland.

2.3.3.2. Cropland Area Ratio (GLC/Reference Map)

Figure 2.8 illustrates the general trends of the GLC products cropland area estimation in the study region. These trends are mainly an overestimation of the crop area. At the country level, land cover products have overestimated the cropland area by a factor greater than 20 in Mauritania, while this factor has an average of less than 2 in other countries (Figure 2.8a). For this reason, the aggregation of area ratios by land cover product (Figure 2.8b) is carried out without Mauritania, so as to reduce bias in the results.

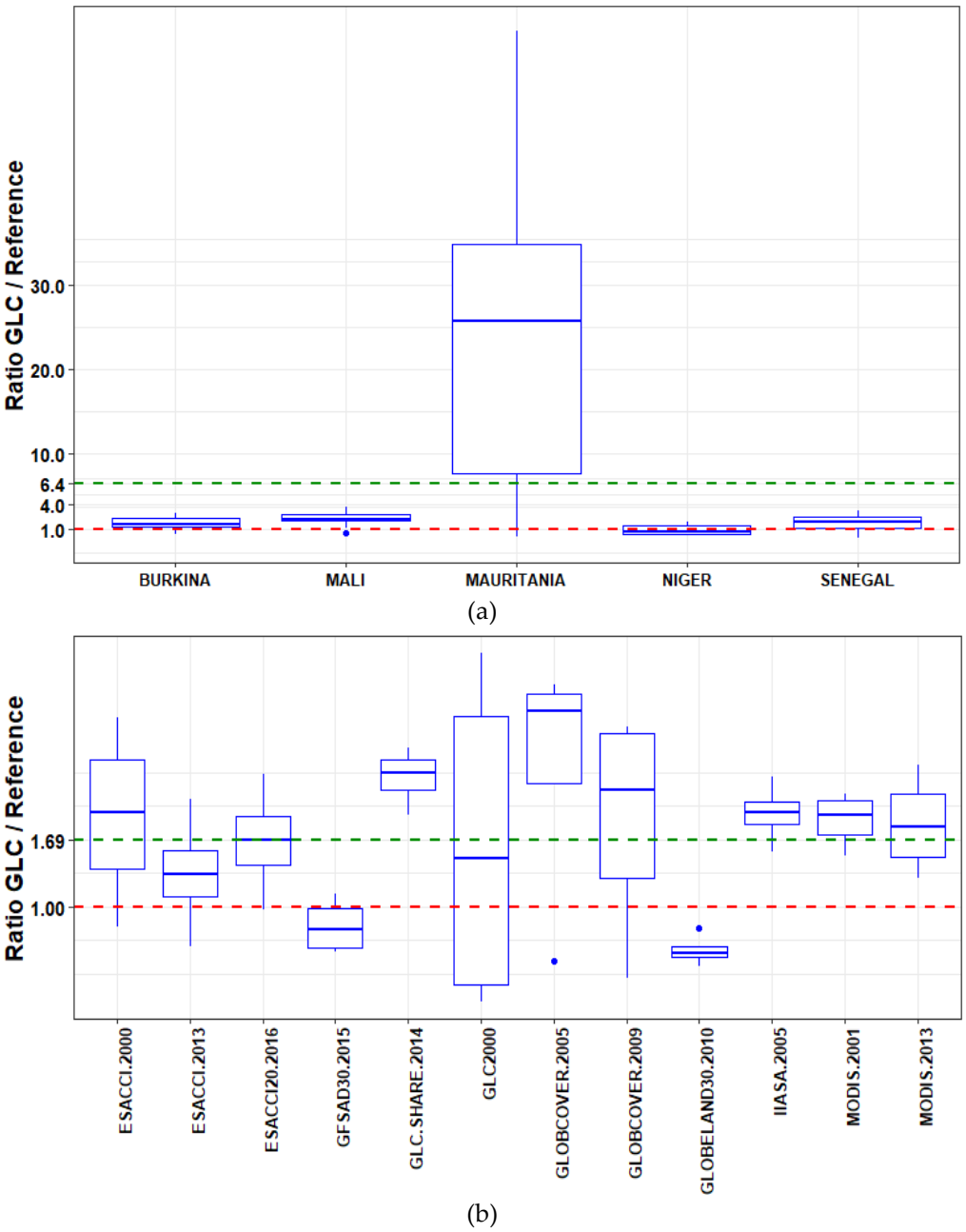

Figure 2. 8. Ratio of mapped and reference crop areas. Aggregated by country (a), and by land cover products (b) with the ideal situation (ratio = 1) in red and the observed average ratio (1.69) in green.

The generalized overestimation of crop areas shown in Figure 2.8b is in line with what has been previously discussed, relative to the difference between omission and commission disagreements. A ratio greater than 1 indicates a tendency, across most of the GLC products, to an overestimation of the cropland area. On average, the GLC datasets overestimate the cropland area by about 69%, although two GLCs (GFSAD30 with a ratio of 0.8 and GlobeLand30's with a ratio of 0.6) underestimate the cropland area. Even if the average ratio of GLC2000 is less than the overall average, this product

presents the most substantial variations in crop areas estimation, followed by GlobCover.

2.4. Discussion

Recently developed land cover datasets (after 2010) seem to have a better accuracy in cropland mapping in the Sahel region (Figures 2.4 and 2.6). This is due not only to the availability of newer sensors with higher spatial, spectral, and radiometric resolutions (e.g., Landsat 8: https://landsat.usgs.gov/landsat-8, and Sentinel 2: https://sentinel.esa.int/web/sentinel/home), but also to the progress made in the implementation of new approaches of satellite image processing, particularly in machine learning techniques (Support Vector Machine, Decision trees, Random forest, Segmentation algorithm). GFSAD30 and GlobeLand30, which have shown better cropland estimation in Western Sahel, compared to the other land cover products, were developed using random forest and pixel–object-based (i.e., an optimization of the pixel-based and object-based methods) classification algorithms, respectively. These new algorithms are becoming popular within the remote sensing community, because of their abilities to accurately classify land cover (Breiman, 2001; Y. Chen et al., 2018). However, at the country and regional scales of this West Africa analysis, using high quality and high density reference information, we found that both GFSAD30 and GlobeLand30 have a cropland class user's accuracy below that reported by the producers; which is in conformity with previous findings in assessing the GlobeLand30 dataset at a country level (Kenya) reported by the authors of (See et al., 2017).

In general, the land cover maps with multiple classes based on coarse spatial resolution (i.e., 300 m or greater) satellite images did not perform well in identifying crop areas in the region of study. At this coarse spatial resolution, it is common to find cropland mixed with fallow and other cover types in the fragmented Sahelian agricultural landscape, adding another level of complexity in land cover classification (Townshend et al., 2000). The best user's accuracy for the mixed cropland class is shown with the European climate change initiative product of the year 2013 at 300 m (ESACCI 2013). This is in large part because the moderate spatial resolution products (i.e., 30 m and 20 m) do not have a mixed class for cropland. GLC2000, developed around the year 2000, with its 1 km pixel size, has the highest disagreement values and the most variable crop area ratio across the five countries. Some improvements have

been made with the ESA CCI land cover series, the GlobCover at 300 m spatial resolution, and MODIS land cover at 500 m. These products have multi-year data (ranging from 1992 to 2015 for ESACCI, 2004 to 2009 for GlobCover, and 2001 to 2013 for MODIS). The results of this study suggest that multi-year products are improving through time, perhaps because of better classification approaches (e.g., handling mixture of cover types in pixels), as data are coming from the same sensors. However, we found a general overestimation of crop areas in this category of land cover product. The specific case of ESA CCI's overestimation of cropland area has been concluded by Laso Bayas et al. (2017) across the Africa continent in previous studies.

Attempts to improve land cover products, particularly for mapping the crop extent, have led to the development of hybrid products with cropland intensity (from 0 to 100%), created by fusing various data sources with different existing land cover datasets. Data fusion is well known approach in remote sensing. Its' goal is to obtain a higher reliability by using multi sources data (Castanedo, 2013). These synergistic or hybrid products are normally at coarser spatial resolution (~1 km) and include GLC SHARE and IIASA Crop intensity products assessed in this study, which both overestimate cropland in West Africa with crop area ratios above the overall average (i.e., 1.69) (Figure 2.8b).

Our results confirm the general observation that coarse pixel size is not suitable for mapping the fragmented cropland landscapes in the West African Sahel. However, expectations for the improved identification of small agricultural fields in West Africa are generally not met with higher resolution products, including the recently released 20 m ESA CCI land cover product based on Sentinel 2 images. Indeed, ESA CCI presents worse agreement in mapping cropland than the 30-m based products like GFSAD30 and GlobeLand30. Even if the year of production could be a factor in the disagreement between those three products (2016 for ESACCI 20 m, 2010 for GlobeLand30, and 2015 for GFSAD30), this raises questions about the approach and training data used to develop the 20 m ESA product for Africa. The spectral and structural similarities of cropland with the surrounding natural vegetation (shrubs, grassland, savanna, and fallow) could also lead to difficulties in correctly mapping crop areas in the region, despite improvements in the spatial resolution (from 1000 m to 20 m).

2.5. Conclusions

In total, eight land cover products were assessed in this study, with a focus on cropland classes across five Western Sahel countries (Burkina Faso, Mali, Mauritania, Niger, and Senegal). These products have been developed for diverse purposes and present different characteristics in terms of input data, algorithm of classification, and consistency.

In general, a low user's accuracy of cropland class and high crop area ratios (overestimation) are observed with coarse spatial resolution (i.e., 300 m or greater) land cover products. However, these products seem to map accurately the mixed cropland class, as the majority of land cover products in this category have more than 25% of the mixed crop user's accuracy. ESACCI 2013 for example reaches a user's accuracy of 76.67% in Niger.

Progress in computational power, combined with the availability of new sensors and optimized algorithms, have led to the development of improved land cover datasets. These datasets at 30 m (GFSAD30 and GlobeLand30) or 20 m (ESACCI 2016) are created sometimes by fusing more than one source of data (e.g., Landsat 8 and Sentinel2). However, while GFSAD30 and GlobeLand30 have shown better accuracy and improvement in the crop area ratio compared to the coarser pixel size products, similar expectations are not met with the 20 m ESA CCI land cover.

Overall, among the studied land cover products, GFSAD30 and GlobeLand30 present better accuracy in identifying crop areas. They have, in the Sahel, an average cropland class accuracy of 68.89% and 64.19% for GlobeLand30 and GFSAD30, respectively, approaching the target accuracy of 75%, although both tend to underestimate crop areas. Given the importance of agriculture for food security and livelihoods in West Africa, the development of remote sensing-based approaches to monitoring agricultural yields is of critical importance. The accurate geolocation and area quantification of the croplands is a necessary first step. Our results suggest a considerable variability in the accuracy of the cropland assessments available in the GLC products. However, gradual improvements associated with newer sensors and higher spatial resolution, coupled with innovations in analytical approaches, have led to increases in the overall accuracy as well as the decreasing quantity and allocation errors. New training and validation datasets, derived using expert local knowledge,

facilitate the error assessment of the global land cover products, and open the door to locally optimized agricultural land use and land cover assessments.

Funding: K.S. was supported by the United States Agency for International Development (USAID) via funding to the Michigan State University Borlaug Higher Education for Agricultural Research and Development (BHEARD) Graduate Research Fellowship Program.

Acknowledgments: This material is based upon work supported by the United States Agency for International Development, as part of the Feed the Future initiative, under the CGIAR Fund, award number BFS-G-11-00002, and the predecessor fund the Food Security and Crisis Mitigation II grant, award number EEM-G-00-04-00013.

2.6. References

Arino, O. (2009). GlobCover 2009. http://epic.awi.de/31046/1/Arino_et_al_GlobCover2009-a.pdf

Arino, Olivier, Bicheron, P., Achard, F., Latham, J., Witt, R., & Weber, J.-L. (2008). The most detailed portrait of Earth. Eur. Space Agency, 136, 25–31.

Arino, Olivier, Gross, D., Ranera, F., Leroy, M., Bicheron, P., Brockman, C., Defourny, P., Vancutsem, C., Achard, F., Durieux, L., & others. (2007). GlobCover: ESA service for global land cover from MERIS. 2007 IEEE International Geoscience and Remote Sensing Symposium, 2412–2415.

Bartholome, E., & Belward, A. S. (2005). GLC2000: a new approach to global land cover mapping from Earth observation data. International Journal of Remote Sensing, 26(9), 1959–1977.

Breiman, L. (2001). Random forests. Machine Learning, 45(1), 5–32.

Castanedo, F. (2013). A review of data fusion techniques. The Scientific World Journal, 2013.

Chen, J., Chen, J., Liao, A., Cao, X., Chen, L., Chen, X., He, C., Han, G., Peng, S., Lu, M., & others. (2015). Global land cover mapping at 30 m resolution: A POK-based operational approach. ISPRS Journal of Photogrammetry and Remote Sensing, 103, 7–27.

Chen, Y., Zhou, Y., Ge, Y., An, R., & Chen, Y. (2018). Enhancing land cover mapping through integration of pixel-based and object-based classifications from remotely sensed imagery. Remote Sensing, 10(1), 77.

CILSS. (2016). Landscapes of West Africa—A window on a changing world. U.S. Geological Survey EROS: Garretson, SD, USA.

Conceição, P., Fuentes-Nieva, R., Horn-Phathanothai, L., & Ngororano, A. (2011). Food security and human development in Africa: strategic considerations and directions for further research. African Development Review, 23(2), 237–246.

Cotillon, S. E. (2017a). West Africa land use and land cover time series.

Cotillon, S. E. (2017b). West Africa land use and land cover time series. In Fact Sheet. https://doi.org/10.3133/fs20173004

Cotillon, S. E., & Mathis, M. L. (2017). Mapping land cover through time with the Rapid Land Cover Mapper—Documentation and user manual: U.S. Geological Survey Open File Report 2017–1012, 23 p., https://doi.org/10.3133/ofr20171012.

ESA-CCI. (2013). Internal Release of Global Land Cover Map with Improved Accuracy over the Existing State of the Art (75.6%). https://www.esa-landcover-cci.org/?q=node/148

Friedl, M. A., Sulla-Menashe, D., Tan, B., Schneider, A., Ramankutty, N., Sibley, A., & Huang, X. (2010). MODIS Collection 5 global land cover: Algorithm refinements and characterization of new datasets. Remote Sensing of Environment, 114(1), 168–182. https://doi.org/10.1016/j.rse.2009.08.016

Fritz, S., See, L., Mccallum, I., You, L., Bun, A., Moltchanova, E., Duerauer, M., Albrecht, F., Schill, C., Perger, C., Havlik, P., Mosnier, A., Thornton, P., Wood-Sichra, U., Herrero, M., Becker-Reshef, I., Justice, C., Hansen, M., Gong, P., … Obersteiner, M. (2015). Mapping global cropland and field size. Global Change Biology. https://doi.org/10.1111/gcb.12838

Fritz, S., You, L., Bun, A., See, L., McCallum, I., Schill, C., Perger, C., Liu, J., Hansen, M., & Obersteiner, M. (2011). Cropland for sub-Saharan Africa: A synergistic approach using five land cover data sets. Geophysical Research Letters, 38(4).

Herold, M., Mayaux, P., Woodcock, C. E., Baccini, A., & Schmullius, C. (2008). Some challenges in global land cover mapping: An assessment of agreement and accuracy in existing 1 km datasets. Remote Sensing of Environment, 112(5), 2538–2556.

Hüttich, C., Herold, M., Wegmann, M., Cord, A., Strohbach, B., Schmullius, C., & Dech, S. (2011). Assessing effects of temporal compositing and varying observation periods for large-area land-cover mapping in semi-arid ecosystems: Implications for global monitoring. Remote Sensing of Environment, 115(10), 2445–2459.

Laso Bayas, J. C., See, L., Perger, C., Justice, C., Nakalembe, C., Dempewolf, J., & Fritz, S. (2017). Validation of automatically generated global and regional cropland data sets: The case of Tanzania. Remote Sensing, 9(8), 815.

Latham, J., Cumani, R., Rosati, I., & Bloise, M. (2014). Global land cover share (GLC-SHARE) database beta-release version 1.0-2014. FAO: Rome, Italy.

Mayaux, P., Eva, H., Gallego, J., Strahler, A. H., Herold, M., Agrawal, S., Naumov, S., De Miranda, E. E., Di Bella, C. M., Ordoyne, C., & others. (2006). Validation of the global land cover 2000 map. IEEE Transactions on Geoscience and Remote Sensing, 44(7), 1728–1739.

Olofsson, P., Foody, G. M., Herold, M., Stehman, S. V, Woodcock, C. E., & Wulder, M. A. (2014). Good practices for estimating area and assessing accuracy of land change. Remote Sensing of Environment, 148, 42–57.

Pontius Jr, R. G., & Millones, M. (2011). Death to Kappa: birth of quantity disagreement and allocation disagreement for accuracy assessment. International Journal of Remote Sensing, 32(15), 4407–4429.

See, L., Laso Bayas, J. C., Schepaschenko, D., Perger, C., Dresel, C., Maus, V., Salk, C., Weichselbaum, J., Lesiv, M., McCallum, I., & others. (2017). LACO-Wiki: A new online land cover validation tool demonstrated using GlobeLand30 for Kenya. Remote Sensing, 9(7), 754.

Tappan, G. G., Cushing, W. M., Cotillon, S. E., Mathis, M. L., Hutchinson, J. A., & Dalsted, K. (2016). West Africa Land Use Land Cover Time Series. U.S. Geological Survey: Sioux Falls, SD, USA.

Townshend, J. R. G., Huang, C., Kalluri, S. N. V, Defries, R. S., Liang, S., & Yang, K. (2000). Beware of per-pixel characterization of land cover. International Journal of Remote Sensing, 21(4), 839–843.

UCL-Geomatics. (n.d.). Land Cover CCI Product User Guide Version 2.0. Retrieved April 10, 2017, from http://maps.elie.ucl.ac.be/CCI/viewer/download/ESACCI-LC-Ph2-PUGv2_2.0.pdf

Wei, Y., Lu, M., & Wu, W. (2018). A comparative analysis of five cropland datasets in Africa. ISPRS Int. Arch. Photogramm. Remote Sens. Spat. Inf. Sci, 1863–1870.

Xiong, J., Thenkabail, P. S., Tilton, J. C., Gumma, M. K., Teluguntla, P., Oliphant, A., Congalton, R. G., Yadav, K., & Gorelick, N. (2017). Nominal 30-m cropland extent map of continental Africa by integrating pixel-based and object-based algorithms using Sentinel-2 and Landsat-8 data on google earth engine. Remote Sensing, 9(10), 1–27. https://doi.org/10.3390/rs9101065

Zhong, L., Gong, P., & Biging, G. S. (2014). Efficient corn and soybean mapping with temporal extendability: A multi-year experiment using Landsat imagery. Remote Sensing of Environment, 140, 1–13.

CHAPTER 3

A high-resolution cropland map for the West African Sahel based on high-density training data, Google Earth Engine and locally optimized machine learning

Paper #2

Samasse, K., Hanan, N. P., Anchang, J. Y., & Diallo, Y. (2020). A high-resolution cropland map for the West African Sahel based on high-density training data, google earth engine, and locally optimized machine learning. *Remote Sensing*. https://doi.org/10.3390/RS12091436

Abstract

The West African Sahel cropland map (WASC30) is a new 30-meter cropland extent product for the nominal year of 2015. We used the computing resources provided by Google Earth Engine (GEE) to fit and apply Random Forest models for cropland detection in each of 189 grid cells (composed of 100 km squares, hence a total of ~1.9 x 106 km2) across five countries of the West African Sahel (Burkina Faso, Mauritania, Mali, Niger, and Senegal). Landsat-8 surface reflectance (Bands 2-7) and vegetation indices (NDVI, EVI, SAVI, and MSAVI), organized to include dry-season and growing-season band reflectances and vegetation indices for the years 2013-2015, were used as predictors. Training data were derived from an independent, high-resolution, visually interpreted sample dataset that classifies sample points across West Africa using a 2-km grid (~380,000 points were used in this study, with 50% used for model training and 50% used for model validation). Analysis of the new cropland dataset indicates a summed cropland area of ~316 x 103 km2 across the 5 countries, primarily in rainfed cropland (309 x103 km2), with irrigated cropland area (7 x103 km2) representing 2% of the total cropland area. At regional scale the cropland dataset has an overall accuracy of 90.1% and a cropland class (rainfed and irrigated) user's accuracy of 79%. At bioclimatic zones scale, results show that land proportion occupied by rainfed agriculture increases with annual precipitation up to 1000 mm. The Sudanian zone (600-1200 mm) has the highest proportion of land in agriculture (24%), followed by the Sahelian (200-600 mm) and the Guinean (1200+) zones for 15% and 4%, respectively. The new West African Sahel dataset is made freely available for applications requiring improved cropland area information for agricultural monitoring and food security applications.

3.1. Introduction

Timely and accurate information on cultivated areas is of paramount importance for food security planning (Latham, 2009; Thenkabail et al., 2009). This is particularly true in developing regions, like the West African Sahel, where most cropland is rainfed and agricultural production is susceptible to fluctuations in precipitation (Hollinger & Staatz, 2015). Earth Observation (EO) satellites can contribute significantly to providing information to the agricultural sector, as they allow for consistent land surface imaging over broad spatial extents (regionally or globally) with high revisit frequency (Atzberger, 2013). That makes these technologies suitable for monitoring vegetation (H. G. Jones & Vaughan, 2010), cropland area (H. G. Jones & Vaughan, 2010; Pérez-Hoyos et al., 2017; Xiong et al., 2017) and agricultural production (Burke & Lobell, 2017; Hong et al., 2019; Löw et al., 2017; Rembold et al., 2019). Optical remote sensing in particular offers unique possibilities for mapping cropland extent, in addition to monitoring the growth and eventual yield of cultivated lands (Kobayashi et al., 2019; Xue & Su, 2017).

The accuracy of remote sensing based land cover (including cropland) products varies considerably depending on the scale of assessment, the statistical approaches adopted and the quality and quantity of training and evaluation data. Samasse et al. (2018) recently reviewed eight global and regional land cover maps (Olivier Arino et al., 2008; Bartholome & Belward, 2005; Bontemps et al., 2015; J. Chen et al., 2015; Friedl et al., 2010; Fritz et al., 2011; Latham et al., 2014; Xiong et al., 2017) using high-density evaluation data for the five countries of the Western Sahel (Burkina Faso, Mali, Mauritania, Niger and Senegal). The study focused uniquely on cropland classes. They found large errors in all existing products, particularly in the coarser resolution (>300 m) products. However, even the higher resolution (~30 m) datasets had accuracy statistics ("user's accuracy") less than 75%, and all existing products were greatly biased to overestimate the area of active cropland in the region. More recent studies benefitted from high spatial resolution data (10 m or less) to map cropland in the region. For example, Tong et al. (2020) used full-year Sentinel-2 NDVI data and Random Forest classifiers to separate cropland from fallow across the Sahel belt (Tong et al., 2020) at 10 m resolution, reporting an overall average accuracy of 88% for crop and fallow classes. However, they also used several land cover products with known moderate or low accuracy for cropland extent to develop the fallow/cropland map. Specifically, the

CGLS LCC 100 m (Buchhorn et al., 2019), and ESA CCI 300 m (Bontemps et al., 2015) maps, used as croplands mask in Tong et al. (2020), have low cropland class-specific accuracy (~60%) (L. Li et al., 2019) and high area overestimation (Samasse et al., 2018), respectively. That may lead, via error propagation, to important misclassifications in the final product, attenuating our ability to retrieve cultivated land area as a precursor to yield modeling and prediction.

The clear need for improvements in cropland area assessments in the Sahel region, coupled with the potential for improvements made possible using higher resolution data, also increases the need for computational resources, new methods, and technical skills for effective processing and analysis. Google Earth Engine (GEE) (Gorelick et al., 2017) is one of the platforms currently facilitating access and processing of larger data volumes for diverse operational applications including cropland mapping. The Landsat data archive, in particular, with 30 m spatial resolution, long temporal record and no cost, provides an opportunity to map large scale agricultural regions consistently and in greater detail (L. Kumar & Mutanga, 2018; Roy et al., 2014). Recent satellite instrument additions (e.g. Copernicus Sentinel Instruments) provide increasing opportunities to combine data from multiple sources for improved spatial, temporal and radiometric resolution.

In this study, we leverage the availability of more than 400,000 land-cover training data points for the year 2013 (Samasse et al., 2018; Tappan et al., 2016), with hundreds of cloud-free Landsat-8 images (for the years 2013-2015), to train locally-optimized Random Forest models predicting presence and absence of rainfed and irrigated agricultural fields across the non-desert (MAP > 200 mm/y) land area of the West African countries of Mauritania, Senegal, Mali, Burkina Faso and Niger. Our analysis grid is composed of 267 (100 x 100 km) grid squares, each processed separately using Google Earth Engine (GEE) to fit and apply locally optimized Random Forest models for cropland detection at 30 meters. We analyze our results to estimate accuracy and uncertainty of the new classification, present summary statistics for cropland in the region, and make the new West African Sahel Cropland dataset (under the name WASC30) freely available for applications requiring improved crop area data for agricultural monitoring and food security.

3.2. Materials and Methods

3.2.1. Reference data

Reference data on presence and absence of rainfed and irrigated agriculture were obtained from the Rapid Land Cover Mapper (RLCM) (Cotillon, 2017a; Cotillon & Mathis, 2017; Tappan et al., 2016) for the year 2013. The RLCM approach uses local experts and visual interpretation of 30 m Landsat images to assess land cover type, sampled at 2 km intervals across West Africa (CILSS, 2016; Cotillon, 2017a; Tappan et al., 2016). While RCLM data are available for several epochs (1975, 2000, 2013), we use only the 2013 data as training data for this study. The dataset provides classification into one of 25 land cover types for each centroid of the 2 km grid, with possible land cover classes including multiple non-agricultural classes, and agricultural classes including rainfed and irrigated cropland. The approach, based on expert visual interpretation, with specific local knowledge of the environments being classified, is expected to show better results than semi- or fully automated classifiers, particularly for the cropland class across West Africa (CILSS, 2016).

Quality control for the reference data was carried out using multiple sources of ancillary data, including thousands of aerial photographs taken by the USGS team, high-resolution verification using Google Earth satellite imagery, and field validation in each country, facilitating systematic verification of land cover assessments (Cotillon, 2017b). In addition, image interpretation and land cover assessments carried out by national experts were reviewed and revised during regular collaborative workshops in West Africa, to ensure consistent practice between country teams and USGS partners. Further details are provided by Samasse et al. (2018).

In this study, we regrouped the 25 land cover classes into 3 classes (rainfed and irrigated agriculture and non-agricultural) and used 50% of the 2 km by 2 km data points for year 2013 as reference information for training the classification algorithm, and the other 50% for assessing the classified product. Reduced data-density in some areas (e.g. on the coastal and desert margins) resulted in a total of 383,464 reference data points (non-crop, rain-fed and irrigated classes) across our West Africa study domain.

3.2.2. Google Earth Engine (GEE)

Google Earth Engine is a cloud-based platform for regional and planetary scale earth observation data retrieval and processing. Its advantage is to store the petabytes

of freely available data (e.g. Landsat imagery) in the cloud, avoiding the need for data download, while providing high-performance parallel computing resources to process large datasets (Gorelick et al., 2017). GEE thus facilitates computationally cumbersome geospatial analysis with minimal local computing and storage resources. GEE makes use of an application programming interface (API in JavaScript or Python), allowing for data processing and visualization at different scales. The GEE platform also implements several Machine Learning algorithms (Support Vector Machine, Random Forest) known to be effective for land cover and land use classification in general, and cropland mapping in particular (Azzari & Lobell, 2017; Johnson, 2019b; Mardani et al., 2019; Xiong et al., 2017).

3.2.2.1. Landsat 8 Surface Reflectance (SR)

The Landsat mission is a joint initiative of the USGS and NASA providing consistent earth observation data at sub-100 m spatial resolution since the 1970s. Surface reflectance data from the Landsat-8 OLI (Operational Land Imager) and TIRS (Thermal Infrared Sensor) is available in GEE from April 2013 to present. Table 1 contains information on the Landsat-8 SR Tier 1 collection spectral bands used in this study.

Table 3. 1. Landsat 8 band description and wavelengths. The 'pixel_qa' band provides metadata on scene quality such as cloud cover for each pixel.
Source : https://developers.google.com/earth-engine/datasets/catalog/LANDSAT_LC08_C01_T1_SR.

Name	Band description	Wavelength (μm)
B2	Band 2 (blue) surface reflectance	0.452-0.512
B3	Band 3 (green) surface reflectance	0.533-0.590
B4	Band 4 (red) surface reflectance	0.636-0.673
B5	Band 5 (near infrared) surface reflectance	0.851-0.879
B6	Band 6 (shortwave infrared 1) surface reflectance	1.566-1.651
B7	Band 7 (shortwave infrared 2) surface reflectance	2.107-2.294
pixel_qa	Pixel quality attributes generated from the CFMASK algorithm.	---

3.2.2.2 Vegetation indices

In addition to the individual band reflectances, remote sensing derived vegetation indices (VI) have been extensively applied to detect vegetation and monitor vegetation condition over large areas. These indices are generally based on the capability of vegetation to strongly reflect incident electromagnetic signal in the near-infrared (NIR) band compared to the optical bands. In this study we calculated four

vegetation indices as candidate predictor variables for the RF classification algorithm to help separate crop and non-crop zones.

NDVI

The Normalized Difference Vegetation Index (NDVI) is commonly used in satellite remote sensing-based vegetation analysis (Fensholt et al., 2009; Olsson et al., 2005; Thenkabail et al., 2009; Vintrou et al., 2012). It is computed using the red (B4) and near-infrared (B5) bands following equation (1).

$$NDVI = (B5 - B4) / (B5 + B4) \quad (1)$$

The NDVI can effectively detect growing vegetation (Tucker, 1979) but gets quickly saturated in high biomass surfaces. In such conditions, other vegetation indices like EVI (Enhanced Vegetation Index) have been proposed to replace or supplement the NDVI.

EVI

The Enhanced Vegetation Index (EVI), described by equation (2) provides improved sensitivity to vegetation condition and changes in high biomass areas as compared to the NDVI, and also reduces the background effect of soil on vegetation index calculation (A. Huete et al., 2002; Miura et al., 2001). In addition to the red and near-infrared bands, EVI includes in the calculation the blue band (B2) to correct atmospheric effects of aerosol.

$$EVI = G * ((B5 - B4) / (B5 + C1 * B4 - C2 * B2 + L)) \quad (2)$$

where G is a gain factor; C1, C2 are the coefficients of the aerosol resistance term, which uses blue band B2 to correct for aerosol influences in the red band B4, and L is the soil-adjustment factor as in SAVI. In this we used the coefficients adopted in the MODIS EVI algorithm, which are L=1, C1=6, C2=7.5, and G=2.5 (Jiang et al., 2008).

SAVI

The soil-adjusted vegetation index (SAVI; Huete, 1988) was developed to compensate for the effects of the soil background in sparsely vegetated areas. Equation (3) is the commonly used expression of SAVI with a soil adjustment factor L. This

factor is found to reduce soil noise using the value L= 0.5 for a wide range of vegetation classes (A. R. Huete, 1988).

$$SAVI= ((B5–B4) / (B5+ B4 + L))*(1+L) \quad (3)$$

MSAVI

The Modified Soil-Adjusted Vegetation Index (MSAVI; (Qi et al., 1994); Eq. 4) was proposed as an improved version of SAVI that minimizes the effect of bare soil (Qi et al., 1994).

$$MSAVI= (2 * B5 + 1 –sqrt ((2 * B5 + 1) ^2–8 * (B5 –B4))) / 2 \quad (4)$$

3.2.3. Random Forest (RF)

We used the random forest (RF) technique as the main classification algorithm in this study. The RF model is an ensemble learning algorithm that can be used to predict both continuous (regression) and categorical (classification) responses. For a classification problem, the response variable is a class which links certain independent values to one of the categories present in the dependent variable (Breiman, 2001). An RF model comprises an ensemble of decision trees, where each tree constitutes a classifier, which can predict the response-variable using a random sub-sample of the independent variables and observations. Each tree uses a sub-ensemble of training values chosen randomly with replacement (i.e. bootstrap sample). The optimum number of predictors used to split data at each tree's node is log(m+1), where m is the total number of predictors involved. An ensemble of diverse trees minimizes the effect of bias from individual trees considerably improving the overall predictive accuracy of the model. The final class prediction is chosen by a maximum vote (classification). It has been shown that by increasing the number of trees in the model, the errors of prediction (also known as out-of-bag errors or OOB errors) converge, reducing problems with overfitting (Breiman, 2001). In this study we used OOB error estimation during the training process to finetune RF model parameters and provide internal cross-validation before independent accuracy assessment.

3.2.4. Gridding and Accuracy metrics

A grid of 100 km by 100 km squares was created using ArcMap based on the extent of the available training data. In total 267 squares (labelled from S1 to S267 in

Figure 3.1) were generated covering the study area. For simplicity, Figure 3.1 shows the positions and labels of the first and last grid-squares. Satellite image (Landsat) data for each square was classified independently using the RLCM reference data to train and evaluate local RF models.

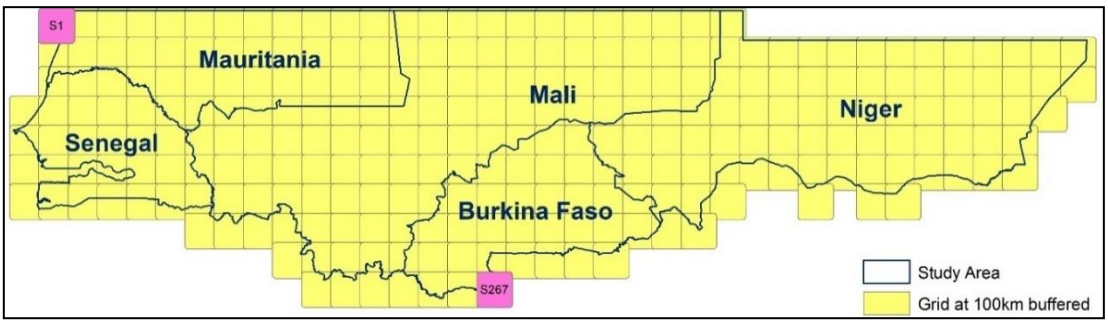

Figure 3. 1. The grid of 100 x 100 km cells.

Classification accuracy in this study was measured using the following metrics: Quantity disagreement (Q), Allocation disagreement (A), Overall Accuracy (OA) and class-specific measures such as User's Accuracy (UA) for Crop class, as suggested by Pontius & Millones (Pontius Jr & Millones, 2011). The new dataset was also validated using detailed local field surveys conducted on agricultural activities at IPR/IFRA, a higher education institution in Mali.

3.2.5. Workflow

Figure 3.2 illustrates the steps employed in developing the cropland extent map, using the GEE platform and Random Forest machine learning approach. Landsat-8 images for each 16-day period were processed for each ~1o grid cell. The Tier 1 Landsat-8 image collection was filtered spatially (Sahel grid level), and temporally (years 2013, 2014, and 2015, to match training data) before being filtered for clouds using the pixel_qa information (Table 1). Cloud-free images were used to compute vegetation indices in GEE using custom functions in JavaScript.

In total twenty bands were exported from GEE as candidate model predictors. Predictors included Landsat 8 surface reflectance bands (B2-B7) and VI averages for growing season (e.g. B2) and dry season (e.g. B2_1), with growing season defined from July-October of each year and November-June considered the dry season. In total, we have twelve (12) surface reflectance and eight (8) vegetation indices (Table 2).

Table 3. 2 Predictors used in the Random Forest classification.

	Wet period (growing period)	Dry period
Surface Reflectance	B2, B3, B4, B5, B6, B7	B2_1, B3_1, B4_1, B5_1, B6_1, B7_1,
Vegetation Indices	NDVI, EVI, SAVI, MSAVI	NDVI_1, EVI_1, SAVI_1, MSAVI_1

The land-cover training data were reclassified to produce three classes corresponding to rain-fed crops (level "1"), irrigated crops (level "2") and the non-crop class (level "0"), with levels 1 and 2 combined as needed to make up the "Crop" class. The training samples were derived by sampling 50% of "Crop" and 50% of "Non-crop" classes selected randomly within each grid cell, representing a stratified random sampling approach. R software was used to fit the RF classifiers external to GEE to benefit from greater model-fitting flexibility in R. Optimal fitted RF models were then used for regional predictions. Predictions of crop (rainfed and irrigated) and non-crop classes were based on the best-fit models and optimal parameters from the tuning process. Classification outputs were initially assessed at grid-cell level using independent reference samples (i.e., samples not used for training and/or OOB error estimation), then grouped at country and regional levels.

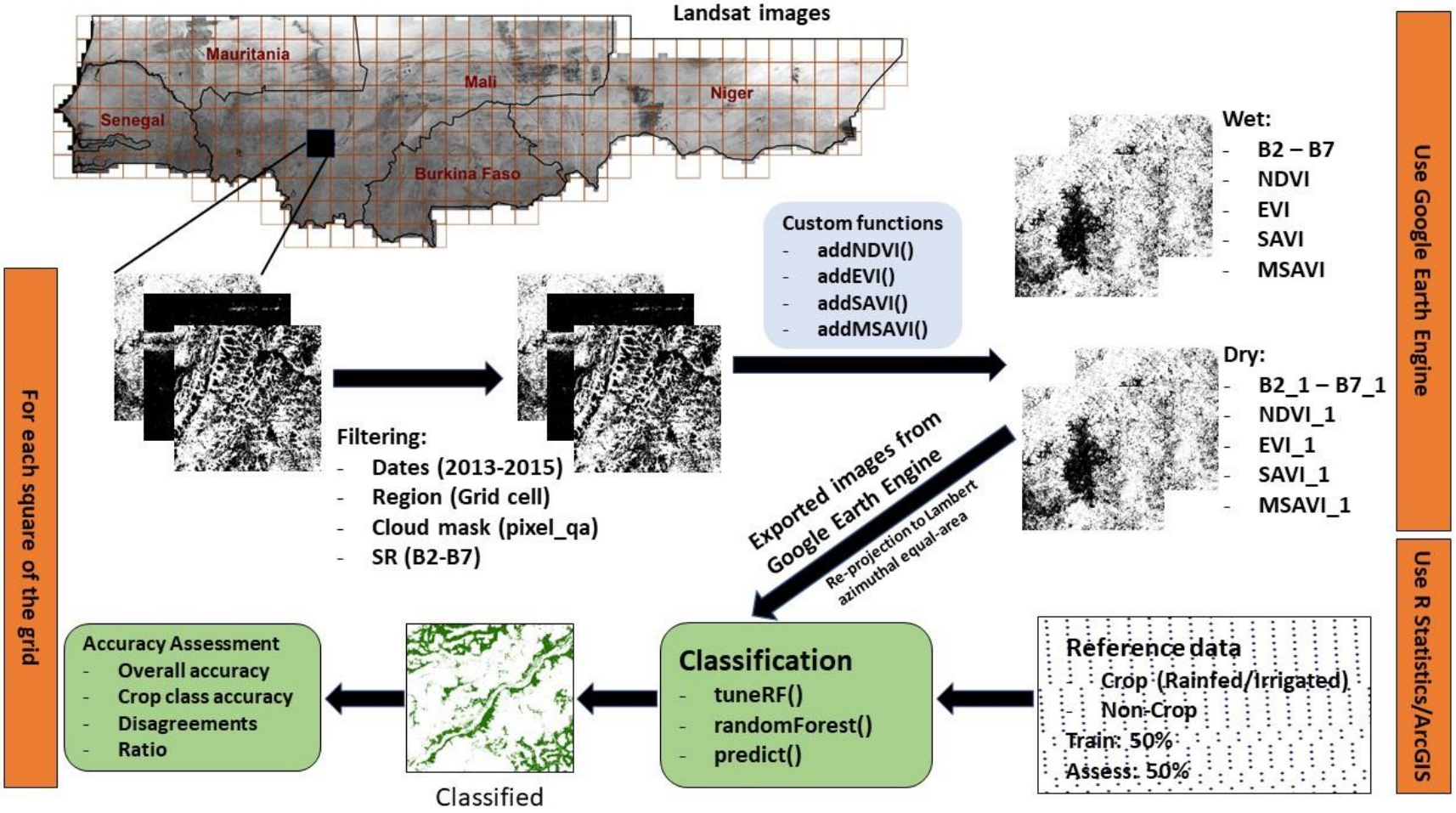

Figure 3. 2 Workflow describing major steps of the cropland dataset development.

3.3. Results

3.3.1. Predictors

The Landsat-8 Tier 1 image collection available on GEE for the study area comprised of 6,803 image scenes as filtered for years 2013, 2014, and 2015. Depending on the location and the time, the number of available images changes due, for example, to the degree of cloud coverage in different years and locations. Figure 3.3 shows that the availability of Landsat images increases in 2014 and 2015, relative to 2013, with the increase related to launch and partial Landsat-8 collection in 2013.

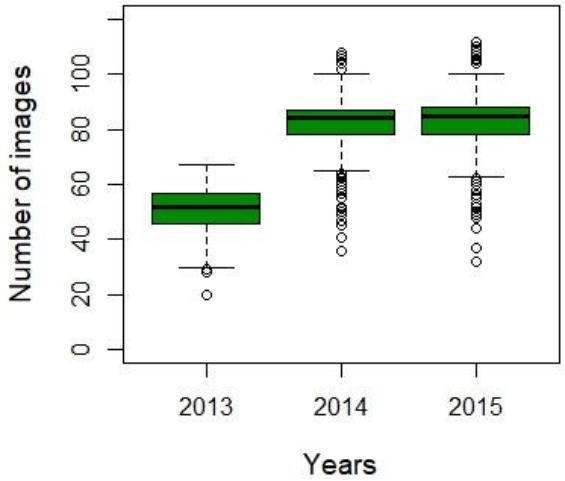

Figure 3. 3. Number of Landsat images per year summarized across West African grid cells, and then processed in GEE for this study. Average number of images represented by thick horizontal black line, standard deviation by green box, 95th percentile by thin horizontal lines, with outliers represented by circles.

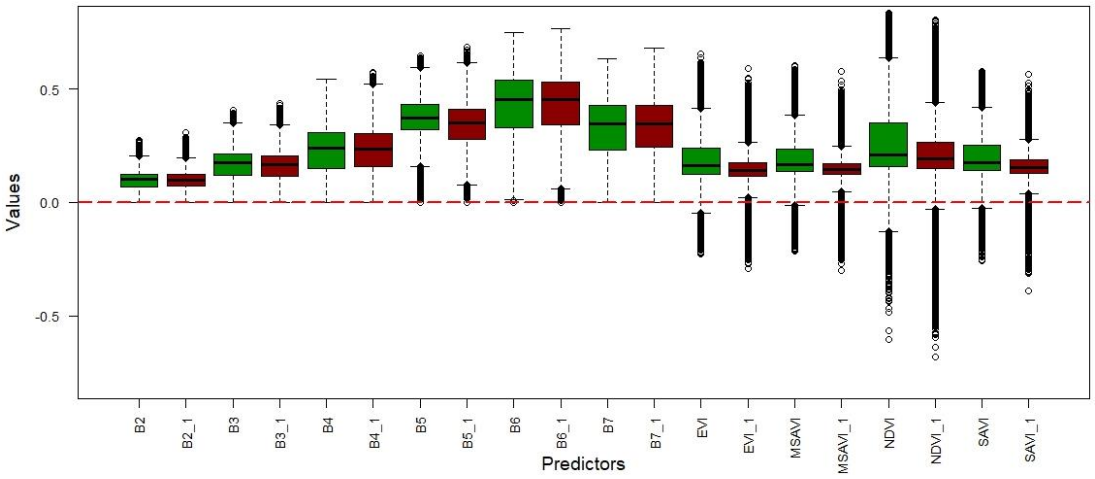

Figure 3. 4. Predictor variables used to train the Random Forest models, showing wet-season averages (green) and dry-season averages (red) for Landsat surface reflectance (SR; bands 2-7) and vegetation index band combinations, averaged across the West African domain (Fig. 5). Mean, standard deviation, percentiles and outliers are as noted for Figure 3.3.

The candidate predictor variables are shown in Figure 3.4. Values of surface reflectance (SR) in Landsat bands are between 0 and 1, while vegetation index (VI) values range between -1 and 1, as expected. On average, the shortwave infrared 1 band

(B6) has the highest reflectance value in both wet and dry periods, probably due to minimal atmospheric attenuation in this part of the electromagnetic spectrum and low surface vegetation moisture on average in the savanna areas which would otherwise lower SWIR reflectance. The second highest value occurs at the near infrared band (B5). This band also shows the most pronounced difference between wet and dry means, showing its sensitivity to green vegetation that is mostly present in the wet seasons. All the vegetation indices (Figure 3.4) show net distinctions between the wet and dry periods, particularly in the range of wet season values.

3.3.2. Reclassified training data

Absence of cropland in the training data examined for some grid squares prevented fitting meaningful local models in these regions. These grid squares are therefore assumed to have little or no agriculture (Fig. 5). Some cells, particularly in the northern drylands lacked any training data (RF algorithm requires >1 class in the training data). In total, 189 cells (~71% of the study domain) include some amount of cropland. The other 78 cells (white cells in Fig. 5) are mainly located in the Northern Sahel and Sahara, where agricultural activities are absent (or occur only intermittently). On average, 2,028 reference data on presence of rainfed and irrigated cropland and non-cropland were available in each of the 189 retained grid cells (~1014 for model training and ~1014 for error assessment).

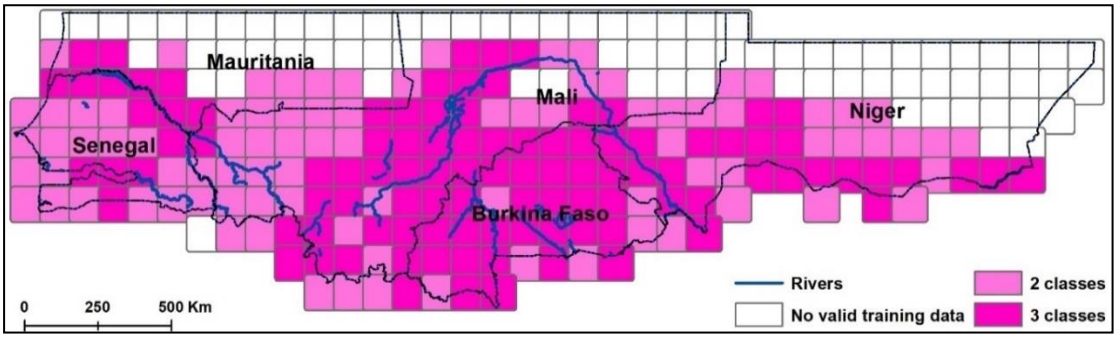

Figure 3. 5. Cells with valid training data (i.e. containing two or more classes (crop and non-crop) after reclassification of the training grid points). 189 cells among the 267 include some cropland in the training data allowing us to run the RF algorithm. 3-classes occur only in those regions with irrigated cropland, mostly associated with the major rivers in the region.

3.3.3. Accuracy at grid level

Results show an average overall accuracy (OA) above 80%, with most 100 km squares having an OA in the range of 75% to 100% (Table 3). Despite the relatively high OA, the reliability of classified product is best measured in terms of the users' accuracy, which quantifies accuracy from the perspective of the user of the classified product. In total, 11% of assessed cells had a user's accuracy less than 50%, 58% were between 50% and 75%, and the remaining 31% has a user's accuracy above 75% (Table 3). On average, accuracy at grid level is 78.8% and 56.6% for OA and UA, respectively. The Supplemental Information (A2) of this document gives further details on grid level assessment.

Table 3. 3. Summary of Overall accuracy and Crop class User's accuracy at grid level.

Overall accuracy				
	No data	0 - 50	50 – 75	75 - 100
Number of cells	99	0	36	132
Average OA	-	-	70.59	87.07
User's accuracy				
Number of cells	99	18	98	52
Average UA	-	22.73	64.10	82.95

3.3.4. Accuracy at country level

Assessment at country-scales indicates that the overall accuracy is around 90% for all the countries, except in Burkina Faso where it is slightly lower at ~77% (Figure 3.6). The country of Mauritania has the highest overall accuracy of 99% but the accuracy to reliably identify crop class from the user's perspective in Mauritania is only about 71%, which is the lowest among the five countries.

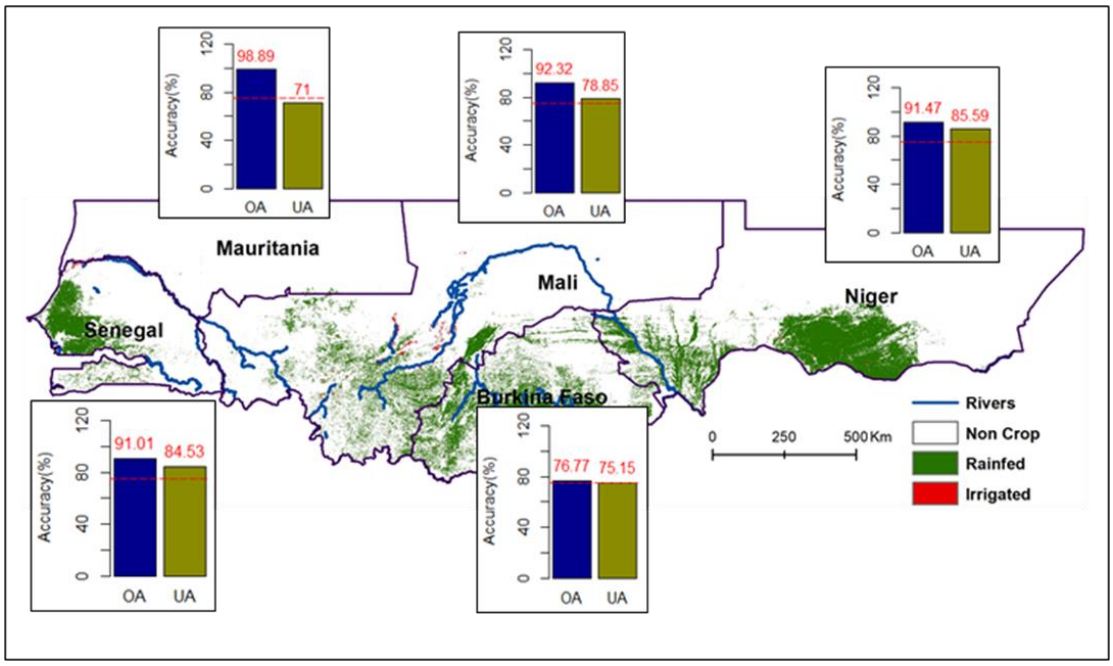

Figure 3. 6. Overall accuracy and User's accuracy by country.

Assuming 75% as targeted value for crop user's accuracy, Mauritania is the only country where the classification performance fails to meet expectation. Highest accuracies occurred in Niger, with 85.6% accuracy, followed by Senegal with 84.5%. Crop user's accuracy in Mali and Burkina Faso is between 75% and 80%.

In terms of crop areas estimation, results show that rainfed agriculture is far more common than irrigated agriculture in the 5 countries, with irrigated cropland occupying only ~2% of the total (Figure 3.7). Cropland area is greatest in Niger (with 119x103 km2 of cropland, representing 37.6% of the total agricultural area in the five Sahelian countries), followed by Burkina Faso (91x103 km2; 28.8%), Mali (67x103 km2; 21.3%), Senegal (38x103 km2; 12.1%), and finally Mauritania (0.6x103 km2; 0.21%) where agriculture is confined to the south of the country and Senegal River Valley (Table 4 and Figure 3.7).

Table 3. 4. Estimated area classified as cropland in each of five Sahelian countries.

	Burkina Faso	Mali	Mauritania	Niger	Senegal	Total
Rainfed crop (km²)	90,799	62,513	372	118,022	37,434	309,139
Irrigated crop (km²)	203	4,615	291	820	758	6,688
Total	91,002	67,128	664	118,841	38,192	315,827

Expressed as fraction of the total irrigated area in the five countries, more than the half of the total irrigated areas are in Mali (69.0%), particularly in the “Office du Niger” region, which is one of the oldest and largest irrigation schemes in West Africa (Zwart & Leclert, 2010). The country of Mauritania, with less than 1% in rainfed agriculture area, has a larger share (4.4%) of the irrigated cropland in the region, more for example than in Burkina Faso with only 3.4% of irrigated cropland (Table 4 and Figure 3.7).

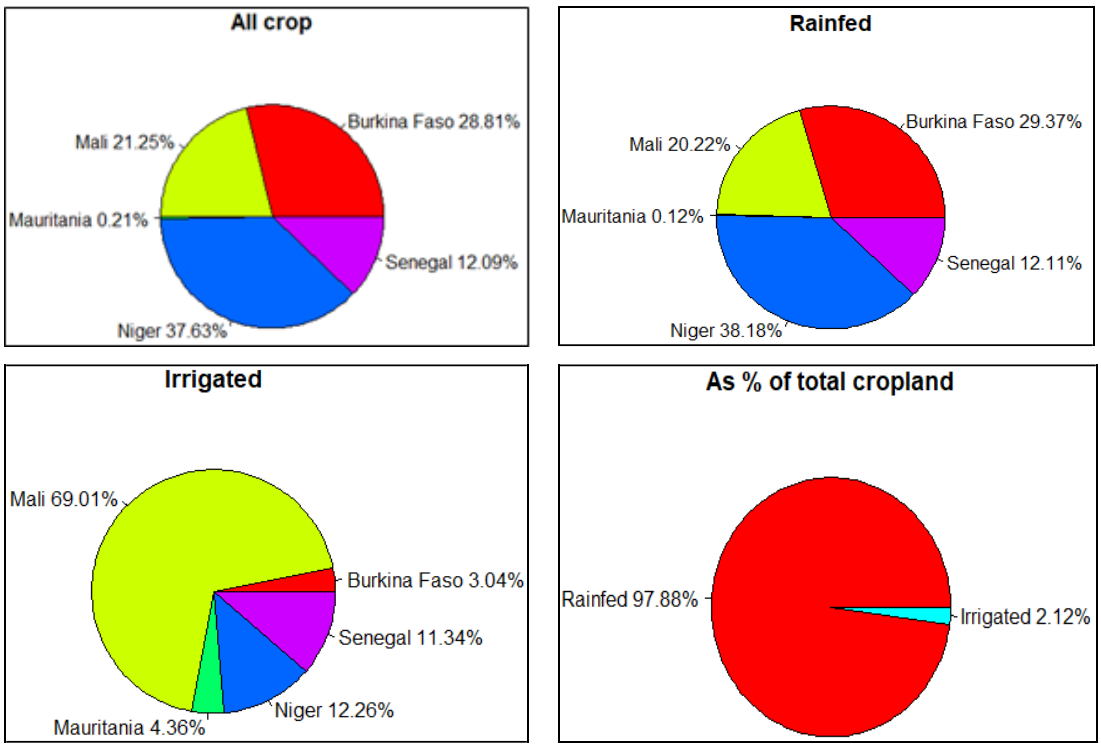

Figure 3. 7. The relative importance (%) of the five Sahelian countries in cropland area across West Africa, showing total cropland area, rainfed and irrigated croplands, and the comparison of rainfed and irrigated cropland area as a fraction of the total.

3.4. Discussion

The 30 m West African Sahel Cropland map (WASC30) covers five Sahelian countries of West Africa and shows in much improved detail than previously available the agricultural zones of West Africa, including the 'breadbasket' regions of Niger, Mali, Burkina Faso and Senegal that are critical to the food security and economies at national and regional scales. We leveraged a distributed and dense sample dataset on actual land cover (Tappan et al., 2016), with Landsat-8 data, to train locally-optimized machine-learning predictors for rainfed and irrigated agriculture using the Google Earth Engine (GEE) platform. Earlier cropland products, covering the Sahelian region,

generally combine irrigated and rainfed agriculture into a single cropland class, with accuracies generally less than 70% (Samasse et al., 2018). The average user's accuracy of the new crop extent map, considering the five countries of Burkina Faso, Mali, Mauritania, Niger, and Senegal (Figure 3.6), is 79%, which is a considerable improvement relative to the best performing earlier products (GlobeLand30, 69% and GFSAD30, 64%; (Samasse et al., 2018)). Our accuracy statistic is also influenced by low accuracy in Mauritania, representing less than 1% of cropland area in the region (Figure 3.7). The user's accuracy for Senegal, Mali, Burkina Faso and Niger (excluding Mauritania) is 81% for the new WASC30 cropland area map. The low accuracy reported for Mauritania is consistent with our previous findings in a study comparing accuracy of cropland classes in 12 pre-existing landcover products (Samasse et al., 2018). Explanations for this include the particularly small size of farms and the low intensity of agricultural activities in this country. However, it must be noted that, despite having lower accuracy compared to other countries, the cropland estimates for Mauritania in our new WASC30 map is an improvement on the pre-existing products.

3.4.1. Irrigated cropland

Based on the estimated crop areas (Table 4), irrigated land represents just 2% of the total cropland area. Thus, a specific accuracy is not reported for this sub-class of "Crop". However, Figure 3.8 shows clearly the intensive irrigation activities in Senegal and Mauritania adjacent to the Senegal River, in Mali in the "Office du Niger" zone, and in Niger adjacent to the Niger River. Irrigated cropland in the region are generally supported by hydroelectric dams on the major rivers (e.g. Niger, Senegal), providing both electricity and increased agricultural production. For example, the Diama dam in Senegal and the Markala dam in Mali are two operational hydroelectric infrastructures promoting intensive irrigated crops production in the Senegal valley and the Office du Niger zone in Mali, respectively (van der Wijngaart et al., 2019; Woodhouse & Ganho, 2011). In Mauritania, 44% of the 664 km2 mapped as cropland is irrigated.

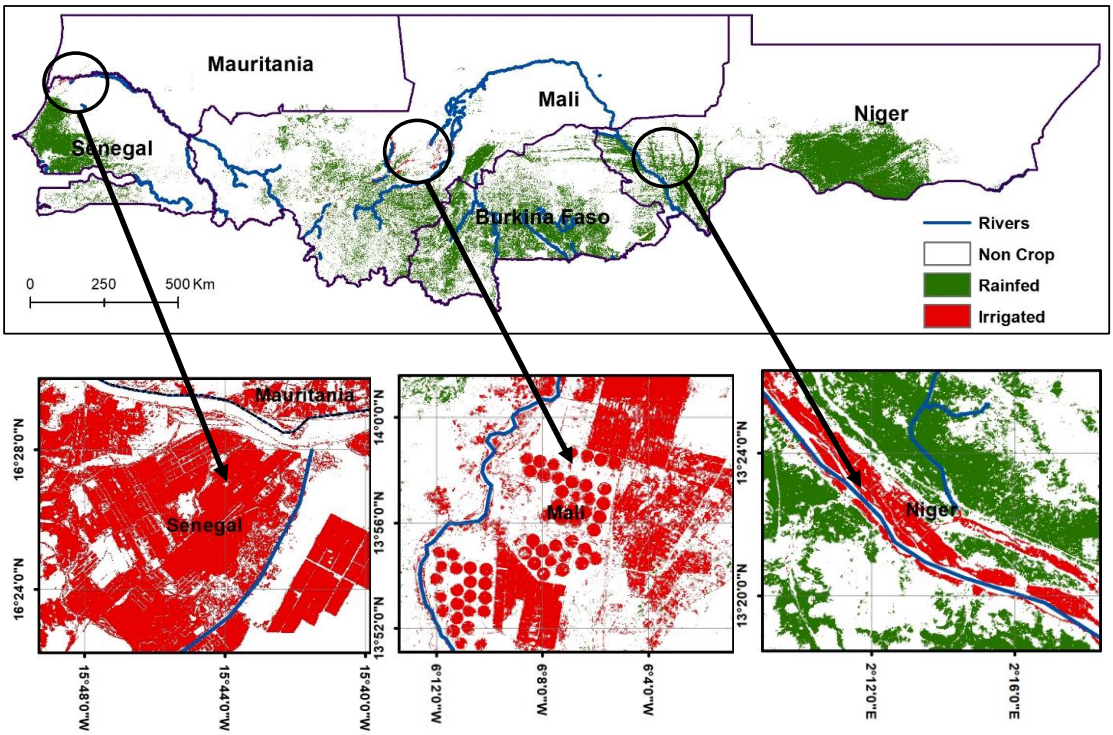

Figure 3. 8. Irrigated cropland adjacent to the Senegal River in South Mauritania and North Senegal, in the Niger River floodplain of Central Mali (with center-pivot irrigation techniques), and adjacent to the Niger River, near Niamey. Rivers are extracted from Hydrological data and maps based on SHuttle Elevation Derivatives at multiple Scales (HydroSHEDS). Extracted areas are 12 x 12 km.

3.4.2. Intensive Rainfed cropland zones

Analysis of the more dominant rainfed cultivated areas shows several "hot spots" of intensive agricultural activities (Figure 3.9). For example, the Seno Plain (red circle), east of the Dogon Plateau in Mali, has been devoted to intensive agricultural activities since the 1930s (Thibaud, 2005). Recent studies using Earth Observation data have reported cropland expansion in this region driven by the need to feed a rapidly increasing population with accelerated expansion between 2000 and 2013 facilitated by modern technology (CILSS, 2016). Rapid population growth and conducive soils, with development of processing infrastructure have also contributed to the high density of rainfed cropland in south-eastern Niger (blue circle). This area, known as the Tarka Plain and Goulbi Agricultural Zone, in the Maradi-Zinder region of Niger is considered to be the most important agricultural zone of Niger (CILSS, 2016). It is an area of enormous agricultural potential, mainly in rainfed cropland (Issoufou et al., 2012). Cereal (Millet, Maize, Sorghum and Rice) cultivation is practiced, with more advanced systems in the Tarka plain, where the rural population density is particularly high. Because of the anthropogenic pressure, it is common to see an integrated system where

agriculture, livestock and forests share the same space (RNCA-NIGER, 2019). Similarly, the West-Central Agricultural Zone in Senegal (black circle), known as the Peanut Basin (Bassin Arachidier) for the suitability of dominant soils to grow peanut, is also characterized by high rural populations, with rainfed agriculture focused on cultivation of peanut, millet, sorghum and beans (FALL, 2009).

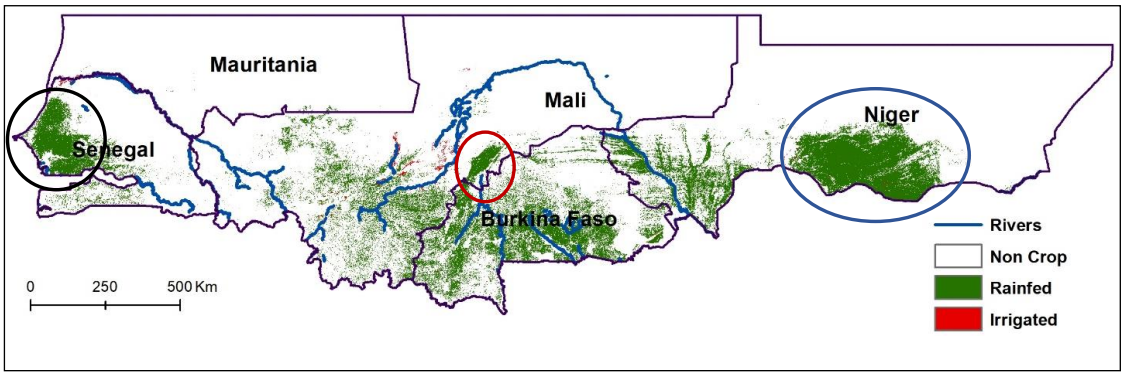

Figure 3. 9. The West African Sahel cropland map (WASC30) with hot spot of intensive rainfed cropland in Senegal, Mali and Niger.

3.4.3. Cropland distribution relative to climate and climate zones

For the purpose of this work, we divided the study area based on the annual precipitation, following a steep gradient of decreasing rainfall from south to north. Figures 3.10 and 11 show the distribution of both rainfed and irrigated cropland as located in the West African Sahel Cropland map (WASC30) under 100 mm rainfall bins. Mean Annual Precipitation (MAP) is derived from eleven years (2005-2015) of CHIRPS (Climate Hazards Group InfraRed Precipitation with Station) data retrieved from Google Earth Engine. Results show that rainfed cropland area generally increases with MAP between 200 mm and 1000 mm MAP, reflecting water limitations to agricultural activities in the arid zones (200-400 mm) and more suitable conditions in the South Sahel and Soudan (400-1000 mm). Above 1000 mm MAP, rainfed cropland proportion declines (Figure 3.11), in part due to shift to forest production and in part since wetter forested zones may have soils unsuitable for agriculture. However, irrigated cropland area is largely decoupled from MAP, being clustered around the flood plains of the perennial rivers in West Africa.

The Saharan desert region (MAP < 200 mm/y; Figure 3.10) constitutes about 61% of the total study area (Table 5). Significant part of northern Mauritania, Mali, and Niger fall in this region. It is generally characterized by an arid climate with high average temperatures, a very low relative humidity and rare and highly irregular

precipitation, making difficult for crop to grow. However, irrigated farming may be present in some areas using appropriate irrigation technologies (Bouzidi, 2011; Hamidat et al., 2003), mainly for small scale production of vegetables. Figure 3.11 shows our results illustrating the very low to non-existent agricultural activities in the Sahara.

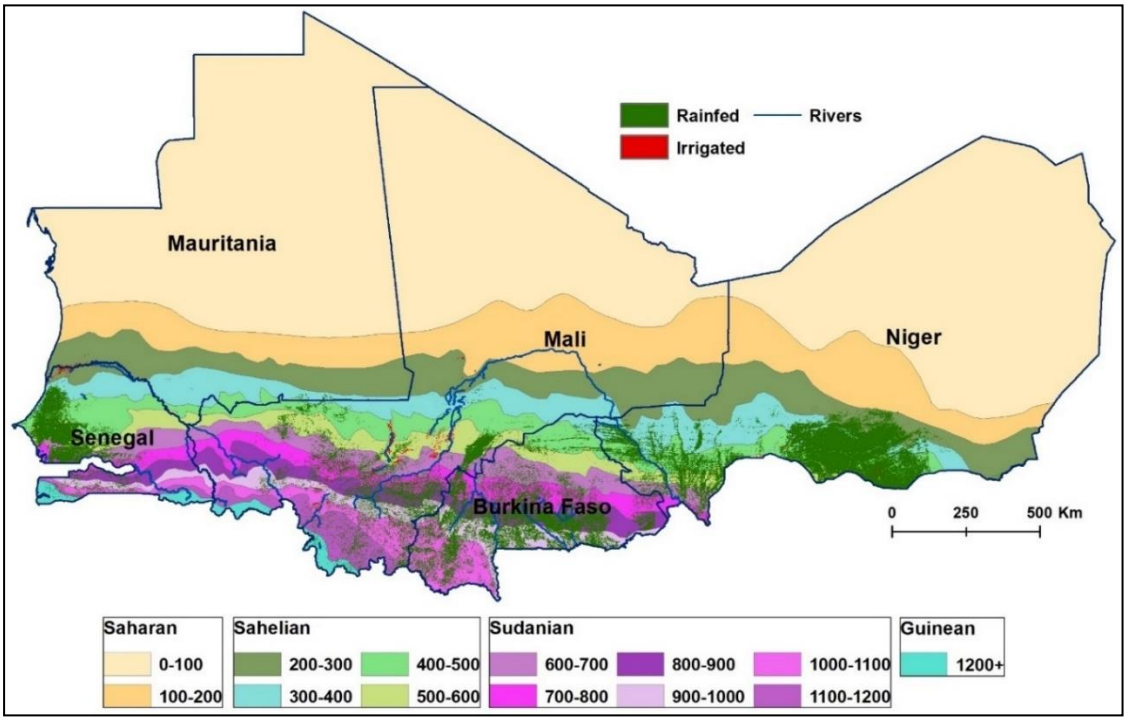

Figure 3. 10. Cropland extent across gradient of mean annual precipitation. Precipitation is an average of 11 years (2005 – 2015) CHIRPS data.

The second largest zone is the Sahelian (200-600 mm), occupying 23% of the total study area. Rainfed cropland intensity increases with annual rainfall (Figure 3.11). Compared to the other climatic zones, the Sahel has the highest proportion of irrigated cropland, as irrigation activities along both Niger and Senegal rivers occur mainly in this climatic zone (Figure 3.10). This irrigation proportion is however, less than 1% against about 15% for rainfed agriculture (Table 5).

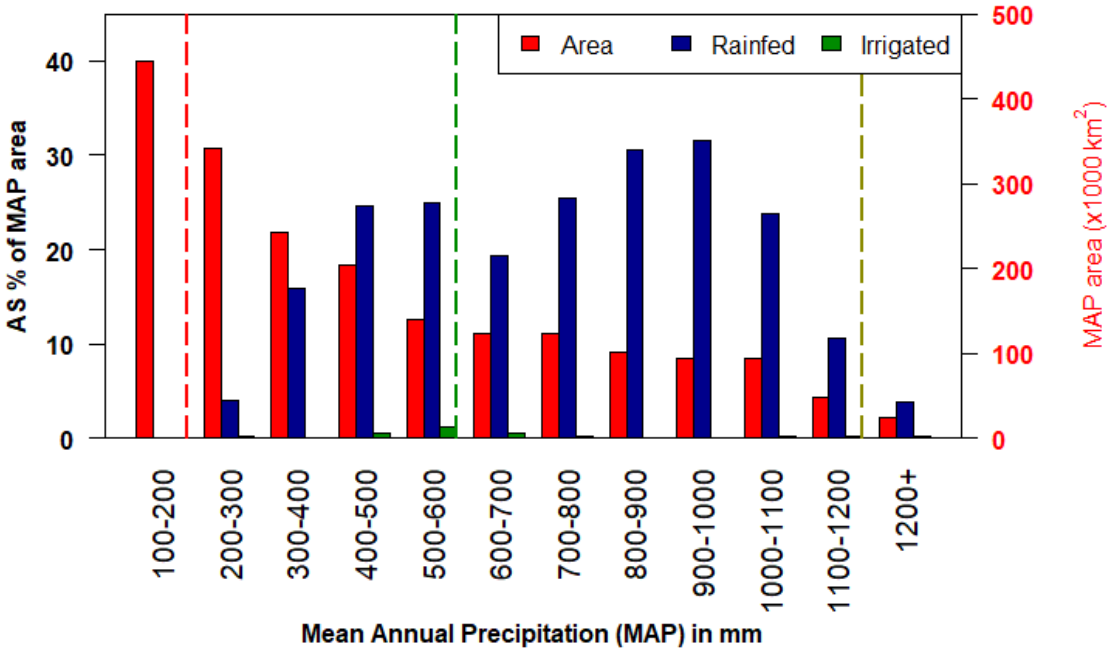

Figure 3. 11. Rainfed and irrigated cropland as percentage of the total area in MAE interval (e.g. The total area of 800-900 mm zone is about 100x103 km2, and the fraction of this area occupied by rainfed cropland is about 30%).

Among the four climatic zones (Figure 3.10), rainfed agriculture activities are most intensive in the Sudanian zone (600 mm – 1200 mm). Representing 15% of the study area, the Sudanian is the third largest climatic zone, after the Sahara and the Sahel. About 24% of this climatic zone is occupied by rainfed cropland (Table 3.5). It covers major cereal production zones in Mali and Burkina Faso, and southern parts of the Peanut Basin in Senegal (Figure 3.10). The precipitation range is also suitable for cash crops (e.g. cotton), root crop and mixed cereal-root system (e.g. Cassava, Yam, Sweet potato, particularly in Southern Mali). Irrigation is not common in the Sudanian zone, largely due to the low occurrence of main rivers in the region.

At more than 1200 mm MAP, the Guinean zone covers little of the total area of the study domain (less than 1%). In this region, some 4% is occupied by rainfed cropland, dominated by root crop cultivation (yams, sweet potatoes, cassava) (SIDIBE, 2007).

Table 3. 5. Proportion of area and cropland by climatic zones in our study domain including Senegal, Mauritania, Mali, Burkina Faso and Niger.

	Saharan	Sahelian	Sudanian	Guinean
% Area	61.02	23.50	14.85	0.63
% Rainfed	0.00	14.79	24.54	3.78
% Irrigated	0.01	0.48	0.26	0.17
% All Cropland	0.01	15.27	24.80	3.95

3.4.4. Fallows in WASC30

The visual interpretation approach adopted for the 2 km RLCM dataset (Cotillon & Mathis, 2017; Tappan et al., 2016), and used as training or reference information in this study, classified large and long-term fallows as savanna. However, in the more intensive rainfed cropland regions with reduced fallow periods, small areas of fallow were generally classified as active agricultural land use. Overall, therefore, we consider that the WASC30 represents active agriculture, inclusive of short-term fallow fields, but exclusive of longer-term fallow (or abandoned) areas that have not been actively cropped in recent years. That makes the final cropland class a reliable reference for developing active cropland extent.

3.4.5. Validation using local scale data

At local scale, our new cropland dataset has been assessed using recent (2012) GPS field surveys mapping land use and land cover at an Agricultural College (IPR/IFRA) in the town of Koulikoro, just north of Bamako. Data was collected in collaboration with Laval University (Quebec, Canada) as part of the PACM research project (Des arbres et des champs contre la pauvreté au Mali). IPR/IFRA is a higher education institution in Mali managing an area of about 380 ha, including experimental farms and other lands for cereals and tree crops production. Figure 3.12 shows that the WASC30 captures the distribution of cultivated areas at IPR/IFRA with an area ratio of 195 ha / 199 ha = 98% (i.e. the WASC30 product underestimates cropland area at this field station by 2%). This slight difference could be attributed to the small size of some sparse experimental plots making difficult their detection in the 30 m Landsat data. No irrigated pixels detected at IPR/IFRA which is consistent with the absence of irrigation trials at the site.

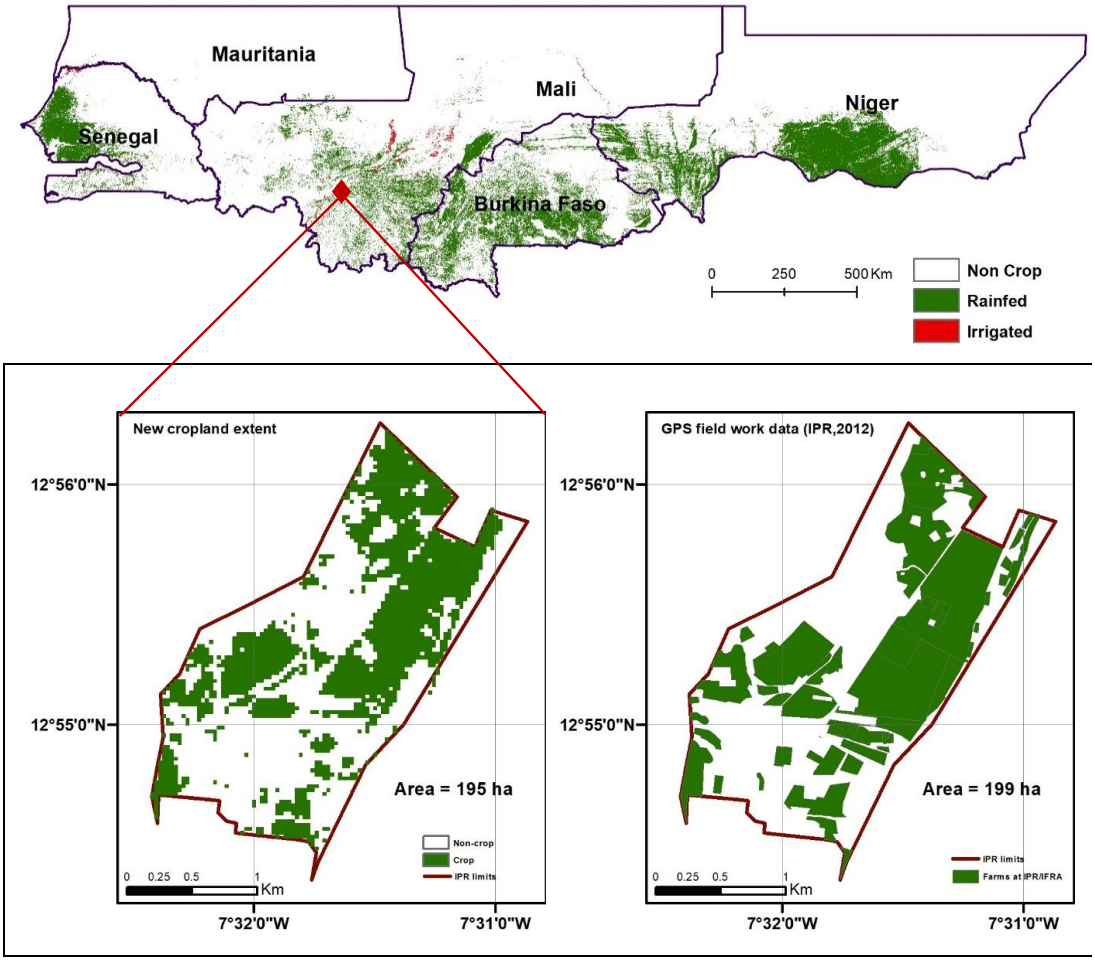

Figure 3. 12. Assessment of the new cropland map (WASC30) using field surveys at IPR/IFRA field station in Mali.

3.5. Conclusions

In this study, the Random Forest ensemble learning method has been applied to individual 100 km grid cells to develop a 30 m Landsat-derived active cropland dataset across five Sahelian countries with unprecedented details and higher accuracy as compared to existing land cover products. The developed dataset has an overall accuracy of 90.1% and a cropland class (rainfed and irrigated) user's accuracy of 79%.

Information derived from the new dataset reveals the total cropland area in West African Sahel to be 316x103 km2 with 7x103 km2 irrigated and 309x103 km2 rainfed. This confirms that agriculture in Sahelian West Africa is almost entirely rainfed. The Sudanian zone (600 mm - 1200 mm) comprises most of the rainfed cultivated areas, while the Sahelian areas in proximity to main rivers presents the highest proportion of irrigated land. Results also show that these irrigation activities in the region remain not well developed, comprising only about 2% of the total cropland area, despite the tremendous potential offered by, for example, the Senegal and Niger rivers. This may

be due to the lack of well-developed infrastructure for irrigation, and high investment costs to manage water and make it available where it is most needed. More efforts in developing irrigated land in Sahel region would expand farmers' production opportunities by reducing risks linked to climate fluctuations.

This study benefitted from the large and regularly distributed RLCM training dataset that allowed us to fit locally optimized random forest models in each of 189 grid cells (each 100 x 100 km) across the five-country study domain. This allowed us to minimize the effects of soil, topographic and climatic differences that would increase errors in models fit at coarser regional and continental scales, thus improving overall accuracy of the final WASC30 product.

Geospatial data in general, and Landsat time series in particular, provide a critical source of information for the important task of producing accurate statistics on cultivated areas, particularly in developing countries where timely accurate georeferenced agricultural data are sometimes missing. The new cropland dataset will contribute to filling this void in West Africa Sahel.

Acknowledgments: K.S. was supported by the United States Agency for International Development (USAID) via funding to the Michigan State University Borlaug Higher Education for Agricultural Research and Development (BHEARD) Graduate Research Fellowship Program. N.P.H. and J.A. were supported, in part, by the NASA SERVIR West Africa Program (Grant # NNX16AN30G). Our particular thanks to Dr. Gray Tappan and colleagues at USGS EROS Data Center who made available the West African Land Cover time series database (https://pubs.er.usgs.gov/publication/fs20173004) that was invaluable as training and validation for this analysis. This material is based upon work supported by the United States Agency for International Development, as part of the Feed the Future initiative, under the CGIAR Fund, award number BFS-G-11-00002, and the predecessor fund the Food Security and Crisis Mitigation II grant, award number EEM-G-00-04-00013.

Appendix 3.A

3.A1. Tuning RF major parameters

Separate RF models were developed for each of the 189 cropland cells. Correlated predictors were removed following the example illustrated by Figure 3.A.4

before fitting models and tuned using the "tuneRF" function in R software. This tuning function helps determine the best number of variables available for splitting at each tree node (mTry) for a number of trees (nTree) based on the minimum values of the Out-Of-Bag (OOB) errors. The chosen values of nTree to run "tuneRF" included 500, 1000, 1500 and 2000. Occurrences of nTree corresponding to the optimal mTry are reported in Figure 3.A.1 (A). It appears that RF models (classifiers) show better performance in 44% of the cells for nTree = 500, and 15% of the cells for nTree = 2000. Between these two limits, 24% and 17% of the cells have shown minimal errors of OOB at nTree = 1000 and nTree = 1500, respectively. Frequency distribution of resulting optimum mTry values from the tuning process is shown on Figure 3.A.1 (B). Numbers 2, 1, 4, 8, 16, and 3 have been used as mTry values to fit the best models for the classification.

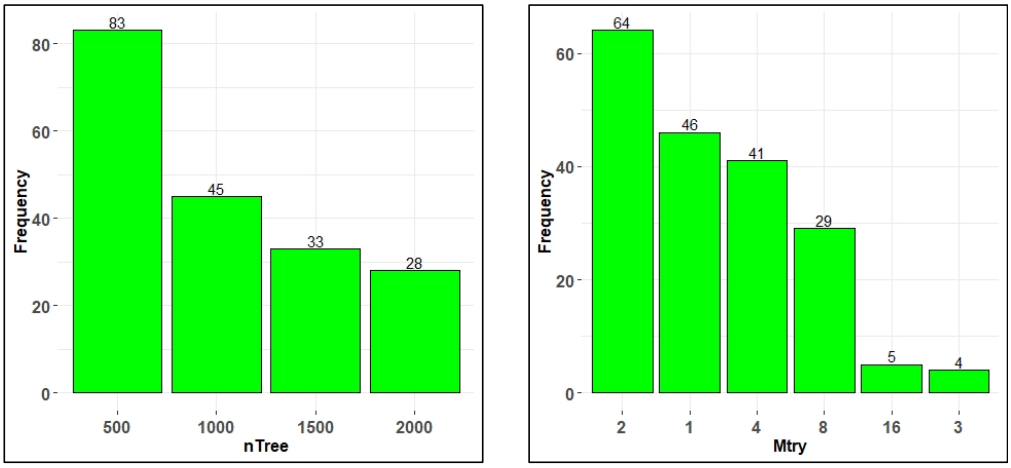

(A) (B)

Figure 3.A. 1 Occurrences of the number of tree (nTree) corresponding to minimum out-of-bag errors (A), and the obtained number of variables available for splitting at each tree node, mTry (B).

The Random Forest (RF) is widely accepted as an efficient ensemble approach for land cover classification using remotely sensed data. It handles well imbalanced data, missing values, and outliers (Pal, 2005). However, tuning RF two major parameters (number of trees: nTree, number of variables available for splitting at each tree node: mTry) to get optimum values may be time and resources consuming, even in parallel processing environments like Google Earth Engine. In this study, we selected nTree in {500, 1000, 1500, 2000} for reduced computational time while ensuring sufficient trees for model convergence (Breiman, 2001). The best mTry for most of the grid cells has been achieved with nTree = 500, others for nTree = 2000, which are the limits of tuned nTree values (Figure 3.A.1(A)). Using a larger range of nTree values

(e.g. including values below 500 and above 2000) could probably result in better mTry, yielding higher classification performance for the final cropland product.

3.A2. Accuracy at grid level

Results on the accuracy assessment are not showing all the 189 trained and classified squares (100 km by 100 km grid unit). Twenty-one (21) of them have been entirely classified as Non-crop. They are considered as NoData for the assessment. The general trend appearing on Figure 3.A.2 is that in average classified squares have an overall accuracy above 80%. For most squares, overall accuracy falls in the range of 75% to 100%. The country of Burkina Faso has the maximum of units with overall accuracy within 50% - 75%, and none in the grid has been classified with a proportion correct less than 50%. This relatively high overall accuracy is contrasted by the crop class specific accuracy. Figure 3.A.3 gives insight into the "Crop" class user's accuracy at grid level. In total, 11% of assessed cells has a user's accuracy less than 50%, 58% of them has theirs between 50% and 75%, and the remaining 31% has a user's accuracy above 75% (Table 3).

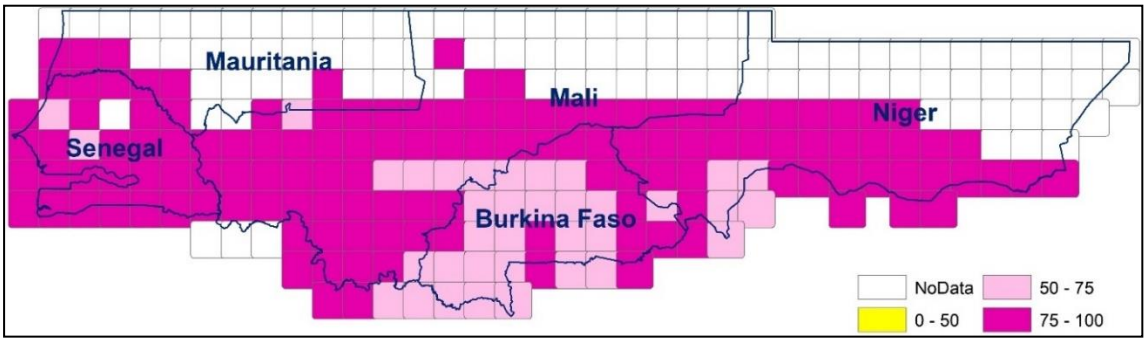

Figure 3.A. 2. Overall accuracy (OA) at grid level.

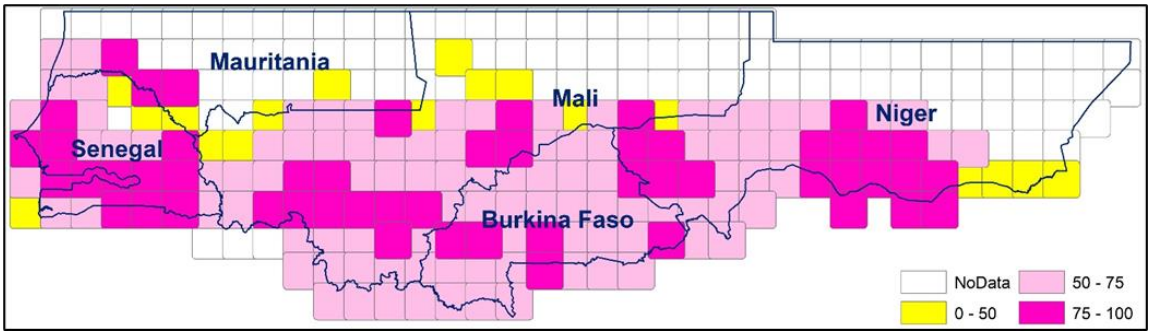

Figure 3.A. 3. Crop User's accuracy at grid level.

3.A3. Correlated variables / predictors

An example of removal of highly correlated variables, based on a correlation coefficient > 0.99 is shown in Fig. A4. In these cases, we anticipate no additional useful explanatory information is available by including both variables. Predictor EVI is

similar to SAVI and MSAVI, thus only MSAVI was maintained to develop the model by the algorithm. Similarly, predictors EVI_1 and SAVI_1 bring the same information as MSAVI_1, they can then be removed, reducing computational time in classifying this grid cell. Since RF is generally robust to correlation correlations <0.99 were permitted.

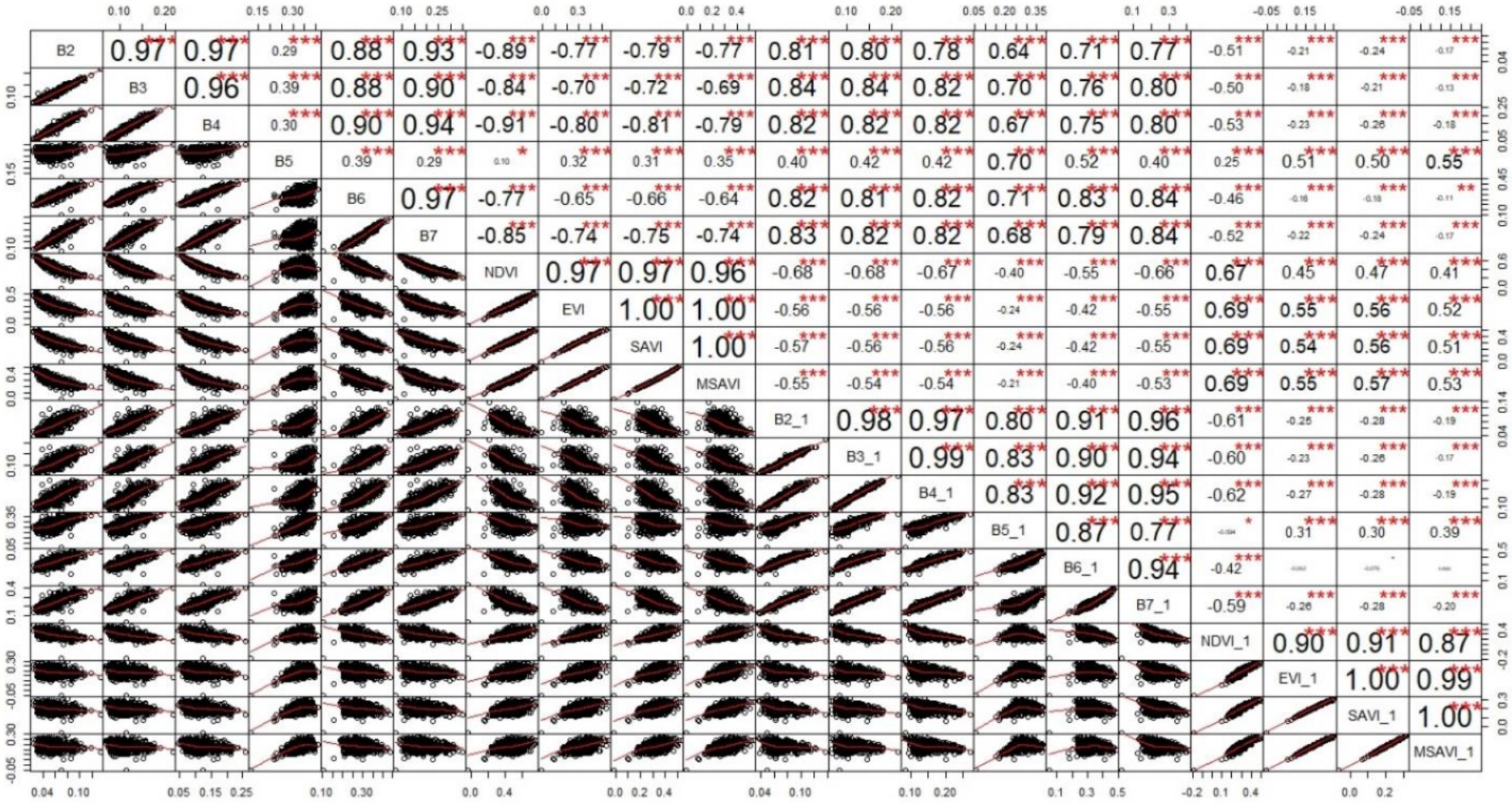

Figure 3.A. 4. Correlated variables.

3.A4. Disagreements analysis

Error of classification, expressed as total disagreement, can be divided into two components which are the quantity disagreement and allocation disagreement (Pontius Jr & Millones, 2011). Quantity disagreement can be interpreted as the differences in the areas allocated to the classes in the reference data and the classified map, and allocation disagreement is related to the misallocation of classified pixels for the same level of quantity agreement (Richards & Jia, 1999). The overall accuracy is the complement of the total disagreement (100% - total disagreement). Figure 3.A.5 illustrates results of the developed cropland map considering these two categories of disagreement at country level. Overall, the highest total disagreement is less than 25%. That means for the 5 countries, overall accuracy is greater than 75%. It also appears that quantity disagreement is more important in Mali, Mauritania, and Niger. Thus, this measure is the major contributor to the map's total disagreement in these countries. The opposite is true for Burkina Faso and Senegal where spatial mismatch of pixels dominates the disagreement. Considering 10% as threshold of disagreement significance, Burkina Faso is the only country exceeding this level.

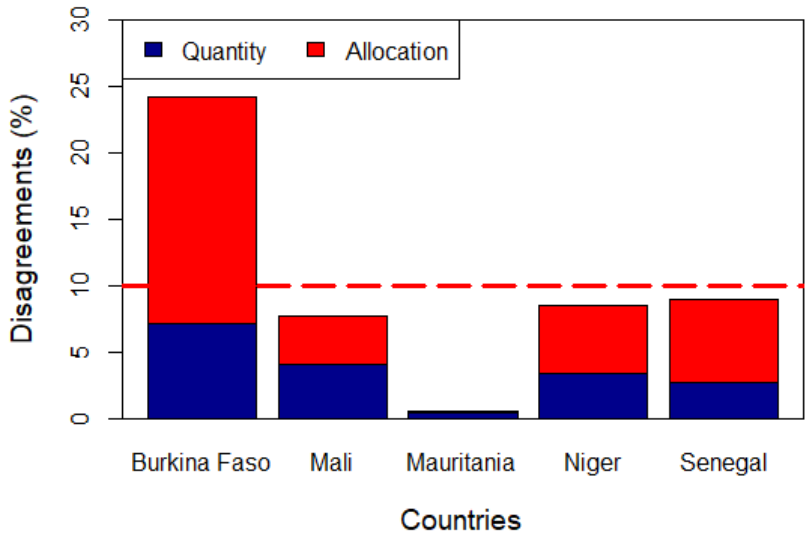

Figure 3.A. 5. Quantity disagreement (quantity = how much cropland) and Allocation disagreement (allocation = where the cropland is) by country

3.6. References

Arino, O., Bicheron, P., Achard, F., Latham, J., Witt, R., & Weber, J.-L. (2008). The most detailed portrait of Earth. Eur. Space Agency, 136, 25–31.

Atzberger, C. (2013). Advances in remote sensing of agriculture: Context description, existing operational monitoring systems and major information needs. Remote Sensing, 5(2), 949–981.

Azzari, G., & Lobell, D. B. (2017). Landsat-based classification in the cloud: An opportunity for a paradigm shift in land cover monitoring. Remote Sensing of Environment, 202, 64–74.

Bartholome, E., & Belward, A. S. (2005). GLC2000: a new approach to global land cover mapping from Earth observation data. International Journal of Remote Sensing, 26(9), 1959–1977.

Bontemps, S., Boettcher, M., Brockmann, C., Kirches, G., Lamarche, C., Radoux, J., Santoro, M., Van Bogaert, E., Wegmüller, U., Herold, M., Achard, F., Ramoino, F., Arino, O., & Defourny, P. (2015). Multi-year global land cover mapping at 300 M and characterization for climate modelling: Achievements of the land cover component of the ESA climate change initiative. International Archives of the Photogrammetry, Remote Sensing and Spatial Information Sciences - ISPRS Archives, 40(7W3), 323–328. https://doi.org/10.5194/isprsarchives-XL-7-W3-323-2015

Bouzidi, B. (2011). Viability of solar or wind for water pumping systems in the Algerian Sahara regions--case study Adrar. Renewable and Sustainable Energy Reviews, 15(9), 4436–4442.

Breiman, L. (2001). Random forests. Machine Learning, 45(1), 5–32.

Buchhorn, M., Smets, B., Bertels, L., Lesiv, M., Tsendbazar, N.-E., Herold, M., & Fritz, S. (2019). Copernicus Global Land Service: Land Cover 100m: epoch 2018: Africa demo. https://doi.org/10.5281/zenodo.3518087

Burke, M., & Lobell, D. B. (2017). Satellite-based assessment of yield variation and its determinants in smallholder African systems. Proceedings of the National Academy of Sciences, 114(9), 2189–2194.

Chen, J., Chen, J., Liao, A., Cao, X., Chen, L., Chen, X., He, C., Han, G., Peng, S., Lu, M., & others. (2015). Global land cover mapping at 30 m resolution: A POK-based operational approach. ISPRS Journal of Photogrammetry and Remote Sensing, 103, 7–27.

CILSS. (2016). Landscapes of West Africa—A window on a changing world. U.S. Geological Survey EROS: Garretson, SD, USA.

Cotillon, S. E. (2017a). West Africa land use and land cover time series. In Fact Sheet. https://doi.org/10.3133/fs20173004

Cotillon, S. E. (2017b). West Africa land use and land cover time series.

Cotillon, S. E., & Mathis, M. L. (2017). Mapping land cover through time with the Rapid Land Cover Mapper—Documentation and user manual: U.S. Geological Survey Open File Report 2017–1012, 23 p., https://doi.org/10.3133/ofr20171012.

FALL, C. A. (2009). État des ressources phytogénétiques pour l'alimentation et l'agriculture dans le monde: Contribution du Sénégal au second rapport. http://www.fao.org/pgrfa-gpa-archive/sen/docs/senegal2.pdf

Fensholt, R., Rasmussen, K., Nielsen, T. T., & Mbow, C. (2009). Evaluation of earth observation based long term vegetation trends—Intercomparing NDVI time series trend analysis consistency of Sahel from AVHRR GIMMS, Terra MODIS and SPOT VGT data. Remote Sensing of Environment, 113(9), 1886–1898.

Friedl, M. A., Sulla-Menashe, D., Tan, B., Schneider, A., Ramankutty, N., Sibley, A., & Huang, X. (2010). MODIS Collection 5 global land cover: Algorithm refinements and characterization of new datasets. Remote Sensing of Environment, 114(1), 168–182. https://doi.org/10.1016/j.rse.2009.08.016

Fritz, S., You, L., Bun, A., See, L., McCallum, I., Schill, C., Perger, C., Liu, J., Hansen, M., & Obersteiner, M. (2011). Cropland for sub-Saharan Africa: A synergistic approach using five land cover data sets. Geophysical Research Letters, 38(4).

Gorelick, N., Hancher, M., Dixon, M., Ilyushchenko, S., Thau, D., & Moore, R. (2017). Google Earth Engine: Planetary-scale geospatial analysis for everyone. Remote Sensing of Environment, 202, 18–27. https://doi.org/10.1016/j.rse.2017.06.031

Hamidat, A., Benyoucef, B., & Hartani, T. (2003). Small-scale irrigation with photovoltaic water pumping system in Sahara regions. Renewable Energy, 28(7), 1081–1096.

Hollinger, F., & Staatz, J. M. (2015). Agricultural Growth in West Africa. Market and Policy Drivers. FAO, African Development Bank, ECOWAS. Pobrano Październik.

Hong, C., Jin, X., Ren, J., Gu, Z., & Zhou, Y. (2019). Satellite data indicates multidimensional variation of agricultural production in land consolidation area. Science of the Total Environment, 653, 735–747. https://doi.org/10.1016/j.scitotenv.2018.10.415

Huete, A., Didan, K., Miura, T., Rodriguez, E. P., Gao, X., & Ferreira, L. G. (2002). Overview of the radiometric and biophysical performance of the MODIS vegetation indices. Remote Sensing of Environment, 83(1–2), 195–213.

Huete, A. R. (1988). A soil-adjusted vegetation index (SAVI). Remote Sensing of Environment, 25(3), 295–309.

Issoufou, W. S., MAHAMANE, A., & OUSSEINI, I. (2012). La Surveillance Ecologique et Environnementale au Niger: Un instrument d'aide à la décision. Options Méditerranéennes: Série B. Etudes et Recherches, 68, 219–230.

Jiang, Z., Huete, A. R., Didan, K., & Miura, T. (2008). Development of a two-band enhanced vegetation index without a blue band. Remote Sensing of Environment, 112(10), 3833–3845.

Johnson, D. M. (2019). Using the Landsat archive to map crop cover history across the United States. Remote Sensing of Environment, 232, 111286.

Jones, H. G., & Vaughan, R. A. (2010). Remote sensing of vegetation: principles, techniques, and applications. Oxford university press.

Kobayashi, N., Tani, H., Wang, X., & Sonobe, R. (2019). Crop classification using spectral indices derived from Sentinel-2A imagery. Journal of Information and Telecommunication, 1–24. https://doi.org/10.1080/24751839.2019.1694765

Kumar, L., & Mutanga, O. (2018). Google Earth Engine applications since inception: Usage, trends, and potential. Remote Sensing, 10(10), 1509.

Latham, J. (2009). FAO land cover mapping initiatives. North America Land Cover Summit, Environment and Natural Resources Service, Food and Agriculture Organization of the United Nations (FAO), 75–95.

Latham, J., Cumani, R., Rosati, I., & Bloise, M. (2014). Global land cover share (GLC-SHARE) database beta-release version 1.0-2014. FAO: Rome, Italy.

Li, L., Tsendbazar, N., Herold, M., & Lesiv, M. (2019). Copernicus Global Land Operations "Vegetation and Energy": MODERATE DYNAMIC LAND COVER CHANGE MAPS, AFRICA 2015-2018.

Löw, F., Biradar, C., Fliemann, E., Lamers, J. P. A., & Conrad, C. (2017). Assessing gaps in irrigated agricultural productivity through satellite earth observations—A case study

of the Fergana Valley, Central Asia. International Journal of Applied Earth Observation and Geoinformation, 59, 118–134. https://doi.org/10.1016/j.jag.2017.02.014

Mardani, M., Mardani, H., De Simone, L., Varas, S., Kita, N., & Saito, T. (2019). Integration of Machine Learning and Open Access Geospatial Data for Land Cover Mapping. Remote Sensing, 11(16), 1907.

Miura, T., Huete, A. R., Yoshioka, H., & Holben, B. N. (2001). An error and sensitivity analysis of atmospheric resistant vegetation indices derived from dark target-based atmospheric correction. Remote Sensing of Environment, 78(3), 284–298.

Olsson, L., Eklundh, L., & Ardö, J. (2005). A recent greening of the Sahel—trends, patterns and potential causes. Journal of Arid Environments, 63(3), 556–566.

Pal, M. (2005). Random forest classifier for remote sensing classification. International Journal of Remote Sensing, 26(1), 217–222. https://doi.org/10.1080/01431160412331269698

Pérez-Hoyos, A., Rembold, F., Kerdiles, H., & Gallego, J. (2017). Comparison of global land cover datasets for cropland monitoring. Remote Sensing, 9(11). https://doi.org/10.3390/rs9111118

Pontius Jr, R. G., & Millones, M. (2011). Death to Kappa: birth of quantity disagreement and allocation disagreement for accuracy assessment. International Journal of Remote Sensing, 32(15), 4407–4429.

Qi, J., Chehbouni, A., Huete, A. R., Kerr, Y. H., & Sorooshian, S. (1994). A modified soil adjusted vegetation index. Remote Sensing of Environment, 48(2), 119–126.

Rembold, F., Meroni, M., Urbano, F., Csak, G., Kerdiles, H., Perez-Hoyos, A., Lemoine, G., Leo, O., & Negre, T. (2019). ASAP: A new global early warning system to detect anomaly hot spots of agricultural production for food security analysis. Agricultural Systems, 168(May 2018), 247–257. https://doi.org/10.1016/j.agsy.2018.07.002

Richards, J. A., & Jia, X. (1999). Remote sensing digital image analysis (Vol. 3). Springer.

RNCA-NIGER. (2019). Le Zonage Agro-écologique du NIGER. https://reca-niger.org/IMG/pdf/Le_zonage_agroecologique_du_Niger_Extraits.pdf

Roy, D. P., Wulder, M. A., Loveland, T. R., Woodcock, C. E., Allen, R. G., Anderson, M. C., Helder, D., Irons, J. R., Johnson, D. M., Kennedy, R., & others. (2014). Landsat-8:

Science and product vision for terrestrial global change research. Remote Sensing of Environment, 145, 154–172.

Samasse, K., Hanan, N. P., Tappan, G., & Diallo, Y. (2018). Assessing cropland area in West Africa for agricultural yield analysis. Remote Sensing, 10(11). https://doi.org/10.3390/rs10111785

SIDIBE, A. (2007). L'état des ressources phytogénétiques pour l'alimentation et l'agriculture au Mali – 2007: Deuxième rapport national.

Tappan, G. G., Cushing, W. M., Cotillon, S. E., Mathis, M. L., Hutchinson, J. A., & Dalsted, K. (2016). West Africa Land Use Land Cover Time Series. U.S. Geological Survey: Sioux Falls, SD, USA.

Thenkabail, P., Lyon, J. G., Turral, H., & Biradar, C. (2009). Remote sensing of global croplands for food security. CRC Press.

Thibaud, B. (2005). Le pays dogon au Mali: de l'enclavement à l'ouverture? Espace, Populations, Sociétés, 1, 45–56.

Tong, X., Brandt, M., Hiernaux, P., Herrmann, S., Rasmussen, L. V., Rasmussen, K., Tian, F., Tagesson, T., Zhang, W., & Fensholt, R. (2020). The forgotten land use class: Mapping of fallow fields across the Sahel using Sentinel-2. Remote Sensing of Environment, 239, 111598.

Tucker, C. J. (1979). Red and photographic infrared linear combinations for monitoring vegetation. Remote Sensing of Environment, 8(2), 127–150.

van der Wijngaart, R., Helming, J., Jacobs, C., Delvaux, P. A. G., Hoek, S., & y Paloma, S. G. (2019). Irrigation and irrigated agriculture potential in the Sahel: The case of the Niger River basin.

Vintrou, E., Desbrosse, A., Bégué, A., Traoré, S., Baron, C., & Seen, D. Lo. (2012). Crop area mapping in West Africa using landscape stratification of MODIS time series and comparison with existing global land products. International Journal of Applied Earth Observation and Geoinformation, 14(1), 83–93.

Woodhouse, P., & Ganho, A. S. (2011). Is water the hidden agenda of agricultural land acquisition in sub-Saharan Africa. International Conference on Global Land Grabbing, 6.

Xiong, J., Thenkabail, P. S., Tilton, J. C., Gumma, M. K., Teluguntla, P., Oliphant, A., Congalton, R. G., Yadav, K., & Gorelick, N. (2017). Nominal 30-m cropland extent map of continental Africa by integrating pixel-based and object-based algorithms using Sentinel-2 and Landsat-8 data on google earth engine. Remote Sensing, 9(10), 1–27. https://doi.org/10.3390/rs9101065

Xue, J., & Su, B. (2017). Significant remote sensing vegetation indices: A review of developments and applications. Journal of Sensors, 2017.

Zwart, S. J., & Leclert, L. M. C. (2010). A remote sensing-based irrigation performance assessment: A case study of the Office du Niger in Mali. Irrigation Science, 28(5), 371–385. https://doi.org/10.1007/s00271-009-0199-3

CHAPTER 4

National scale crop type mapping for the major subsistence cereal crops of Mali, West Africa

Paper #3

In preparation for submission

Abstract

In arid and semi-arid West Africa, agricultural production and regional food security depend largely on small-scale subsistence farming and rainfed crops, both of which are vulnerable to climate variability and drought. Efforts made to improve crop monitoring and our ability to estimate crop production (areas planted and yields by crop type) in the major agricultural zones of the region are critical paths for minimizing climate risks and supporting food security planning. In the present study, georeferenced plot data (N=13,000) collected by the Malian Department of Agriculture, Landsat 8 remotely sensed data, rainfall, and terrain information are combined to train a random forest classifier predicting crop type at 30 m for the major subsistence cereals (maize, millet, upland rice, and sorghum) cultivated in Mali. Tested with about 2,500 independent samples, using an unbiased area error matrix, the new crop type map has an overall agreement of 78.3%. The 21.7% disagreements are caused mainly by spatial allocation disagreement representing errors in "where the crop type is", with relatively small errors in total area assessments. The developed crop type map offers unprecedented information on subsistence farming intensity, crop areas and the proportion of different crops in different regions and administrative subdivisions ("communes") of Mali. At country-scale for 2017, total subsistence cropland areas are estimated at 1,300,211 ha ±70,360 for maize, 1,813,937 ha ±78,829 for millet, 239,550 ha ±36,061 for rice, and 1,297,346ha ± 76,656 for sorghum. Analyses for maize, sorghum and millet confirms that planting intensity (i.e. crop type fraction in a region), is primarily a function of the rainfall regime. Pearl millet dominates production in Sahelian and upper Sudanian climatic zones (400 – 800 mm/y), sorghum is predominant in most parts of the central Sudanian zone (800-1000 mm/y), while maize is the primary cereal crop in the upper Sudanian to Guinean zones (>1000 mm/y). By

contrast, small-scale (non-irrigated) rice cultivation is concentrated in river valleys where rice is planted during high-water seasons and as river levels decline in the dry season. Thus, rice farms are present in all four climatic zones along the main stems and tributaries of the Niger, Baoulé and Bani rivers. The outcomes of this study, and potential for the analysis to be repeated for other years, constitute a major advance for our understanding of food production systems in Mali and potential for improved crop yield modelling. This analysis provides spatially explicit information on location and probable crop types that can be used to enhance the precision of bioclimatic and remote sensing based yield forecasting and information and analyses on possible food insecurity to help stave off famine early.

4.1. Introduction

Rapid population growth, increasing temperatures, drought and extreme rainfall events are major factors contributing to food insecurity in the Sahel, making this region one of the most food-insecure regions in the world (Sissoko et al., 2011). According to the Food and Agriculture Organization (FAO) and the World Food Programme (WFP), the Central Sahel area, covering large parts of Burkina Faso, Mali and Niger, is a hotspot of acute food insecurity because of the combination of variable rainfall and emerging conflict leading to internal displacement of communities (FAO & WFP, 2020). In the Sahelian region, agriculture is primarily based on rainfed crops, and agricultural production systems are often structurally inadequate to manage inherent climatic variability, making the sector more vulnerable as climate risks increase (Barbier et al., 2009; der Geest & Dietz, 2004). In addition, in recent years the region has experienced recurrent political instabilities, with associated economic and livelihood challenges particularly for rural communities. In such conditions, crop failure or significant yield decreases may occur with either rainfall irregularities or extreme temperatures during the rainy season (Vignaroli et al., 2016), and longer-term yield reductions may occur with soil degradation and lack of access to fertilizer (Adams et al., 2016; Breman et al., 2001). Thus, additional efforts are needed to improve crop monitoring and our ability to estimate crop production in the major agricultural zones of the region. Crop area estimation, crop type mapping, and early estimates of crop yields are critical paths for minimizing climate risks in rainfed agriculture systems and to support food security planning (e.g. Bolton & Friedl, 2013; Samasse et al., 2020; Shahhosseini et

al., 2020; Wang et al., 2019). As satellite remote sensing is increasingly improving in spatial and temporal resolution, it can contribute significantly to systems that collect information on crop type and seasonal production at national and regional geographical scales (Lambin et al., 1993).

Satellite remote sensing-based tools and models for agricultural yield prediction have been used for decades in the Sahelian region, through different regional and national initiatives in collaboration with international institutions, to allow near-real-time monitoring during the cropping season. For example, the USAID Famine Early Warning System Network (FEWS-NET) combines biophysical remote sensing and socio-economic methodologies (Brown, 2008) to provide monitoring and early warning support to decision makers responsible for responding to humanitarian crises, including famine and food insecurity. The main FEWS-NET satellite remote sensing-based inputs include rainfall and seasonal vegetation growth inferred from vegetation index time-series (Ross et al., 2009). An example of an analysis tool promoted by FEWS NET is the Early Warning eXplorer (EWX), which is an interactive web-based mapping tool allowing users to visualize continental-scale rainfall estimates (RFE and the Climate Hazard group InfraRed Precipitation with Stations, CHIRPS), land surface temperature (LST) and normalized difference vegetation index (NDVI) data and anomalies during the crop growing season (FEWS NET, 2020). To be effective in crop condition monitoring, the RFE, CHIRPS, LST, and NDVI information should be filtered based on crop locations. Thus, knowledge of where croplands are, and which crops are planted, is of critical importance for operational crop monitoring. Several previous studies have examined crop/non-crop areas using remotely sensed data at different scales (Fritz et al., 2011; Lambert et al., 2016; Ramankutty, 2004; Samasse et al., 2020; Thenkabail et al., 2009; Tong et al., 2020; Xiong et al., 2017). However, few of these studies focused on crop specific location mapping at regional scale, particularly in the Sahelian countries.

Spatially explicit crop type information is critical for a variety of applications in agricultural monitoring, guiding investments and policies for improving food security (Jin et al., 2019; Wang et al., 2019). The traditional method of estimating crop type acreage in most developing regions is through field surveys and application of statistical methods to

derive nationwide agricultural statistics. For example, in Mali, a stratified random sampling method is used to select samples for area, type and yield estimation of major crops. Each region (stratum) in the Malian sampling scheme is sub-divided into sub-regions named “SE” ("sous-échantillon"). An SE is composed of about 700 rural households that constitute the basic sampling units. The sampling process starts by randomly selecting a certain number of “SE” in each Region, then randomly selecting 10 farms in each selected “SE”. Areas for different crop types are calculated for all fields on the selected farms, with estimated field areas summed to derive crop type acreage information at SE scale. From SE to region scale, results are extrapolated using statistical methods. Only the extrapolated crop area information is reported and shared with partners such as FAO representatives for official reports. The inability to assess the probable error of the extrapolation process, combined with difficulties related to accessing and surveying some regions due to conflicts, constitute major weaknesses of this method to estimate crop type area at the country level. As remote sensing imagery continues to increase in spatial and temporal resolution, it is becoming a powerful input from which to create crop type maps, particularly at field scale (Wang et al., 2019), and this constitutes a viable alternative for improving traditional methods of area estimation. In addition, crop type mapping is widely accepted as a critical first step in forecasting crop yields using remote sensing, as different crop types have different seasonal growth patterns and phenology (Maselli & Rembold, 2001).

In this study, we use field observations of crop type provided by the Malian Department of Agriculture to train random forests classifiers to map crop identities at field scale for the entire country of Mali in 2017, using precipitation, terrain, surface reflectance, and vegetation indices as predictors. The WASC30 cropland dataset, which maps croplands across West Africa with no information on crop type (Samasse et al., 2020), is used as a mask to prevent the new crop type map from predicting the presence of crops in areas not mapped as rainfed cropland. Maize, millet, rice, and sorghum are the major subsistence cereal crops mapped. These four crops constitute about 98% of nationwide cereal production in Mali (Ministère de l’Agriculture, 2018).

Results show that Landsat datasets and random forest Classifier are reliable for crop type mapping in a semi-arid region like the Sahel. The new crop type dataset for Mali will

be made available for online access to agricultural modeling communities, researchers, and early warning systems developers with high resolution crop type mask for maize, millet, rice, and sorghum.

4.2. Methods

4.2.1. Crop type data (dependent variable)

In total, ~13,000 field-based samples of actual crop type were used to develop the crop type map. These samples include geo-localized plots distributed in all seven regions of Mali, recording the presence of maize (n = 2,057), pearl millet (n = 3,092), rice (n = 1,000), and sorghum (n = 2,258) (Figure 4.1). Other crops including fonio, groundnut, beans, onions, wheat, root crops, and other vegetables constitute a fifth class (other crops, n = 4,496). A sixth class (n = 8,000) named “non-crop” (which, include fallow and non-cropland areas in the spatially randomized sample) is extracted from the West African Sahel Cropland 30 (WASC30; Samasse et al., 2020). Field data with GPS coordinates were collected by the statistical and planning service of the Malian Department of Agriculture during the 2017 and 2018 agricultural surveys. Irrigated agriculture is not included in this analysis; thus, field data were limited to rainfed plots (for maize, sorghum and millet), and a smaller number of flood-recession rice fields (i.e. small scale agriculture in river flood plains where rice is planted as flood waters recede).

Considering the four (4) major cereals (maize, millet, rice, and sorghum), Figure 4.1 shows that agricultural activities occur mainly in central to southern Mali, following the mean annual precipitation (MAP) gradient, which increases from North to South. Low MAP in northern Mali creates non-suitable conditions for agricultural activities in most areas, except for isolated millet cultivation and rice along river corridors.

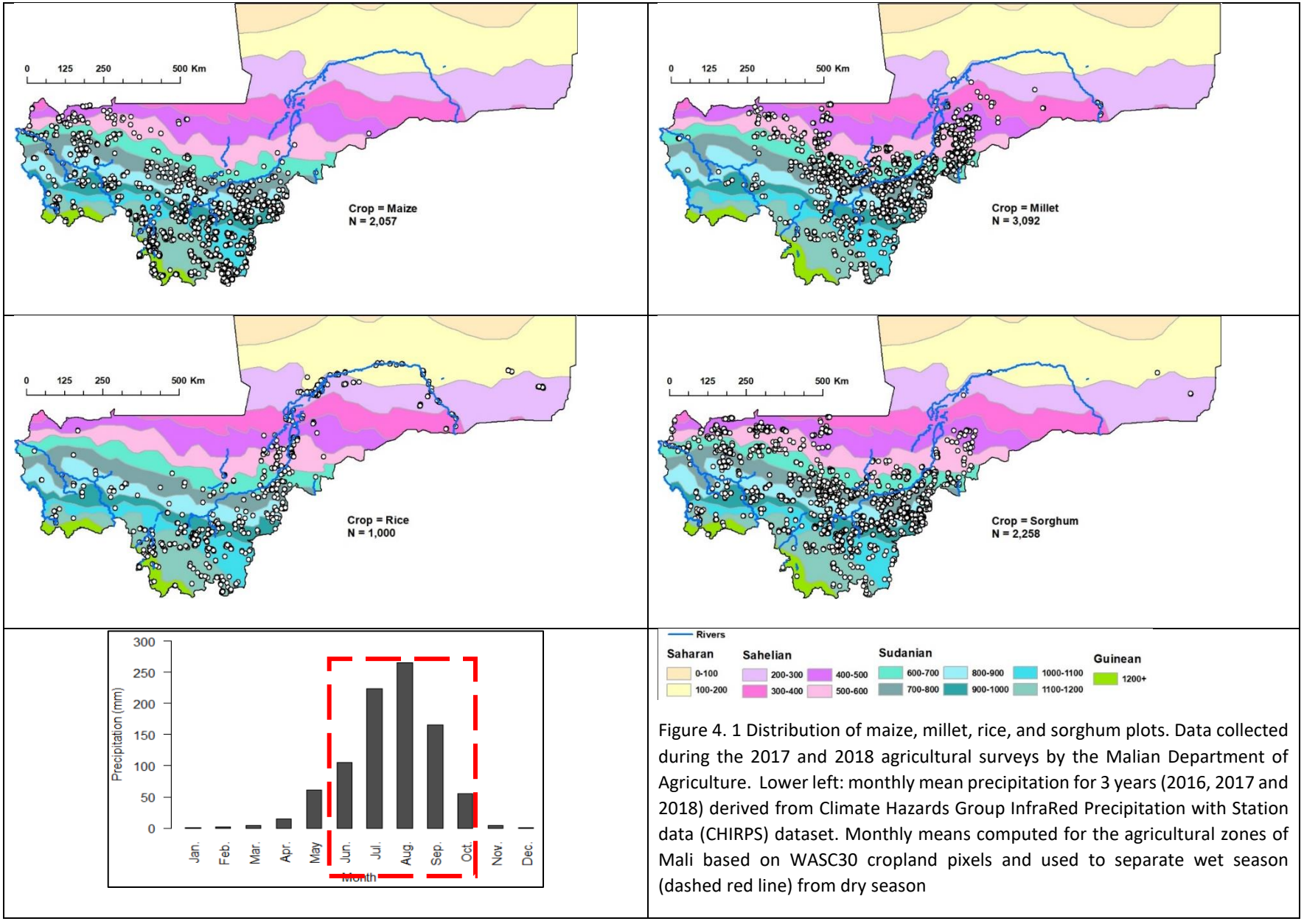

Figure 4. 1 Distribution of maize, millet, rice, and sorghum plots. Data collected during the 2017 and 2018 agricultural surveys by the Malian Department of Agriculture. Lower left: monthly mean precipitation for 3 years (2016, 2017 and 2018) derived from Climate Hazards Group InfraRed Precipitation with Station data (CHIRPS) dataset. Monthly means computed for the agricultural zones of Mali based on WASC30 cropland pixels and used to separate wet season (dashed red line) from dry season

4.2.2. Climate, remote sensing, and edaphic data (independent variables)

Surface reflectance, vegetation indices, precipitation (rainfall) and terrain information (elevation and slope) are used as candidate predictor variables in the random forest classifier (Table 1). Predictor variables are averaged for three years (2016, 2017, and 2018) using the Google Earth Engine (GEE) platform. As cropping activities typically coincide with the rainy season, crop growth conditions are primarily linked to the amount and regularity of precipitation. For this reason, remote sensing and climate predictors are divided in two groups (wet and dry season). The wet season corresponds to the growing season of major crops in Mali, generally from June to September, while the dry season is composed by months with no or low monthly precipitation (Figure 4.1; Appendix A).

Table 4. 1. Predictors extracted from Google Earth Engine platform. Variables names with _1 suffix correspond to dry season (e.g. NDVI_1) while those without the suffix are for the wet season (e.g. NDVI)

Predictors	Data source
Surface reflectance Wet period: B2 to B7 Dry period: B2_1 to B7_1	Landsat 8, 30 m
Vegetation indexes Wet period: NDVI, EVI, SAVI, MSAVI Dry period: NDVI_1, EVI_1, SAVI_1, MSAVI_1	
Precipitation Wet period: PRECIP Dry period: PRECIP_1	CHIRPS v2.0 Daily, 0.05 degree
Terrain Elevation, Slope	NASA SRTM Digital Elevation 30m

4.2.3 Random Forest Model

Random forest (RF) is an ensemble machine learning algorithm that can be used to predict both continuous (regression) and categorical (classification) responses. It is used in this study for classification of crop species. An RF model comprises an ensemble of

decision trees, where each tree can predict the response-variable using a random sub-sample of the independent variables and observations. Each tree uses a sub-ensemble of training values chosen randomly with replacement (i.e. bootstrap samples). The optimum number of predictors used to split data at each tree's node is *sqrt(m)*, where m is the total number of predictors involved. An ensemble of diverse trees minimizes the effect of bias from individual trees considerably improving the overall predictive accuracy of the model. In classification problems, the final predicted value is chosen by output majority voting of individual trees. It has been shown that by increasing the number of trees in the model, the errors of prediction (also known as out-of-bag errors or OOB errors) converge, reducing problems with overfitting (Pal, 2005).

To develop and test our new crop type map, the reference dataset (actual crop types) was divided into a training set (80%) and a validation set (20%). We used estimation based on the OOB errors during the training process to fine tune the number of predictors at each tree node (*mtry*) before training the model to predict crop type classes for the country of Mali. Appendix B gives details on tuning parameters and optimal outputs. In addition to the internal cross-validation assessment occurring during the training process to fine-tune RF model parameters, and external testing with unused data in the training process, the resulting crop type map was also masked using the WASC30 cropland dataset (Samasse et al., 2020) to avoid confusion with natural vegetation (that might have similar seasonal trends as some crop species) and thus omit predictions in non-cropland areas. Finally, the area of each of the four crops is compared to agricultural statistics for the study years available at national level.

4.3. Results

4.3.1. Random forest model evaluation

Although the technique of bagging used by the random forest algorithm offers the possibility to examine error derived from samples out-of-bag, in this analysis we used independent data samples (20% of the reference data). These data were not used during the training process and thus provide fully independent data to test model accuracy. The method of accuracy assessment suggested in Pontius & Millones (2011), based on quantity disagreement (Q) and allocation disagreement (A), was employed to characterize errors in prediction for each of the five crop classes (Maize: 1, Millet: 2, Rice: 3, Sorghum: 4, and Other crops: 5). In our study, the quantity disagreement represents errors in “how much" crop of each type there is, while the allocation disagreement quantifies error in “where" the crop is located. A detailed application of these accuracy metrics in land cover maps assessment can be found in Samasse et al. (2018). The overall accuracy of the newly developed crop type map is 78.3% for an average disagreement of 21.7% (Table 2). Error due to the spatial locations of each crop type constitutes the largest component of the total error. In terms of class-specific disagreements, Figure 4.3 confirms that allocation disagreement is the most important error factor in all five crop type classes (maize, millet, rice, sorghum, other crops), but its value is less than 10% for all but the Other crops class.

Alternative class-specific accuracy metrics used in many studies are the user’s accuracy and producer’s accuracy (e.g. Congalton, 1991; Hasmadi et al., 2009; Konduri et al., 2020; Shao & Wu, 2008). User’s accuracy for each of the different crop types is above 75% (Table 2) with the highest value observed for rice (94.05%). That is, our crop type predictions have relatively high reliability. For producer’s accuracy, maize and millet are the most correctly mapped classes with accuracy above 85% (maize: 86.12%; millet: 87.40%) followed by sorghum (75.25%). However, producer’s accuracy for rice is relatively low, below 60%. The producer’s accuracy informs on how often real features on the ground are correctly shown on the classified map. Table 2 reports commission and omission errors as well, which are the complement of user’s accuracy and producer’s accuracy, respectively. In general, higher commission to omission error corresponds to overestimation of cropland, while higher omission to commission error is equivalent to

underestimation of cropland. Thus, based on the testing dataset, our crop type map overestimates maize and millet areas, while areas for rice, sorghum, and other crops are underestimated. The largest difference between commission and omission errors is observed in rice, suggesting that rice cropping areas may be greatly underestimated.

Table 4. 2. Accuracy statistics derived from the unbiased error table using the testing dataset. See Appendix B for complete error tables and accuracy metrics.

	Maize	Millet	Rice	Sorghum	Other crops	All crops
User's Accuracy	77.12	78.77	94.05	77.92	77.91	
Producer's Accuracy	86.12	87.40	52.96	75.25	69.86	
Commission error	22.88	21.23	5.95	22.08	22.09	
Omission error	13.88	12.60	47.04	24.75	30.14	
Quantity Disagreement						5.31
Allocation Disagreement						16.36
Overall accuracy						78.33

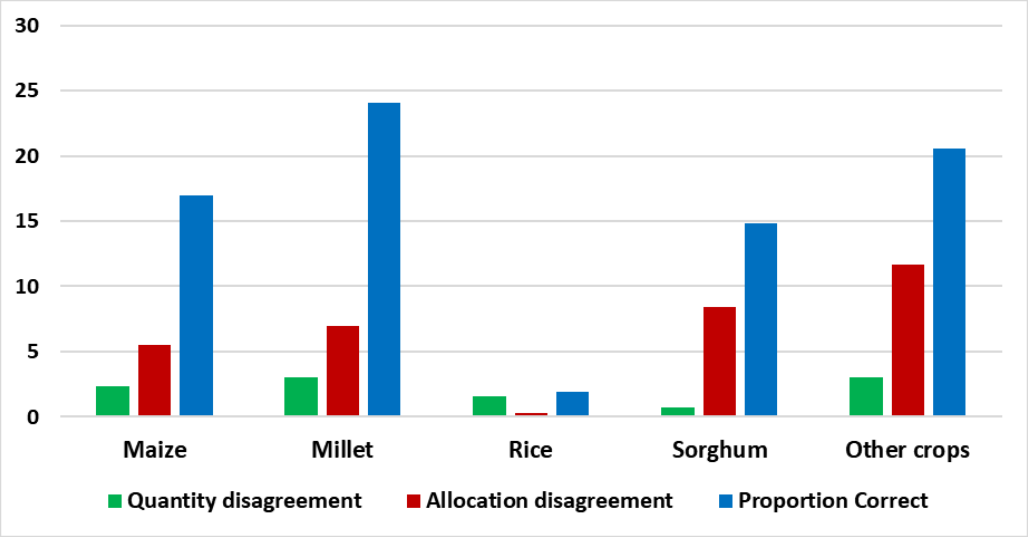

Figure 4. 2. Quantity disagreement, Allocation disagreement, and Fraction correct for the different crop classes. Fraction correct is the contribution of a specific class to the overall accuracy

4.3.2. Spatial distribution of major cereal crops

Figure 4.4 shows the estimated 2017 spatial distribution for the major rainfed subsistence cereal crops of Mali as predicted by our fitted machine learning model. Pixels misclassified in non-agricultural zones, or in irrigated agricultural zones, were masked using the WASC30 rainfed crop class (Fig. 4C). The "Other crops" class includes fonio, groundnut, beans, onions, wheat, root crops, and other vegetables which are widely

distributed close to villages. Overall, millet is cultivated primarily in northern and central Mali, sorghum in central to southern, and maize in the southern regions of the country. From North to South, following the MAP, pearl millet dominates agricultural activities in areas averaging up to 800 mm of precipitation, sorghum is concentrated between 800 to 1000 mm, and areas above 1000 mm are dominated by maize farms. Rice fields are more present in the Inner Niger Delta plains and along the Niger, Bani and Baoulé rivers, not necessarily following the MAP gradient.

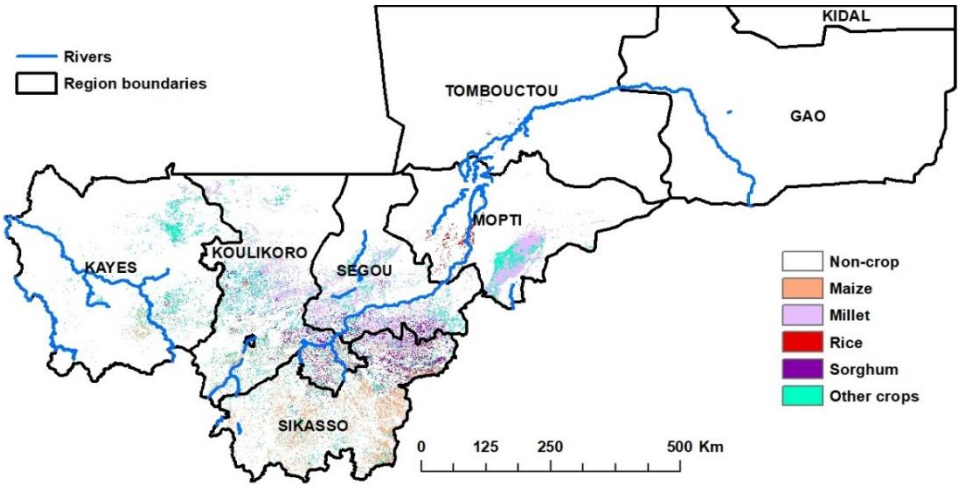

(B)

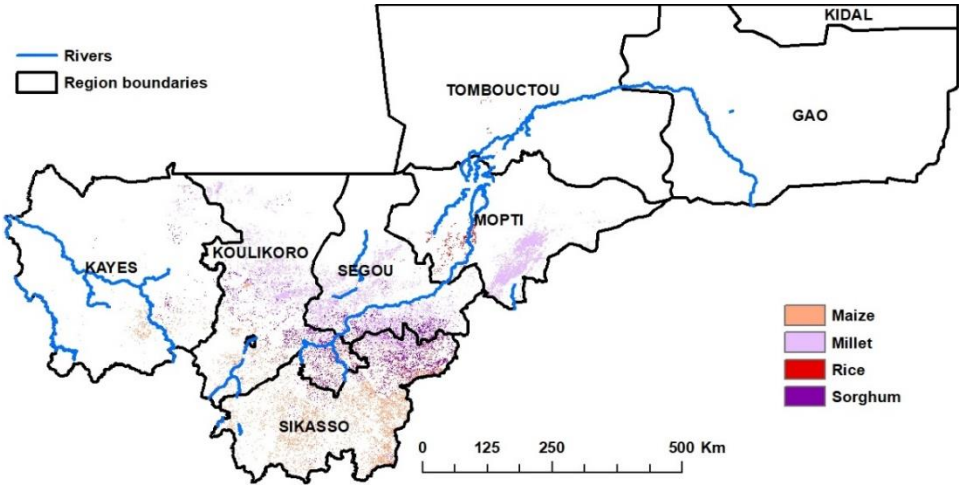

(C)

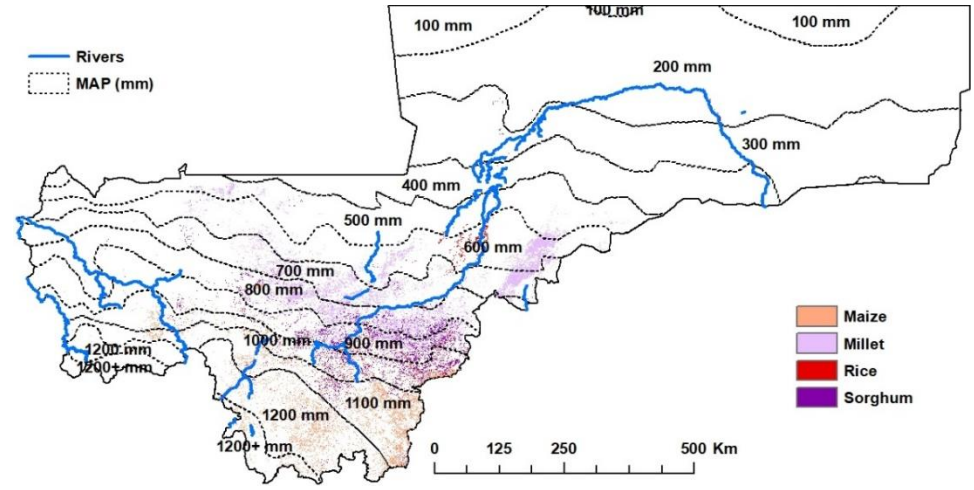

Figure 4. 3. Crop type mapping for Mali in 2017: (A) all classes including non-crop, (B) maize, millet, rice, and sorghum only, (C) maize, millet, rice and sorghum map using the WASC30 cropland database to omit non-cropland areas. Mean Annual Precipitation (MAP) in (C) is derived from CHIRPS v2.0 for years 2005 – 2015

4.4. Discussion

4.4.1. Cultivated areas for major crop types

The cultivated area devoted to each of the four major cereals for the country of Mali is detailed in Table 3. By using the area-based unbiased error matrix suggested by Olofsson et al. (2014), we estimated areas and the confidence intervals (CI) and then compared our estimates to the reported cultivated areas by the Malian Ministry of Agriculture (MMA) for 2017/2018 campaign. Based on our results, MMA statistics overestimate millet and sorghum areas by 14-24% and 15-30%, respectively. The estimated areas planted to maize is similar in our crop type map to those of the reported cultivated areas by MMA (with a ratio of 95-100%. However, MMA reports considerably less rainfed rice than our estimates (an underestimation of 16-30%; Table 3). Differences between our remote sensing-based crop type acreage and the reported statistics may come from various sources. Firstly, the MMA estimation is based on statistical methods of extrapolation using randomly selected ground surveys following geographic stratification. While sampling error is nominally 12% the MMA recognizes that errors associated with statistical extrapolation techniques may be much larger (Ministère de l'Agriculture, 2018). Secondly, considering the large extent of the country and difficulties accessing some areas due to security concerns, sampling of farmers in some local-scale administrative subdivisions (e.g. Commune level) is reduced, limiting samples size and statistical inference based only on field data. In this context, our approach to mapping cultivated areas by crop type at national scale using earth observation data and the power of machine learning techniques, could be a good alternative to reduce survey costs and improve accuracy, particularly in insecure regions.

Table 4. 3. Cultivated cropland areas (non-irrigated) for the country of Mali in 2017 for the major cereal crops and comparison with the national agricultural statistics (MMA). The ratio is calculated by dividing national statistics by the new crop type area estimates times 100.

	Area (ha)	± 95% CI	Area -95% CI	Area + 95% CI	National statistical data (2017) (ha)	Ratio (%)	Ratio ±95% CI
Maize	1,300,211	70,360	1,229,851	1,370,571	1,233,008	94.8	90.0 -100.3
Millet	1,813,937	78,829	1,735,107	1,892,766	2,155,729	118.8	113.9 -124.2
Rice	239,550	36,061	203,489	275,610	191,969	80.1	69.7 – 94.3
Sorghum	1,297,346	76,656	1,220,691	1,374,002	1,585,986	122.3	115.4 -129.9

4.4.2. Fractional cultivated area by crop type

The fraction of cultivated area devoted to each of the major subsistence crops in a region reflects both the bioclimatic suitability of each crop to the region, interacting with the cultural and economic decision-making of individual farmers. *A priori* understanding of crop ratios for the major subsistence crops can also provide critical inputs to crop yield modeling based either on climate data or remote sensing of greenness. In this study, crop type fractions were calculated at administrative level 3 (*Commune* in French) and in climatic zones (MAP 100 mm isohyets). Figure 4.5 shows that agriculture activities in Mali are concentrated in five regions (Kayes, Koulikoro, Sikasso, Segou, and Mopti). In each of these regions, all four major cereals are planted yearly, however the fractions in different crops varies greatly. In the northern regions, our results show that rice is the most cultivated crop in Tombouctou, and Gao, along the Niger river. At the *Commune* level, maize constitutes the predominant crop in Sikasso and parts of Kayes and Koulikoro; millet is equally planted in Mopti, central Segou, and Koulikoro; while the distribution of sorghum is relatively more even across all five regions. In addition to Tombouctou and Gao, rice is also common on the flood plains of the Inner Niger Delta in the regions of Mopti and Segou while being locally cultivated in the lowlands and river valleys of the Sikasso, Kayes and Koulikoro regions (Fig. 5). The fifth crop type (Other crops) is widely distributed, reflecting small-scale vegetable cultivation for household consumption and sale at markets, and with high fraction values in the Kayes region, probably due to the importance of groundnut farms in this region and export opportunities to neighboring Senegal.

Following the climatic zones as illustrated in Figure 4.6, the Saharan zone (MAP < 200 mm/y) which has very little cropped area is dominated by rice fields along the Niger river. In the Sahelian zone (200-600 mm/y), millet is the main rainfed crop, with rice cultivated in the river valleys. This zone includes the Inner Niger Delta plains known for their suitability to grow both rainfed and irrigated rice (Fig. 5). The Seno plains of the Mopti region, identified by Samasse et al. (2020) as one of the most intensive rainfed agricultural zones of Mali is dominated by millet cultivation (Fig. 5). Relatively important fractions of other crops observed in the Sahelian zone could be related to onions and other vegetables cultivated in Dogon uplands and the Office du Niger zone. The Sudanian zone which has

~25% total area in cropland (Samasse et al., 2020) constitutes the most important rainfed agricultural production zone of Mali, because of the quantity and period of rainfall per year (600 mm – 1200 mm; 4-6 months). All mapped crop types are common in the Sudanian zone, with millet dominant in the drier areas (700 mm – 800 mm), sorghum in intermediate rainfall zones (800 mm – 1000 mm) and maize in areas with >1000 mm/y (Fig. 6). Other crops are also significantly present in this climatic zone, including root crops (e.g. yams, potatoes, sweet potatoes) that are suitable for growing under the zone humidity conditions. In the Guinean zone (>1200 mm/y) areas are generally dominated by forests and agricultural intensity declines (Samasse et al., 2020). This climatic zone occupies a small part of the Sikasso and Kayes regions (Figure 4.6). Maize is the most cultivated crop followed by a variety of other crops (primarily root crops).

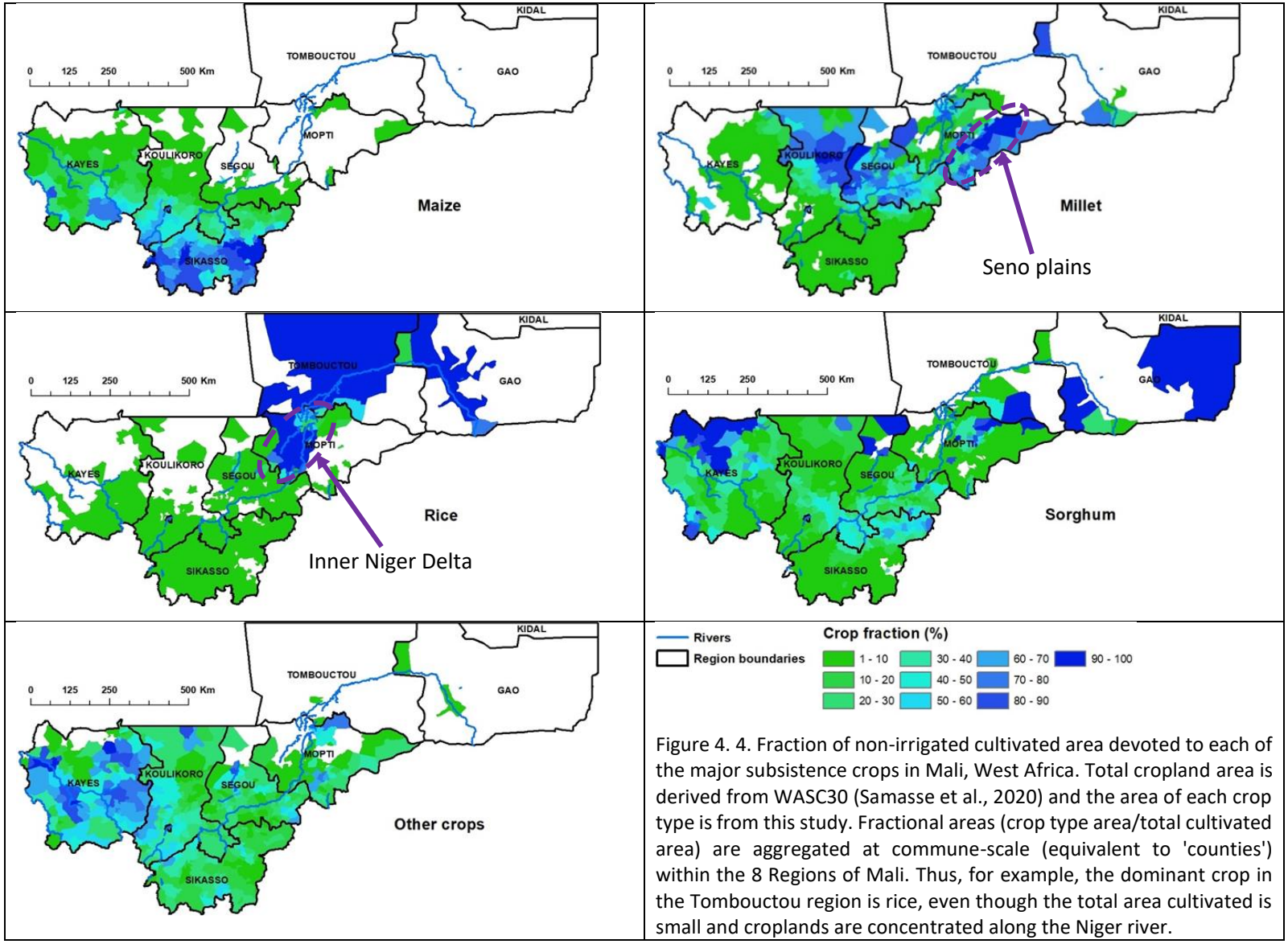

Figure 4. 4. Fraction of non-irrigated cultivated area devoted to each of the major subsistence crops in Mali, West Africa. Total cropland area is derived from WASC30 (Samasse et al., 2020) and the area of each crop type is from this study. Fractional areas (crop type area/total cultivated area) are aggregated at commune-scale (equivalent to 'counties') within the 8 Regions of Mali. Thus, for example, the dominant crop in the Tombouctou region is rice, even though the total area cultivated is small and croplands are concentrated along the Niger river.

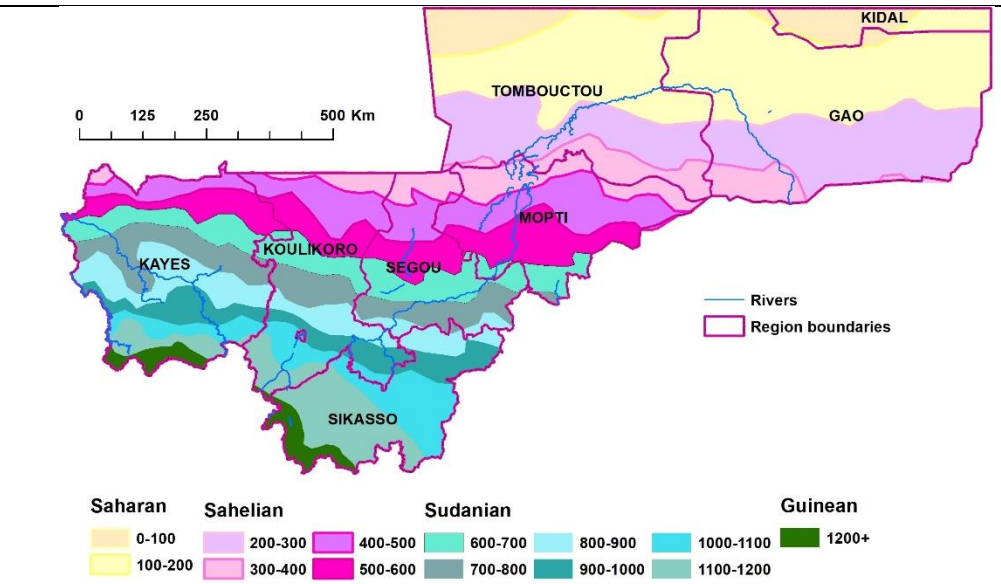

(A)

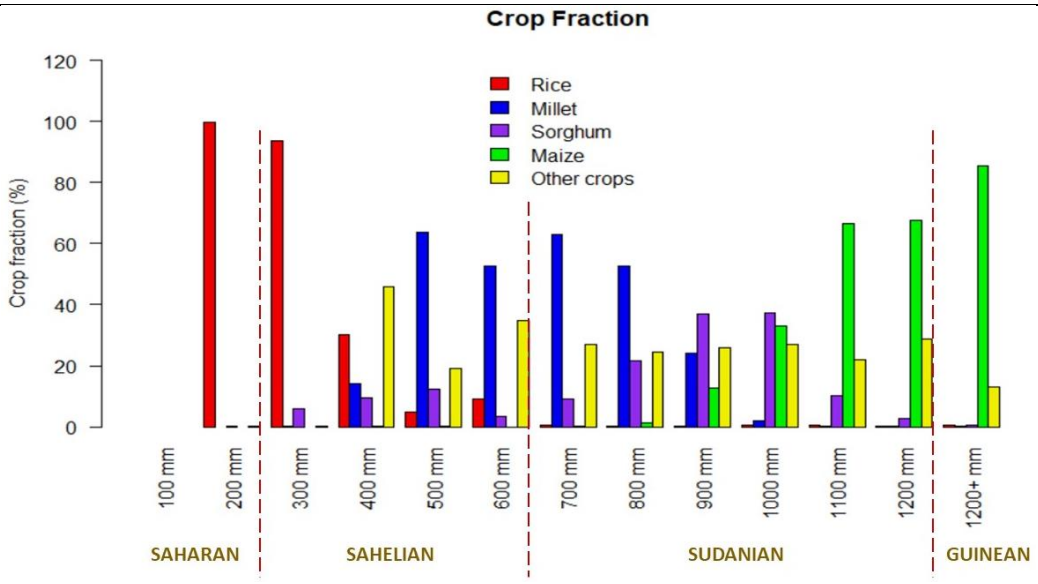

(B)

Figure 4. 5. Association of crop types and climate zones in Mali, West Africa. (A) Agroclimatic zones based on long-term mean annual rainfall (MAP), and (B) the fraction of different crop types grown in each 100 mm MAP interval.

4.5. Conclusions

A new 30 m - crop type map of rainfed maize, millet, rice, and sorghum has been developed for the country of Mali in West Africa using satellite remote sensing data and machine learning techniques. The nominal year is 2017. Overall, total accuracy is ~78% with class-specific accuracies between 77% and 94% for user's accuracy, and 53% and 87% for producer's accuracy. Our analysis also shows that allocation disagreement (related to crop type spatial location error), as compared to quantity disagreement (related to crop type area estimation error), constitutes the most important source of classification errors in the new dataset, and more than 80% of this total allocation disagreement is contributed by the Other crops class. That is, the developed crop type product is equally reliable in both area estimation and spatial allocation for all four subsistence cereal crops (i.e. maize, millet, rice, and sorghum).

In the period of study, area estimations show that millet is the most planted cereal across the country, followed by maize and sorghum. Rainfed and recession (i.e. flood plain) rice is mainly cultivated along the major rivers and occupies a much smaller area than the three subsistence cereal crops. An aggregate crop class ("other crops") includes small-scale vegetable gardens for household consumption that are widespread across Mali, and local specialty crops (onions, groundnuts, cotton) for local markets and export.

From north to south, the analysis of cultivated areas demonstrates the association of crop types with the mean annual precipitation gradient. Rainfed and recession rice is the exception to this pattern because this crop is cultivated in river valleys and depressions where annual flooding decouples the crop from local rainfall. Thus, rice farms are present, but at different intensity, in all four climatic zones from Saharan to Guinean. However, in addition to the precipitation regime, the intensity of a specific crop proportion in a particular geographical region may be influenced by other factors such as cultural, social, and market considerations that may favor particular crops in specialist agricultural zones.

Gaining an accurate understanding of the distribution of the major subsistence cereal crops at 30 m spatial resolution for the whole country of Mali is a critical contribution for decision making in food security planning. It allows area estimations to be disaggregated into individual crop types at a relatively fine spatial resolution appropriate to Sahelian field-

sizes, which can be used to improve yield statistics at different administrative subdivisions levels (from local to national scales). As agricultural production is estimated by knowing both crop areas and average yields for each crop in a particular area, estimating these two variables constitutes the major components of all operational agricultural monitoring systems. More detailed information on not only cropland area (Samasse et al., 2020) but specific crop types (this study) also allows for improved planning and development interventions relative to agronomic enhancement (improved seeds, fertilizer) and other agricultural inputs. Results found in this study confirm that crop type can be accurately estimated using a combination of remotely sensed data, ground data, and ensemble machine learning techniques. Crop type information, whether mapped at the scale of individual fields or aggregated to estimate fraction of different crops planted at county (commune) scale, is an essential step forward towards the longer-term goal to monitor and forecast agricultural yields for improved food security and famine early warning for the rural populations of Mali.

Appendix 4.A: Independent variables

In addition to weather (Precipitation, Temperature), and terrain (Elevation, Slope) information, we used four vegetation indices (NDVI, EVI, SAVI, MSAVI) derived from Landsat 8 surface reflectance, as predictors to fit RF machine learning models.

4.A.1. Climate (Precipitation)

Precipitation is extracted based on plot locations from the Climate Hazards Group InfraRed Precipitation with Station data (CHIRPS) (Funk et al., 2015). CHIRPS is a quasi-global rainfall dataset combining 0.05° (~6 km) resolution satellite imagery with in-situ station data to create gridded rainfall time series for diverse applications including crop monitoring. The CHIRPS dataset is freely available from 1981 to present. In this study, we computed and used as predictors the long-term (2000-2018) mean total rainfall during dry and wet seasons (Figures 4.A.1 and A1).

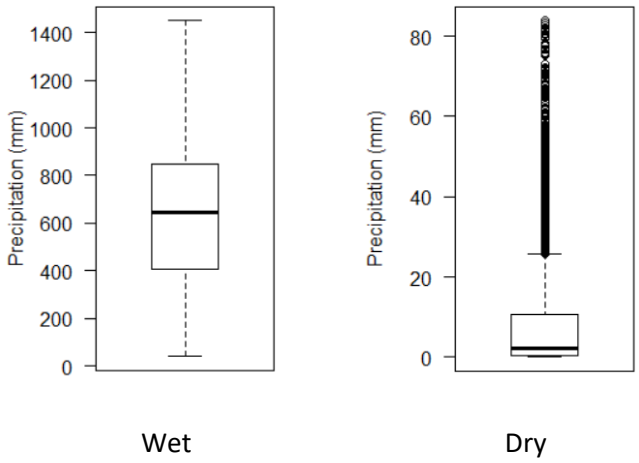

Figure 4.A. 1 Distribution of wet and dry season long-term mean precipitation across 13,000 Malian Ministry of Agriculture (MMA) field survey sites

4.A.2. Vegetation indexes (NDVI, EVI, SAVI, MSAVI)

Remote sensing derived vegetation indices (VI) have been extensively applied to detect vegetation, monitor vegetation condition, and map cropland over large areas (Samasse et al., 2020). These indices are generally based on the capability of vegetation to strongly reflect incident electromagnetic signal in the near-infrared (NIR) band compared to the optical bands. In this study, four of these vegetation indices are computed from

Landsat 8 surface reflectance and used as candidate predictor variables for the random forest model to help classify major cereal crops across the country of Mali. These VI are the Normalized Difference Vegetation Index (NDVI), the Enhanced Vegetation Index (EVI), the Soil Adjusted Vegetation Index (SAVI), and the Modified Soil-Adjusted Vegetation Index (MSAVI) (Figure 4.A.2).

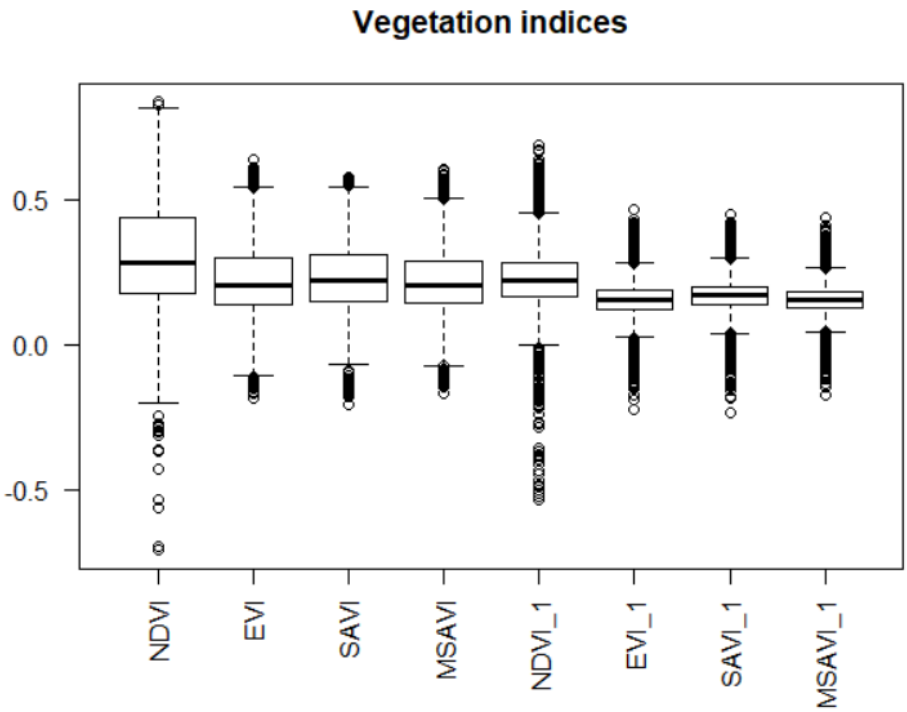

Figure 4.A. 2. Distribution of vegetation index values across ~13,000 MMA field survey sites used as predictors for regression models. Values for all four VI are extracted from GEE for wet and dry season months (suffix '_1' indicates dry season).

4.A.3. Terrain

Information on terrain elevation and slope could bring supplemental insights on estimating and understanding crop yield. The Shuttle Radar Topography Mission (SRTM) digital elevation data is an international research effort that obtained digital elevation models on a near-global scale (Farr et al., 2007). The SRTM V3 product used in this study (Figure 4.A.3) is provided by NASA JPL and available on the Google Earth Engine platform. It is a high-resolution elevation dataset, 1 arc-second (approximately 30m), and has undergone a void-filling process.

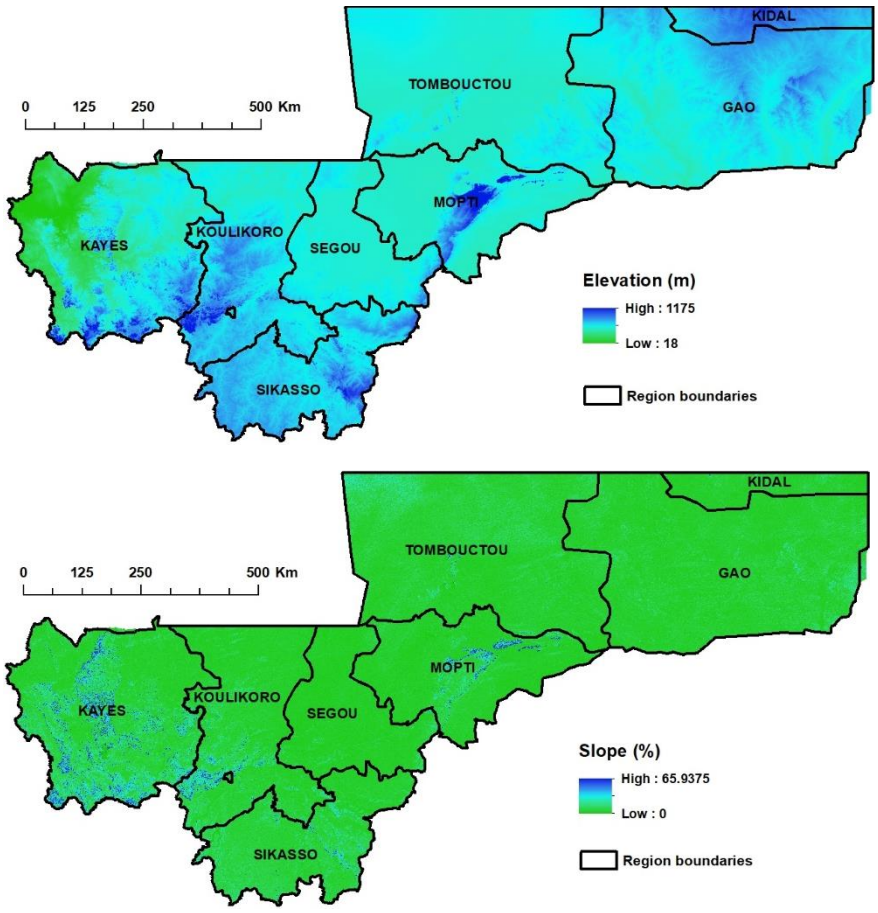

Figure 4.A. 3. Elevation and slope used as terrain information. Slope is computed from SRTM dataset available in Google Earth Engine (GEE)

Appendix 4.B. Random Forest Model

4.B.1 Tuning parameters

The *tuneRF ()* function in the R software is used to tune random forest hyper parameter *mtry* which minimizes the Out-Of-Bag (OOB) error for a given number of trees (*nTree*). An optimal value of *mtry* was computed for values of trees selected from 500 to 5000 with 500 intervals (i.e. 500, 1000, 1500, 2000, 2500, 3000, 3500, 4000, 4500, and 5000). The best tuned values of *mtry* and *nTree* are 24 and 3000, respectively (Table B1).

Table 4. 4. Out-Of-Bag error and best mtry for different number of trees, from 500 to 5000. nTree = 3000 gave the best fitted model

mtry	*OOB.error*	*nTree*
24	0.43109	3000
24	0.43109	3500
16	0.43109	5000
16	0.431505	4000
24	0.431624	2000
24	0.431743	2500
16	0.431921	4500
24	0.432336	500
16	0.432514	1500
24	0.43287	1000

The RF model trained using the best *mtry* and *nTree* is used to predict maize, millet, rice, and sorghum locations at 30 m spatial resolution across the country of Mali.

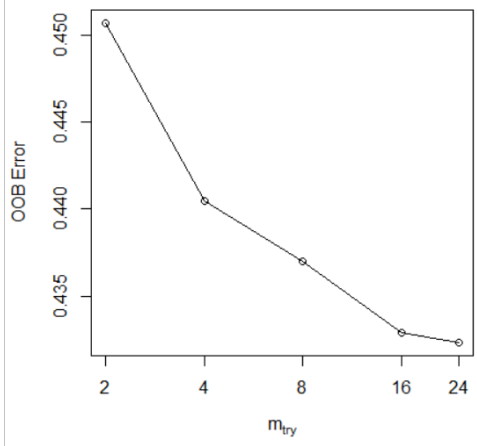

500

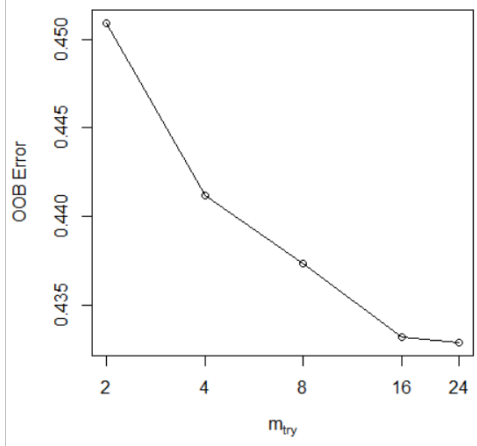

1000

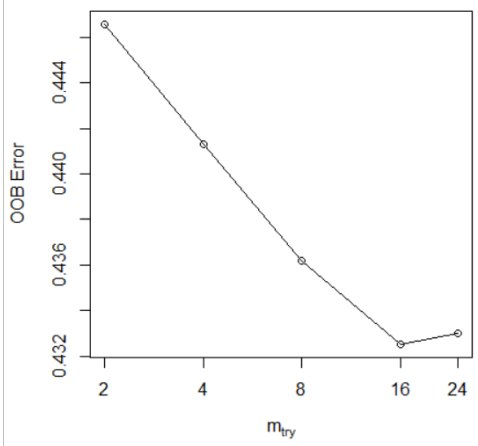

1500

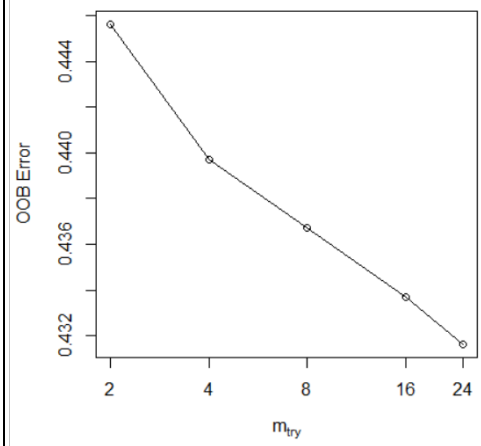

2000

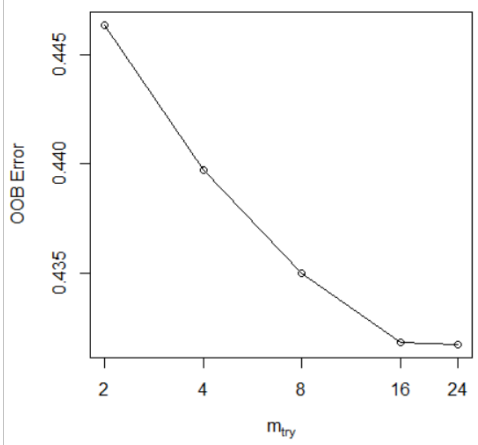

2500

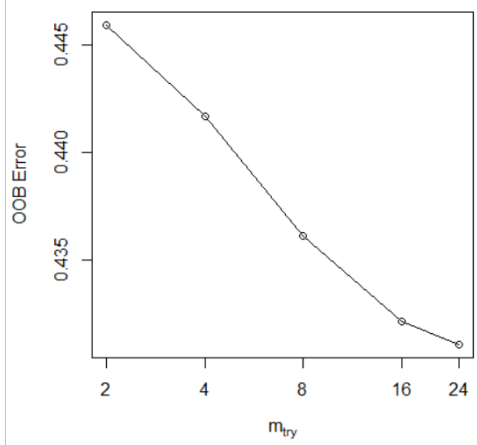

3000

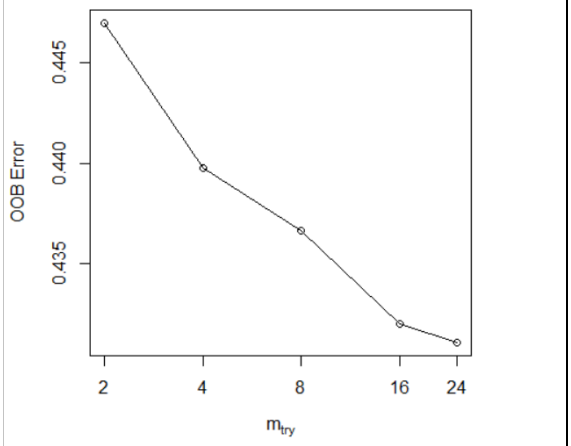

3500

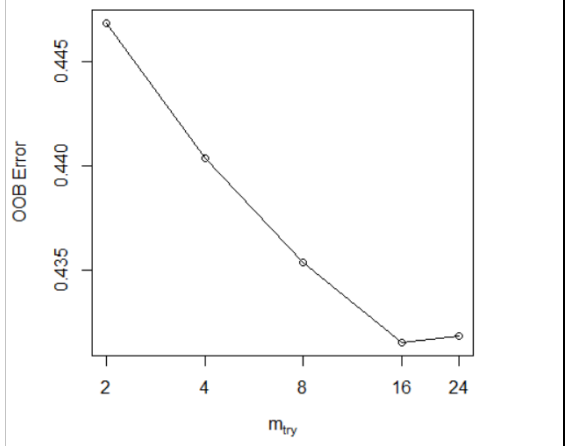

4000

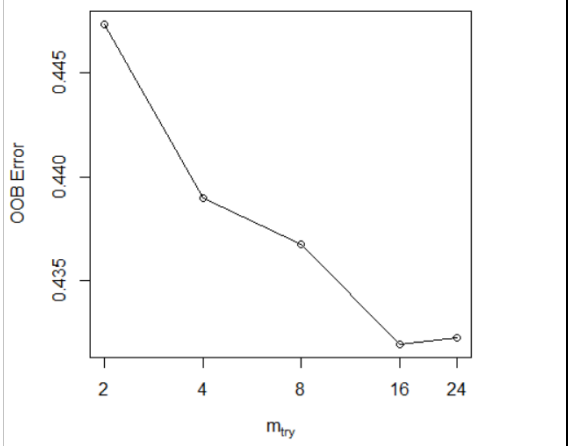

4500

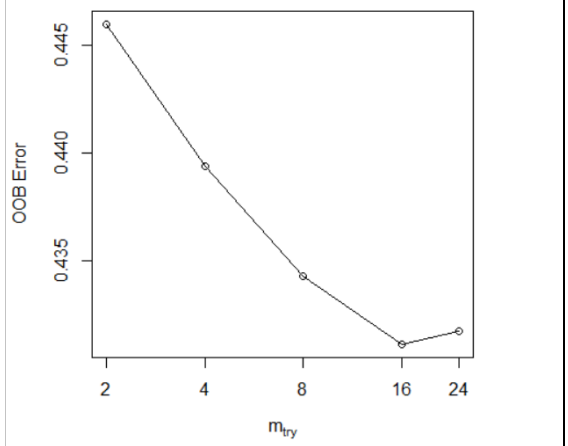

5000

Figure 4.B. 1. Out-Of-Bag error and best mtry for all number of trees values, lying from 500 to 5000. nTree = 3000 gave the best fitted model as illustrated by the ranked table (Table 4)

4.B.2. Fitted model

The best fitted model's output is the following.

```
Call:
 randomForest(formula = class ~ ., data = data_train, ntree = opt_ntree,
mtry = opt_mtry, importance = TRUE)
               Type of random forest: classification
                     Number of trees: 3000
No. of variables tried at each split: 24

        OOB estimate of  error rate: 43.1%
Confusion matrix:
     0   1    2   3   4    5 class.error
0 5696 101  221  51  58  375   0.1239619
```

```
1  203 486  151  18 212  565   0.7027523
2  213 144 1226   6 210  679   0.5052462
3  194  89   43 289  44  122   0.6299616
4  196 224  394  19 234  732   0.8699277
5  361 426  784  40 387 1655   0.5469477
```

4.B.3. Variables importance and Error plots

The Random forest algorithm offers the possibility to rank variables, which is useful for interpreting the results. The most influential predictors in our best fitted model are those related to weather (Precipitation) and terrain (Elevation). Surface reflectance in near-infrared (NIR; Band 5) and shortwave infrared (SWIR; Band 7), are more important in predicting crop type than the first highly ranked vegetation index, which is NDVI. The other vegetation indices (i.e. EVI, SAVI, and MSAVI), for both wet and dry seasons, seem to have lower significance on the RF classifier outcomes in this analysis (Figure 4.B,2).

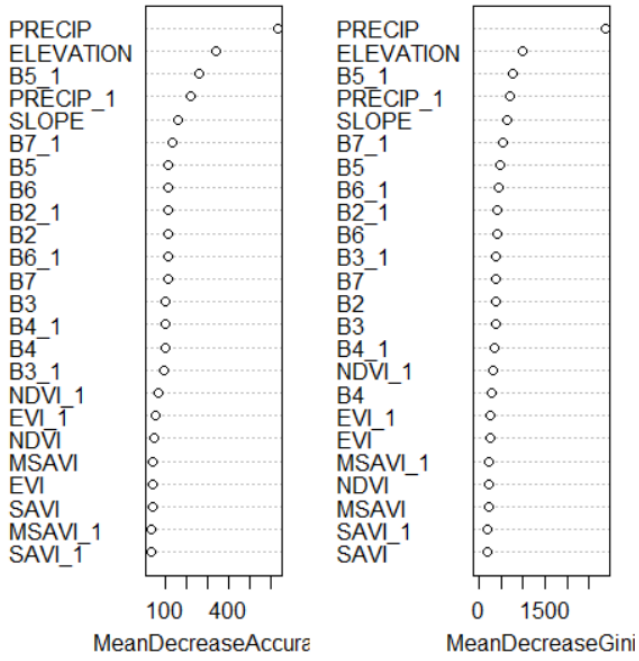

Figure 4.B. 2. Variables' importance for mean decrease in accuracy and mean decrease in node impurity

4.B.4. Testing the model

Table 4. 5. Error matrix based on testing samples. N is the total number of pixels by categories

	Maize	Millet	Rice	Sorghum	Other crops	Sum	N
Maize	327	12	19	26	40	424	16132517
Millet	8	501	4	36	87	636	22361209
Rice	2	0	158	1	7	168	1498883
Sorghum	12	19	3	307	53	394	13921521
Other crops	59	65	13	60	695	892	19379749
							67238494

Table 4. 6. Error matrix based on population estimate as suggested by (Pontius Jr & Millones, 2011)

	Maize	Millet	Rice	Sorghum	Other crops
Maize	0.1698	0.0062	0.0099	0.0135	0.0208
Millet	0.0038	0.2403	0.0019	0.0173	0.0417
Rice	0.0002	0.0000	0.0192	0.0001	0.0009
Sorghum	0.0058	0.0092	0.0014	0.1480	0.0256
Other crops	0.0175	0.0193	0.0039	0.0178	0.2060

Table 4. 7. Accuracy metrics by crop types

	Maize	Millet	Rice	Sorghum	Other crops	All crops
Quantity Disagreement	2.78	3.72	1.66	2.72	2.11	6.50
Allocation Disagreement	5.42	6.69	0.27	5.17	12.73	15.13
Proportion Correct	18.50	26.20	2.10	9.12	22.46	78.37
User’s Accuracy	77.12	78.77	94.05	77.92	77.91	
Producer’s Accuracy	87.24	88.68	53.90	63.21	72.59	

4.6. References

Adams, A. M., Gillespie, A. W., Kar, G., Koala, S., Ouattara, B., Kimaro, A. A., Bationo, A., Akponikpe, P. B. I., Schoenau, J. J., & Peak, D. (2016). Long term effects of reduced fertilizer rates on millet yields and soil properties in the West-African Sahel. Nutrient Cycling in Agroecosystems, 106(1), 17–29.

Barbier, B., Yacouba, H., Karambiri, H., Zoromé, M., & Somé, B. (2009). Human vulnerability to climate variability in the Sahel: farmers' adaptation strategies in northern Burkina Faso. Environmental Management, 43(5), 790–803.

Bolton, D. K., & Friedl, M. A. (2013). Forecasting crop yield using remotely sensed vegetation indices and crop phenology metrics. Agricultural and Forest Meteorology, 173, 74–84. https://doi.org/10.1016/j.agrformet.2013.01.007

Breman, H., Groot, J. J. R., & van Keulen, H. (2001). Resource limitations in Sahelian agriculture. Global Environmental Change, 11(1), 59–68.

Brown, M. E. (2008). Famine early warning systems and remote sensing data. In Famine Early Warning Systems and Remote Sensing Data. https://doi.org/10.1007/978-3-540-75369-8

Congalton, R. G. (1991). A review of assessing the accuracy of classifications of remotely sensed data. Remote Sensing of Environment, 37(1), 35–46.

der Geest, K., & Dietz, T. (2004). A literature survey about risk and vulnerability in drylands, with a focus on the Sahel. In The impact of climate change on drylands (pp. 117–146). Springer.

FAO, & WFP. (2020). FAO-WFP early warning analysis of acute food insecurity hotspots. July, 1–25. http://www.fao.org/3/cb0258en/CB0258EN.pdf

Farr, T. G., Rosen, P. A., Caro, E., Crippen, R., Duren, R., Hensley, S., Kobrick, M., Paller, M., Rodriguez, E., Roth, L., & others. (2007). The shuttle radar topography mission. Reviews of Geophysics, 45(2).

FEWS NET. (2020). USGS FEWS NET Data Portal. https://earlywarning.usgs.gov/fews

Fritz, S., You, L., Bun, A., See, L., McCallum, I., Schill, C., Perger, C., Liu, J., Hansen, M., & Obersteiner, M. (2011). Cropland for sub-Saharan Africa: A synergistic approach using five land cover data sets. Geophysical Research Letters, 38(4).

Funk, C., Peterson, P., Landsfeld, M., Pedreros, D., Verdin, J., Shukla, S., Husak, G., Rowland, J., Harrison, L., Hoell, A., & Michaelsen, J. (2015). The climate hazards infrared precipitation with stations - A new environmental record for monitoring extremes. Scientific Data. https://doi.org/10.1038/sdata.2015.66

Hasmadi, M., Pakhriazad, H. Z., & Shahrin, M. F. (2009). Evaluating supervised and unsupervised techniques for land cover mapping using remote sensing data. Geografia: Malaysian Journal of Society and Space, 5(1), 1–10.

Jin, Z., Azzari, G., You, C., Di Tommaso, S., Aston, S., Burke, M., & Lobell, D. B. (2019). Smallholder maize area and yield mapping at national scales with Google Earth Engine. Remote Sensing of Environment, 228, 115–128.

Konduri, V. S., Kumar, J., Hargrove, W. W., Hoffman, F. M., & Ganguly, A. R. (2020). Mapping crops within the growing season across the United States. Remote Sensing of Environment, 251, 112048.

Lambert, M. J., Waldner, F., & Defourny, P. (2016). Cropland mapping over Sahelian and Sudanian agrosystems: A Knowledge-based approach using PROBA-V time series at 100-m. Remote Sensing, 8(3). https://doi.org/10.3390/rs8030232

Lambin, E. F., Cashman, P., Moody, A., Parkhurst, B. H., Pax, M. H., & Schaaf, C. B. (1993). Agricultural Production Monitoring in the Sahel Using Remote Sensing: Present Possibilities and Research Needs. Journal of Environmental Management. https://doi.org/10.1006/jema.1993.1047

Maselli, F., & Rembold, F. (2001). Analysis of GAC NDVI data for cropland identification and yield forecasting in Mediterranean African countries. Photogrammetric Engineering and Remote Sensing.

Ministère de L'Agriculture. (2018). Plan de campagne agricole consolidé et harmonisé 2018/2019.

Olofsson, P., Foody, G. M., Herold, M., Stehman, S. V, Woodcock, C. E., & Wulder, M. A. (2014). Good practices for estimating area and assessing accuracy of land change. Remote Sensing of Environment, 148, 42–57.

Pal, M. (2005). Random forest classifier for remote sensing classification. International Journal of Remote Sensing, 26(1), 217–222. https://doi.org/10.1080/01431160412331269698

Pontius Jr, R. G., & Millones, M. (2011). Death to Kappa: birth of quantity disagreement and allocation disagreement for accuracy assessment. International Journal of Remote Sensing, 32(15), 4407–4429.

Ramankutty, N. (2004). Croplands in West Africa: A Geographically Explicit Dataset for Use in Models. Earth Interactions. https://doi.org/10.1175/1087-3562(2004)8<1:ciwaag>2.0.co;2

Ross, K. W., Brown, M. E., Verdin, J. P., & Underwood, L. W. (2009). Review of FEWS NET biophysical monitoring requirements. In Environmental Research Letters. https://doi.org/10.1088/1748-9326/4/2/024009

Samasse, K., Hanan, N. P., Anchang, J. Y., & Diallo, Y. (2020). A high-resolution cropland map for the West African Sahel based on high-density training data, google earth engine, and locally optimized machine learning. Remote Sensing. https://doi.org/10.3390/RS12091436

Samasse, K., Hanan, N. P., Tappan, G., & Diallo, Y. (2018). Assessing cropland area in West Africa for agricultural yield analysis. Remote Sensing, 10(11). https://doi.org/10.3390/rs10111785

Shahhosseini, M., Hu, G., & Archontoulis, S. V. (2020). Forecasting Corn Yield With Machine Learning Ensembles. Frontiers in Plant Science. https://doi.org/10.3389/fpls.2020.01120

Shao, G., & Wu, J. (2008). On the accuracy of landscape pattern analysis using remote sensing data. Landscape Ecology, 23(5), 505–511.

Sissoko, K., van Keulen, H., Verhagen, J., Tekken, V., & Battaglini, A. (2011). Agriculture, livelihoods and climate change in the West African Sahel. Regional Environmental Change, 11(1), 119–125.

Thenkabail, P., Lyon, J. G., Turral, H., & Biradar, C. (2009). Remote sensing of global croplands for food security. CRC Press.

Tong, X., Brandt, M., Hiernaux, P., Herrmann, S., Rasmussen, L. V., Rasmussen, K., Tian, F., Tagesson, T., Zhang, W., & Fensholt, R. (2020). The forgotten land use class: Mapping of fallow fields across the Sahel using Sentinel-2. Remote Sensing of Environment, 239, 111598.

Vignaroli, P., Rocchi, L., De Filippis, T., Tarchiani, V., Bacci, M., Toscano, P., Pasqui, M., & Rapisardi, E. (2016). The Crop Risk Zones Monitoring System for resilience to drought in the Sahel. In Geophysical Research Abstracts.

Wang, S., Azzari, G., & Lobell, D. B. (2019). Crop type mapping without field-level labels: Random forest transfer and unsupervised clustering techniques. Remote Sensing of Environment. https://doi.org/10.1016/j.rse.2018.12.026

Xiong, J., Thenkabail, P. S., Tilton, J. C., Gumma, M. K., Teluguntla, P., Oliphant, A., Congalton, R. G., Yadav, K., & Gorelick, N. (2017). Nominal 30-m cropland extent map of continental Africa by integrating pixel-based and object-based algorithms using Sentinel-2 and Landsat-8 data on google earth engine. Remote Sensing, 9(10), 1–27. https://doi.org/10.3390/rs9101065

CHAPTER 5

Preliminary analysis of crop yield predictions using satellite and environmental data for maize production in Mali, West Africa

Paper #4

In preparation for submission

5.1. Introduction

Information on crop area and yield is critical for agricultural development in low-income countries because it contributes to a parsimonious allocation of scarce resources dedicated to the agricultural sector and constitutes a fundamental input for planning and making important decisions related to food security issues (Wineman et al., 2019). The two variables (crop area and yield) are required to estimate agricultural production. In Mali, like in other developing countries, crop area and yield are estimated by combining field assessments and statistical methods to extrapolate area and average yield from plots to administrative subdivisions scales. In general, errors due to these statistical estimations are not accurately known (Ministère de l'Agriculture, 2018), making these estimates poor. As alternatives to improve crop yield estimation accuracy and reduce costs induced by traditional methods of field surveying, various yield modeling approaches are used for both short-term and scenarios-based long-term predictions of yield. Two of these modeling approaches are process-based models which dynamically simulate crop growth and yield formation processes (e.g. Holzworth et al., 2014; Jones et al., 2003; Williams et al., 1989) and statistical models which relate yield to various predictors (e.g., soils. rainfall) based on empirical relationships derived from measured or observed historical data (e.g. Kern et al., 2018; Li et al., 2019).

Whether they are process-based or empirical models, crop yields predictions require timely and spatially resolved information on weather, soil, crop type and management. As satellite remotely sensed data are continuously improving in terms of spatial and temporal resolutions, they become valuable inputs forecasting crop yields on a large-scale basis using models, particularly in data-deficit regions such as the Sahel. Several previous

studies have examined how variables derived from satellite data, such as vegetation indices and soil moisture, can be combined with meteorological and other environmental information for improved process-based or statistical crop yield modelling. For example, Li et al. (2019) developed multiple statistical modeling methods for predicting rainfed corn yield in the U.S. Midwest. They combined satellite variables, such as MODIS land surface temperature and Enhanced Vegetation Index (EVI) with climate variables which include monthly mean vapor pressure deficit, mean air temperature, and monthly precipitation. Their results showed that satellite variables used alone as predictors give improvements in yield predictions compared to models based on climate variables alone. Remote sensing can also be used to estimate crop growth indicators, which can be integrated with crop growth simulation in process-based models for improved predictions. This technique, commonly known as data assimilation, has proven to be the most promising approach to increasing crop growth and yield estimation accuracy (Y. Xie et al., 2017). For example, Thorp et al. (2010) assimilated measured LAI in the DSSAT-CSM-Wheat model using forcing and updating methods. The forcing method consists of replacing a simulated state variable with a remote sensing observation, while in the updating approach the model state variables are continuously updated whenever an observation is available. A third method is "steering" which aims to re-initialize (e.g., sowing date, planting density) or re-parameterize (e.g., canopy and growth parameters) the crop growth model in a way that minimizes the difference between simulated and measured data (Ines et al., 2013). The assumption of this latter method is that the variable derived from remotely sensed data is free of error or that the level of data error is acceptable to be propagated within the modelling system. However, satellite data assimilation in process-based models is not an easy task and, as these models are point-based simulators, we still need further processing to spatialize model outputs for yield estimation at larger scale (e.g. Venkatesan & Pazhanivelan, 2018).

More recently, in parallel with process based and statistical models, machine learning techniques have been applied with satellite-derived datasets as predictors for crop yield predictions. In all cases, it has been found that machine learning models outperformed regular statistical approaches. Techniques of machine learning include multivariate regression, random forest, support vector machine, boosted regression trees, and artificial

neural networks (Cai et al., 2019; Khaki & Wang, 2019; A. Li et al., 2007; Peng et al., 2020; Schwalbert et al., 2020). Machine learning models have advantages to treat the dependent variable (crop yield) as an implicit function of predictors (e.g. climate, soil), allowing for highly non-linear functions when needed (Khaki & Wang, 2019).

In this study, we focus on crop yield of maize, a critical staple crop for many rural communities in Mali, using yield data from geo-localized plots provided by the Malian Department of Agriculture as reference data to train two machine learning models (Random Forest and Boosted Regression Trees) for yield modelling and predictions. All predictors were extracted for maize fields using the recently developed crop type map, which is used as a mask (Samasse et al., 2020). In total, 80% of 553 plot samples were used to train machine learning models, the remaining 20% were held apart for model testing and error quantification. Prediction performance was initially tested for independent plots in the training year (2017). Separately, we tested the ability of models fitted to data in 2017 to be used for forecasting yields in 2018.

5.2. Methods

5.2.1. Dependent variable (maize yield)

Agricultural statistics data, including yields by crop type, are sampled annually by the Statistics and Planning Agency of the Malian Department of Agriculture. For this analysis, field data reported maize yields are the dependent variable. To reduce redundancy in the training dataset, a minimum distance of 200 m between plots has been observed, and only pure maize fields are included in this analysis. In total, we have 553 maize yield samples distributed across Mali to train the models. They are a subset of the dataset used to develop the crop type map detailed in Chapter 4 (Samasse et al., 2020). Basics statistics of the training dataset are shown in Figure 5.1, with average maize yields of about 2,000 kg/ha but with considerable variability between samples. Spatially, Figure 5.2 shows locations of maize plots for 2017. We focused on the Koulikoro Region to illustrate spatial distribution of maize plots across the region.

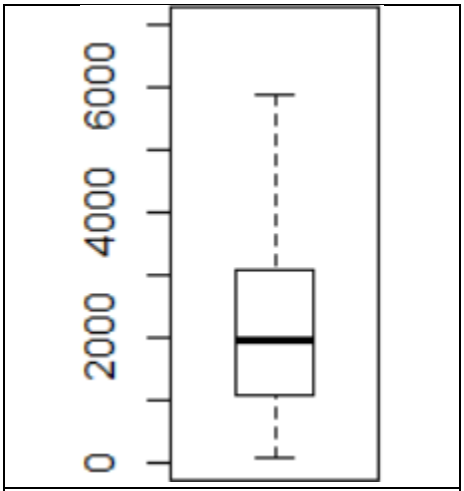

N = 553, mean = 2144.6 kg/ha, sd = 1321.7 Kg/ha

Figure 5. 1. Maize yield training dataset used in this study, after removing outliers. Year = 2017.

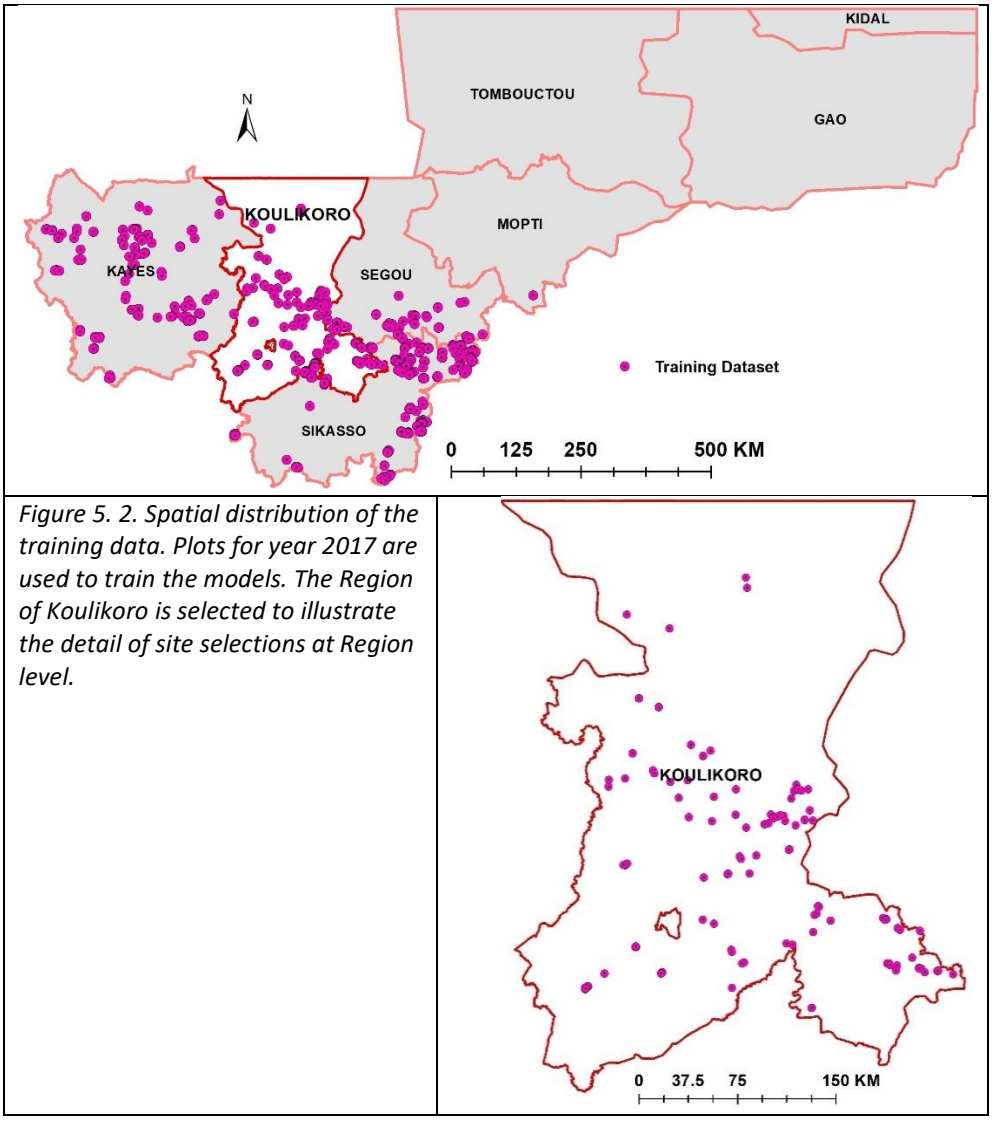

Figure 5. 2. Spatial distribution of the training data. Plots for year 2017 are used to train the models. The Region of Koulikoro is selected to illustrate the detail of site selections at Region level.

5.2.2. Independent variables or Predictors

The candidate independent data used to model maize yield variability across Mali include growing season meteorological variables (monthly cumulative rainfall, temperature), Landsat-8 measurements of growing season vegetation indices including the normalized difference vegetation index (NDVI), enhanced vegetation index (EVI), and normalized difference water index (NDWI). Full details are provided in Appendix 5.A.

5.2.3. Models

In this study, two machine learning techniques, Random Forest (RF) and Boosted Regression Trees (BRT), are used for maize yield predictions. Climate, and satellite-derived vegetation indices are used as independent variables. All datasets were projected to WGS84 before extracting values for the locations of the dependent maize plots. Both RF and BRT models are assessed using internal cross-validation before accuracy assessment using independent validation data in both 2017 (year of the training data) and 2018.

5.2.3.1. Random Forest

Random Forest (RF) modeling is an ensemble learning algorithm that can be used to predict both continuous (regression) and categorical (classification) responses. The regression forms are used in this study to model yield variability. An RF model comprises an ensemble of decision trees, where each tree can predict the response variable using a random sub-sample of the independent variables and observations. Each tree uses a sub-ensemble of training values chosen randomly with replacement (i.e. the bootstrap sample). The optimum number of predictors used to split data at each tree's node is $log(m+1)$, where m is the total number of predictors involved. An ensemble of diverse trees minimizes the effect of bias from individual trees, considerably improving the overall predictive accuracy of the model. In regression, the final predicted value is chosen by averaging output of individual trees. It has been shown that by increasing the number of trees in the model, the errors of prediction (also known as out-of-bag errors or OOB errors) converge, reducing problems with overfitting (Pal, 2005). In this study we used estimation based on the RMSE error during the training process to fine-tune RF model hyper-parameters (*mtry* and *ntree*).

5.2.3.2. Boosted Regression Trees

Boosted Regression Tree (BRT) models combine decision tree algorithms and boosting methods. They are an ensemble learner, as they repeatedly fit many decision trees to improve the accuracy of the final model. BRT models use a boosting approach to fit new trees. Boosting consists of giving a higher probability to data that was poorly modelled by previous trees to be selected to fit the new tree. That is, after fitting the first tree, the model

will consider prediction errors to fit the next tree. This is not the case in RF models where trees are built independently using random subsets of the training dataset. Training data points are selected at equal probability. By considering the fit of previous trees, BRT models try continuously to improve predictions accuracy. In this study, we used the Gradient Boosted Model (GBM) approach implemented in R statistics. Three major parameters are tuned to get optimal predictions of maize yield. These parameters are the number of trees, the interaction depth, and the shrinkage.

5.3. Results

5.3.1. Model selection

In Machine Learning techniques, getting parameters for optimal predictions is sometimes tedious and time consuming. All tuning processes have been done using the package Caret in R statistics. We first fitted models using all twenty (20) predictors for both RF and BRT, and monthly-based models afterward. Table 1 shows model performance in all cases. Based on tuning results, the best fitted model is the one using all predictors (Model 0: Full model) in both RF and BRT. For all five models, RF presents a lower RMSE in predicting maize yield for both 2017 and 2018 testing datasets as compared to BRT.

Table 5.1 Within-season diagnostic and between-season predictive model accuracy metrics for RF and BRT. Within-season diagnostic models use 20% independent test data for 2017, where training and test data share aspects of growing season conditions and the models rely on end of season yields for training (thus considered diagnostic models). The between-season predictive models use models fitted using 2017 data, with new data on weather and VI from 2018 to make "true" predictions of 2018 maize yields with varying lead-time and input data.

	Within-season diagnostic models 2017 dataset, 20 % of training, N = 110		Between-season predictive models 2018 dataset, N = 638	
	RMSE		RMSE	
	RF	BRT	RF	BRT
Model 0: Full model	362.0	449.9	706.7	973.7
Model 1: June-July	378.3	492.2	835.1	1079.7
Model 2: June-August	366.1	537.8	756.9	1020.0
Model 3: Weather	507.9	568.6	857.3	1169.3
Model 4: VI	454.6	752.4	858.7	938.0

Figure 5.3 illustrates plots of observed against predicted yields using the 20% reserved testing data in 2017 and independent yield data for 2018. RMSE values resulting from predicting yields for 2018 (707 kg/ha and 974 kg/ha) are approximately twice those in 2017 (362 kg/ha and 450 kg/ha). However, the RF model performs considerably better than the BRT model in all cases. In 2018 predictions, we also have weak linear relationships between predicted and observed values, as explained by the R^2 values, 20% and 14% for RF and BRT, respectively.

	RF	BRT
2017 current season	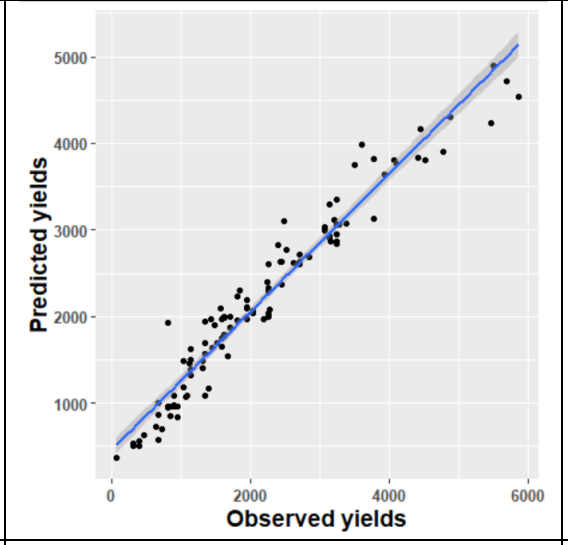	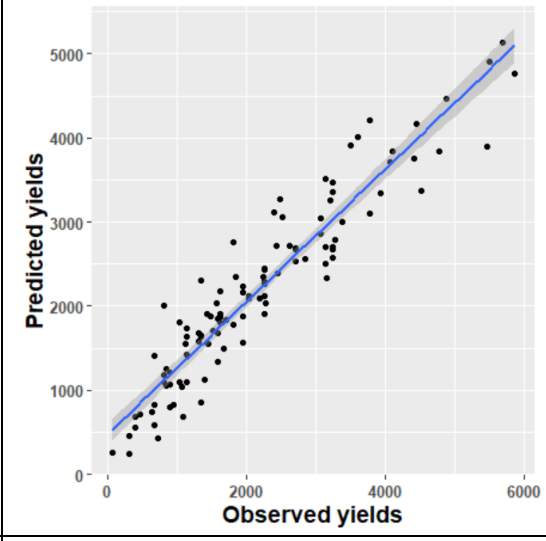
	R2 = 0.94; RMSE = 362.0538	R2 = 0.89; RMSE = 449.9059
2018 predicted based on 2017	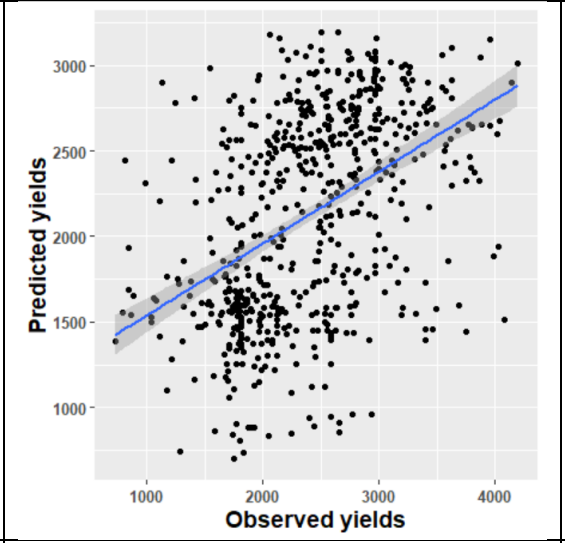	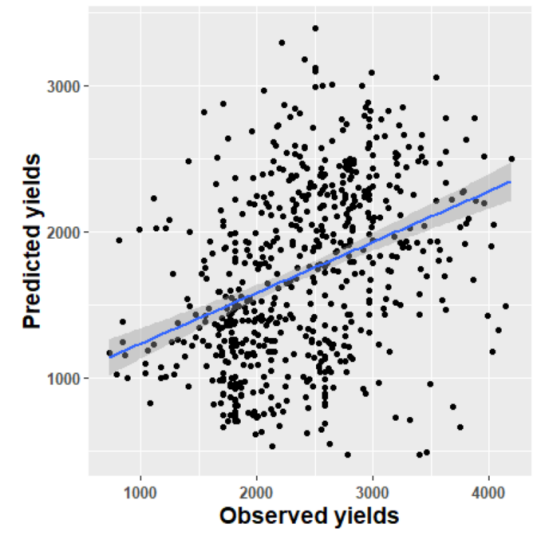
	R2 = 0.20; RMSE = 706.6981	R2 = 0.14; RMSE = 973.6933

Figure 5. 3. Best models for RF and BRT. Predicted yields are in kg/ha.

5.3.2. Variable importance

Based on the best model using the RF algorithm, all twenty predictors seem to have a non-negligible influence in building the model. However, climate variables (precipitation and air temperature) appear to be the most influential predictors (Figure 5.4). The first most important variable among vegetation indices (VI) is the NDWI, followed by EVI and NDVI. At monthly level, climate predictors extracted during August (month 8) are the most frequent in the five first most influential variables. At the same time, VI in August are the variables which contribute to increase model's performance.

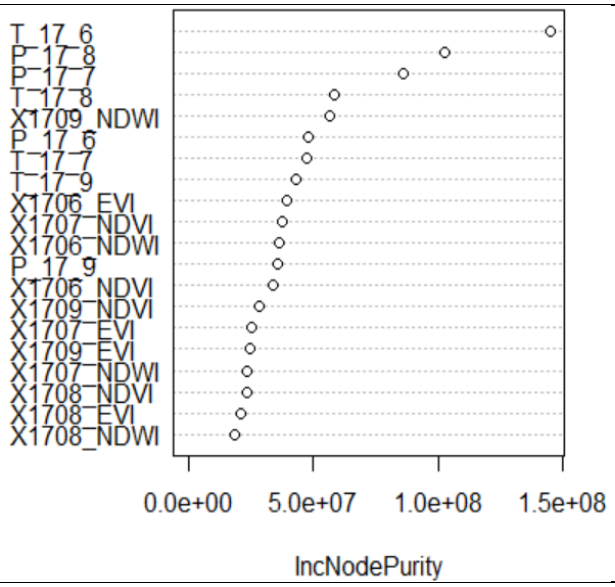

T_17_6 T_17_7 T_17_8 T_17_9	Temperature in June, July, August, September
P_17_6 P_17_7 P_17_8 P_17_9	Precipitation in June, July, August, September
X1706_NDVI X1707_NDVI X1708_NDVI X1709_NDVI	NDVI values in June, July, August, September
X1706_EVI X1707_EVI X1708_EVI X1709_EVI	EVI values in June, July, August, September
X1706_NDWI X1707_NDWI X1708_NDWI X1709_NDWI	NDWI values in June, July, August, September

Figure 5. 4: Variable importance plots for RF best model

5.3.3. Variable Partial Dependence

The Partial Dependence Plots (PDP) tell us the relationship between the dependent variable (maize yield) and the predictor variables (Figure 5.5). Figure 5.5 shows the PDP for the five most important predictors as ranked by the RF best predicting model. Maize yield increases with precipitation but decreases with mean air temperature. Yield is more impacted by temperature in August than in June, particularly at higher temperatures (above 28^{o}C); Figure 5.5. Regarding precipitation, increases in rainfall during August are more influential on predicted yield than July, but in both cases, yield increases with the amount of precipitation. For NDWI VI, higher values in September appear to lead to lower predicted yield, perhaps reflecting the impact of late rainfall on grain maturation and final yield.

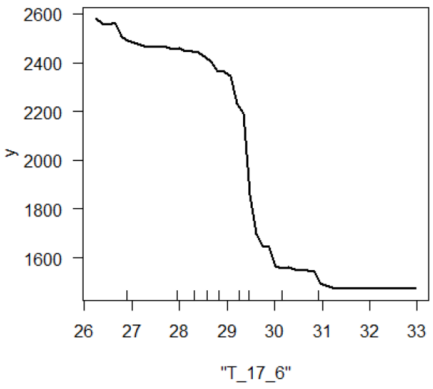

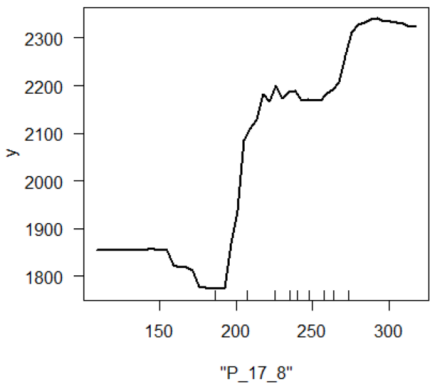

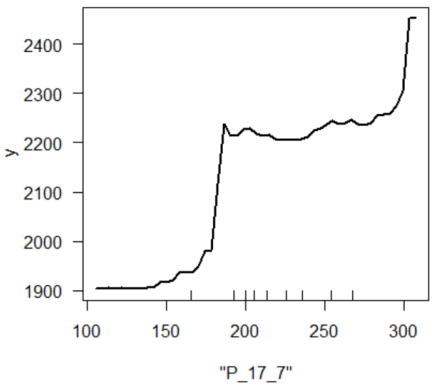

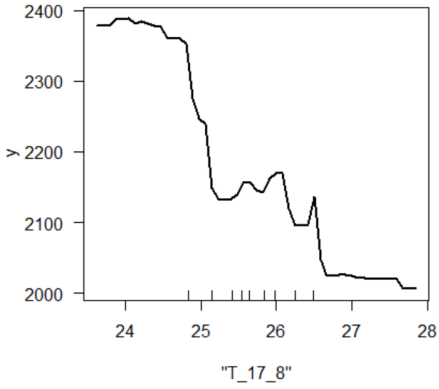

Figure 5. 5. Partial dependence plots for the five most important predictors as ranked by RF full model. P_17_7 and P_17_8 are precipitation in July and August of year 2017, respectively. T_17_6 and T_17_8 for 2017 mean air temperature in June and August, respectively. X1709_NDWI is NDWI vegetation index for September 2017.

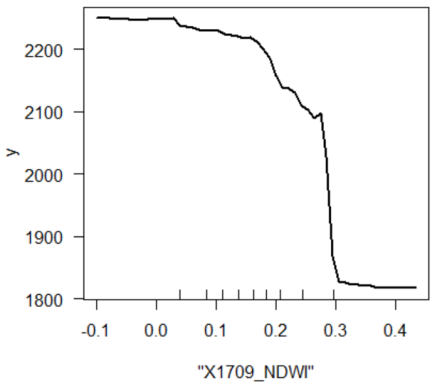

5.4. Discussion and Conclusions

In this study, we presented crop yield prediction based on the ensemble machine learning approach, using climate data and vegetation indices derived from satellite remote sensors. Results showed better maize yield prediction performance with random forest compared to boosted regression trees. This performance of random forest models is in line with results found by Peng et al. (2020) in maize and soybean yields estimation across the United States, and Leroux et al. (2019) who predicted maize yield in Burkina Faso (West Africa).

Results of testing the best model with out-of-sample (i.e. fully independent) data (20% of the 2017 observed yields) are promising. The 'full model' (Model 0) uses data on rainfall, temperature and vegetation indices through the entire growing season (June-September, corresponding to the beginning of maize harvest in Mali). Using Model 0 it was possible to predict maize yields with an RMSE of 362 kg/ha. Similar RMSE values were found for predictions using data extending only through July (378 kg/ha) and through August (366 kg/ha), suggesting that yield predictions greater than 1 or 2 months might be possible. These results are encouraging compared to previous studies.

However, prediction errors (RMSE) increase dramatically when trying to use models fitted using 2017 yield data to forecast maize yield in 2018 (year +1). Overall, models developed using 2017 data present lower reliabilities in predicting maize yield for a future agricultural season using climate (precipitation, temperature) and vegetation indices (NDVI, EVI, and NDWI) for the new growing season. With an RMSE of 706 kg/ha obtained in 2018, prediction error increases by more than 300 kg/ha compared to model performance in 2017. Results remain similar to findings of Leroux et al. (2019), who obtained an RMSE of 637 kg/ha predicting maize yields in years that were not included in fitting their models, against an error of 258 kg/ha resulting using a within-season cross-validation approach.

Vegetation indices derived from satellite remote sensing have been widely used in crop yield modeling. The main findings in this study are that models based only on VI data (i.e. without input of seasonal rainfall and temperature data) perform much less well than

combined models (Table 5.1). Among the candidate VI data, the Normalized Difference Vegetation Index (NDVI) performed better in predicting independent 2017 samples, as compared to the Normalized Difference Water Index (NDWI), and the Enhanced Vegetation Index (EVI), while the NDWI had lower RMSE for 2018 data. That is, with NDVI, EVI, and NDWI used alone and separately to fit random forest models, we obtained RMSEs of 494 kg/ha, 623 kg/ha, and 577 kg/ha, respectively for testing using out-of-sample independent data, and 984 kg/ha, 888 kg/ha, and 812 kg/ha for 2018 data, respectively (Appendix B).

NDWI of September is the most influential predictor, probably because of the importance of water availability for the maize crop at this growing step, and NDWI sensitivity to water content in semiarid region. However, the NDVI index has higher occurrences among the five most important predictors (Figure 5.6). June is considered in this study as the first month of crop growing season, and is the most influential month in the VI-based model. However, predictors extracted in August, the month with the maximum quantity of precipitation (Figure 5.6), seem to bring less information in the learning process compared to the other three months (i.e. June, July, and September).

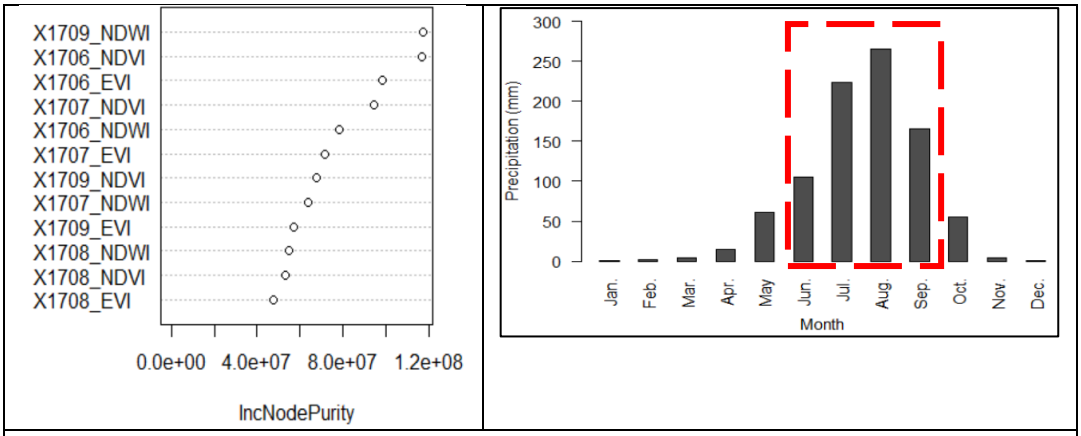

Figure 5. 6. Variables importance for NDVI, EVI, and NDWI

Overall, results found in this analysis on maize yield predictions using machine learning techniques at plot levels for the whole country of Mali are encouraging and constitute an important step to the development of operational satellite remote sensing based crop yield forecasting applications in support of food production estimates. This

early estimate of crop yield information represents an input in decision making at local and national levels in agricultural production management. In this study, Random forest algorithms provide better prediction performance than boosted regression trees and capture the complex relationships between maize yield, seasonal weather and satellite VI predictors. The analysis of variables importance provides an opportunity to identify variables with the most predictive power, but the model does not provide any further possibility to control or understand the internal functions that link maize yield to these variables. Another weakness of the fitted models in our study is the low performance in predicting yield out of the period of study. However, as additional data become available, it may be possible to further improve the predictive power of the models.

Results for yield predictions in 2017 showed that Random Forest ensemble approaches have a higher performance in predicting maize yields across Mali as compared to Boosted Regression Trees. NDVI, EVI, and NDWI derived from Landsat 8 optical bands are reliable contributors for maize yields estimation at field scale in a semi-arid region like the Sahel. However, models developed using data from 2017 were considerably less effective in forecasting yields in 2018. This suggests that season-specific variables (timing of rainfall, temperatures and other agronomic variables) are significant in controlling end of season yields, such that models fitted in the prior year are probably not going to be effective in a later year. High within-year predictive ability, as found here for maize yields in 2017, can be useful for food security planning purposes, if they can be produced with minimal delay following harvest (e.g. 1-2 weeks). Such model would provide managers an effective ability to interpolate between field measurements of yield to provide a more comprehensive understanding of the current year's harvest across the country than available using only field samples. For true yield forecasting, while the 2018 example shown here was less effective, it may be that RF models trained with many years of data would include sufficient inter-annual variability to produce acceptable (useful) yield forecasts.

Appendix 5.A: Independent variables

5.A.1. Climate (Precipitation, Temperature)

Precipitation and temperature are extracted based on cropped plots locations from the Climate Hazards Group InfraRed Precipitation with Station data (CHIRPS) (Funk et al., 2015) and the Famine Early Warning Systems Network (FEWS NET) Land Data Assimilation System (FLDAS) (McNally et al., 2017), respectively. CHIRPS is a quasi-global rainfall dataset combining 0.05° (~6 km) resolution satellite imagery with in-situ station data to create gridded rainfall time series for diverse applications including crop monitoring. CHIRPS dataset is freely available from 1981 to present. While FLDAS includes information on many other climate-related variables including moisture content, humidity, evapotranspiration, average air and soil temperature. The main goal of FLDAS was to support regions which lack sufficient weather data for food security assessments. It In this study, we computed and used as predictors the total rainfall and the mean air temperature (Figure 5.A.1) for each of the four months of crop growing season in Mali.

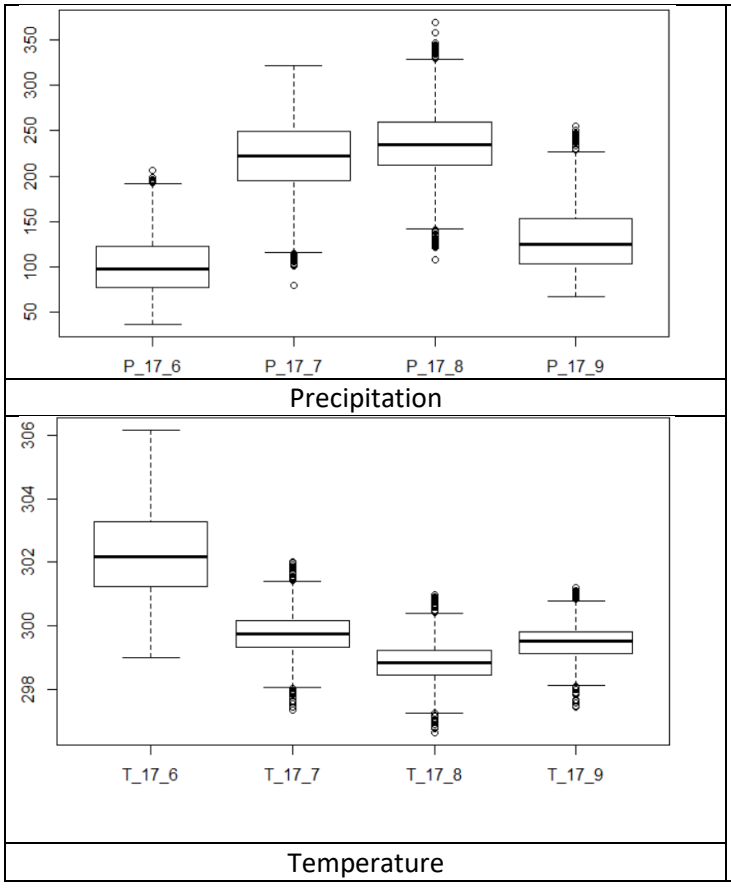

Figure 5.A. 1. Monthly total precipitation and average temperature.

5.A.2. Vegetation indices (NDVI, EVI, NDWI)

Remote sensing derived vegetation indices (VI) have been extensively applied to detect vegetation, monitor vegetation condition, and map cropland over large areas (Samasse et al., 2020). These indices are generally based on the capability of vegetation to strongly reflect incident electromagnetic signal in the near-infrared (NIR) band compared to the optical bands. In this study three vegetation indices are computed from Landsat 8 surface reflectance and used as candidate predictor variables for the Random Forest and Boosted Regression Trees regression models to help predict maize yields across the country of Mali. These VI are the Normalized Difference Vegetation Index (NDVI), the Enhanced Vegetation Index (EVI), and the Normalized Difference Water Index (NDWI). The 8-day composites of NDVI, EVI, and NDWI, created from all Landsat 8 scenes, available on Google Earth Engine platform are used in this study.

NDVI

The Normalized Difference Vegetation Index (NDVI) is commonly used in satellite remote sensing-based vegetation analysis. It is computed using the red (0.64-0.67 µm) and near-infrared (0.85-0.88 µm) bands. The NDVI can effectively detect growing vegetation and has been numerously applied for cereal crop yield modelling in different regions and under different climate conditions. However, in high biomass surfaces NDVI gets quickly saturated. In such conditions, other vegetation indices like EVI (Enhanced Vegetation Index) have been proposed to replace or supplement it.

EVI

The Enhanced Vegetation Index (EVI) provides improved sensitivity to vegetation condition and changes in high biomass areas as compared to the NDVI. It also reduces the background effect of soil on vegetation index calculation. In addition to the red and near-infrared bands, EVI includes in the calculation the blue band (0.45-0.51 µm).

NDWI

The Normalized Difference Water Index (NDWI) is sensitive to changes in liquid water content of vegetation canopies. NDWI is less sensitive to atmospheric effects than NDVI. Because of its sensitivity to water content in vegetation, NDWI can be used as complementary to NDVI and EVI. It may therefore better capture the effect of drought on crop yields (Gu et al., 2008). By using Landsat 8 surface reflectance, NDWI is derived from the Near infrared band and the Short-Wave infrared band (1.57-1.65 µm). Gao (1996) gives more details on NDWI calculation and its potential applications.

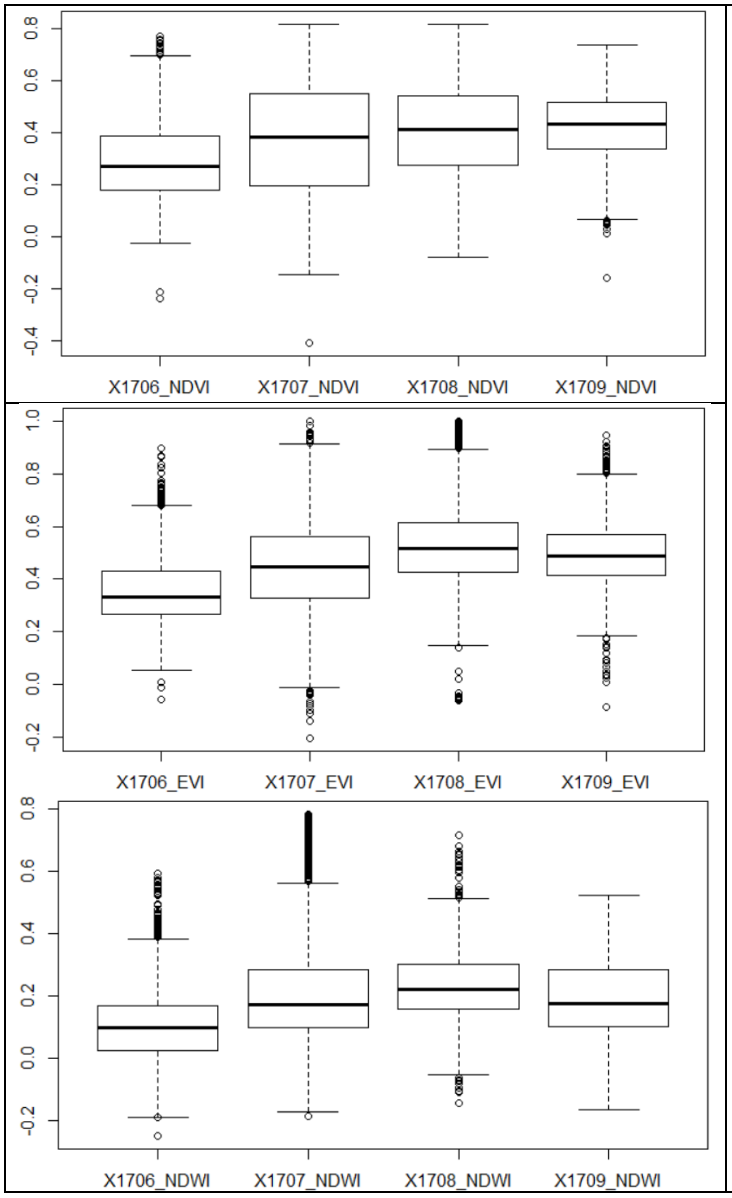

Figure 5.A. 2. Vegetation Indices used as predictors for regression models. Values for all three VI are extracted from GEE using the crop type map as mask. They range from -1 to 1 with a maximum average value in August.

Appendix 5.B: Model selection

Model 0: Full model

Predictors	"P_17_6" "P_17_7" "P_17_8" "P_17_9" "T_17_6" "T_17_7" "T_17_8" "T_17_9" "X1706_NDVI" "X1707_NDVI" "X1708_NDVI" "X1709_NDVI" "X1706_EVI" "X1707_EVI" "X1708_EVI" "X1709_EVI" "X1706_NDWI" "X1707_NDWI" "X1708_NDWI" "X1709_NDWI"	
	RF	BRT
Variable importance	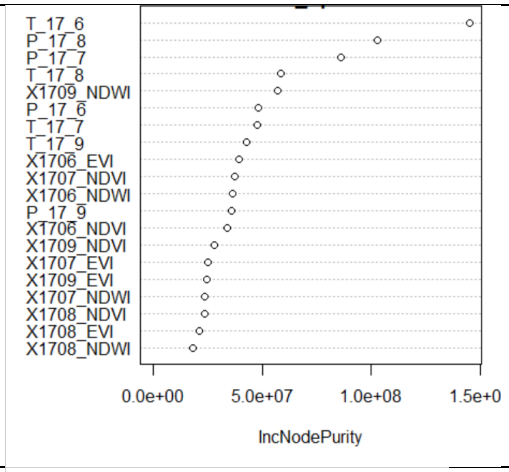	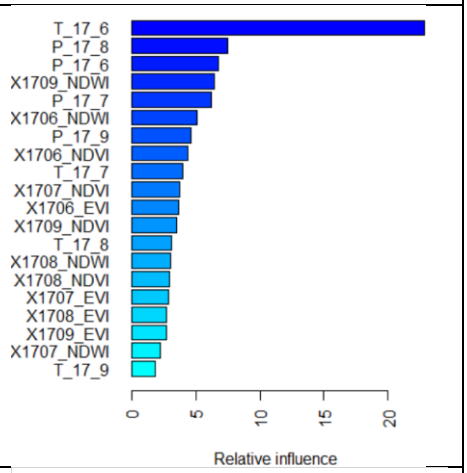
Test 20%	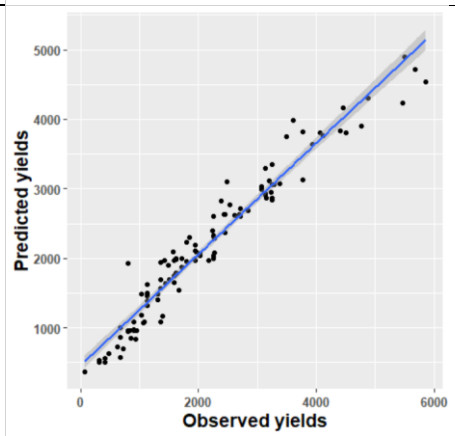	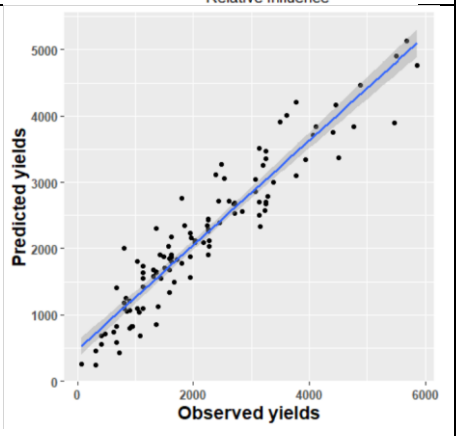
	R2 = 0.94; RMSE = 362.0538	R2 = 0.89; RMSE = 449.9059
Test 2018	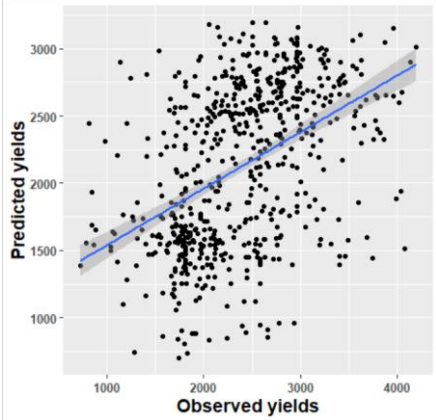	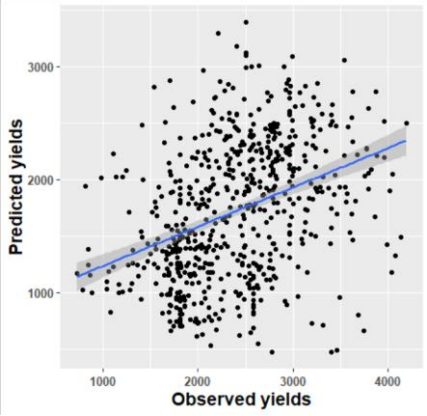
	R2 = 0.20; RMSE = 706.6981	R2 = 0.14; RMSE = 973.6933

Model 1: June-July

Predictors	"P_17_6" "P_17_7" "T_17_6" "T_17_7" "X1706_NDVI" "X1707_NDVI" "X1706_EVI" "X1707_EVI" "X1706_NDWI" "X1707_NDWI"	
	RF	BRT
Variable importance	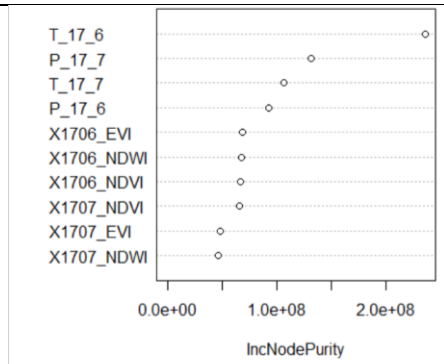	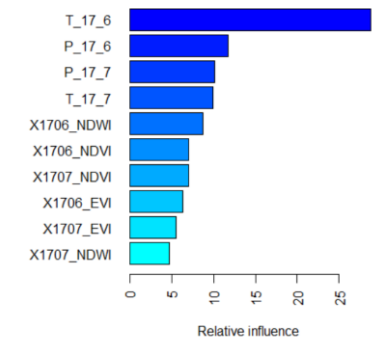
Test 20%	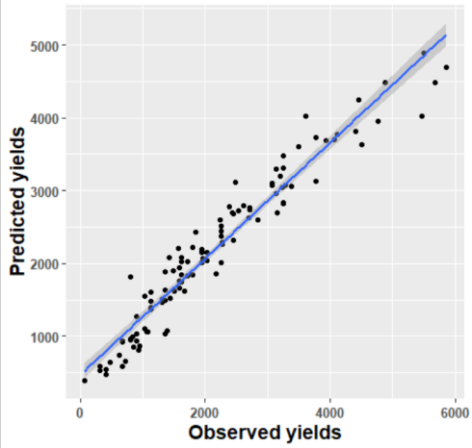	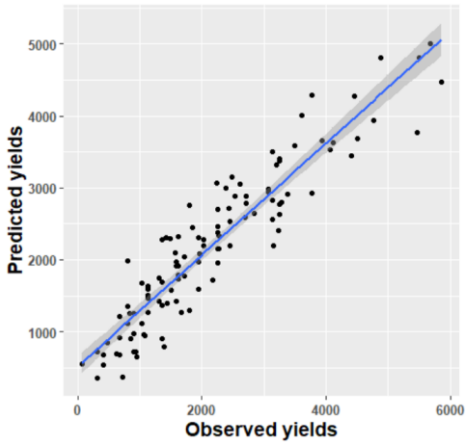
	R2 = 0.93; RMSE = 378.2635	R2 = 0.86; RMSE = 492.163
Test 2018	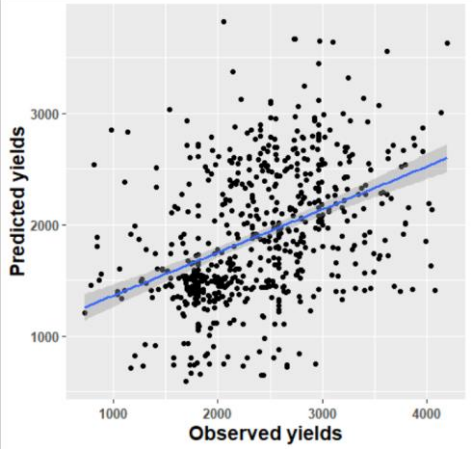	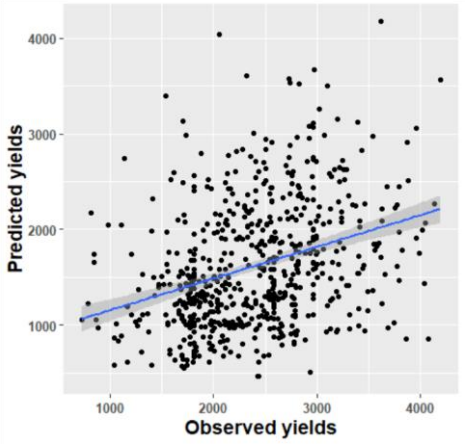
	R2 = 0.17; RMSE = 835.1378	R2 = 0.11; RMSE = 1079.688

Model 2: June-August

Predictors	"P_17_6" "P_17_7" "P_17_8" "T_17_6" "T_17_7" "T_17_8" "X1706_NDVI" "X1707_NDVI" "X1708_NDVI" "X1706_EVI" "X1707_EVI" "X1708_EVI" "X1706_NDWI" "X1707_NDWI" "X1708_NDWI"	
	RF	BRT
Variable importance	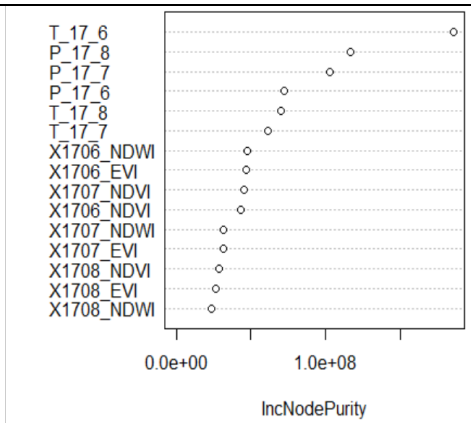	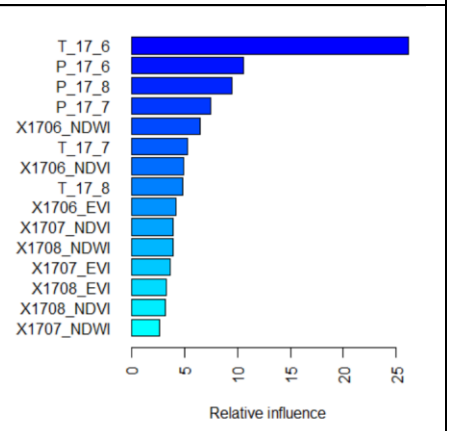
Test 20%	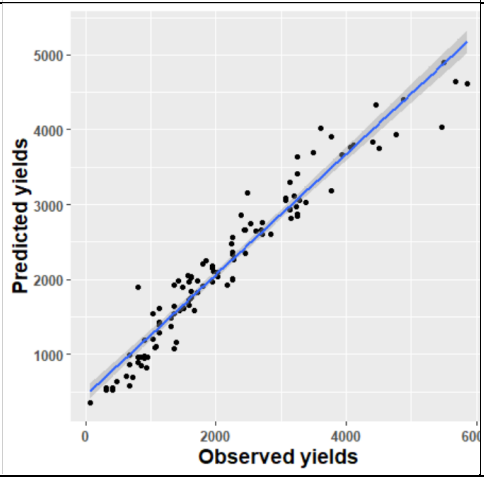	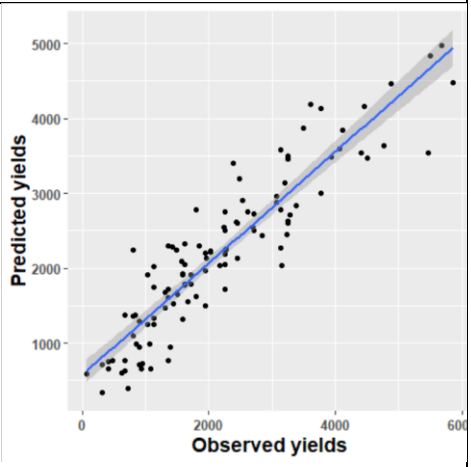
	R2 = 0.94; RMSE = 366.1159	R2 = 0.83; RMSE = 537.8349
Test 2018	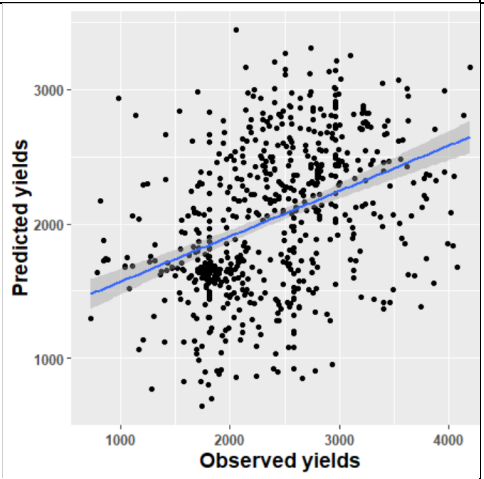	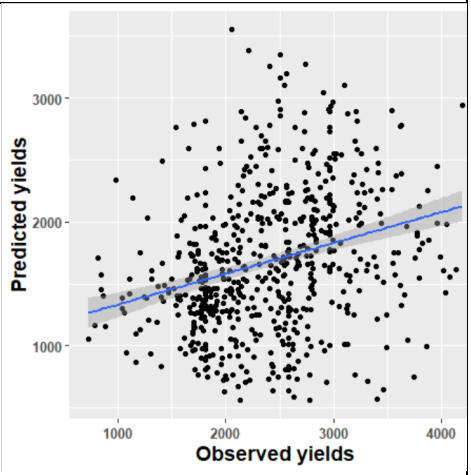
	R2 = 0.15; RMSE = 756.9454	R2 = 0.08; RMSE = 1019.951

Model 3: Weather

Predictors	"P_17_6" "P_17_7" "P_17_8" "P_17_9" "T_17_6" "T_17_7" "T_17_8" "T_17_9"	
	RF	BRT
Variable importance	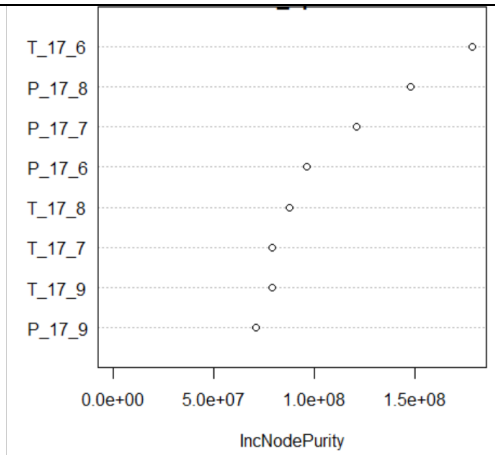	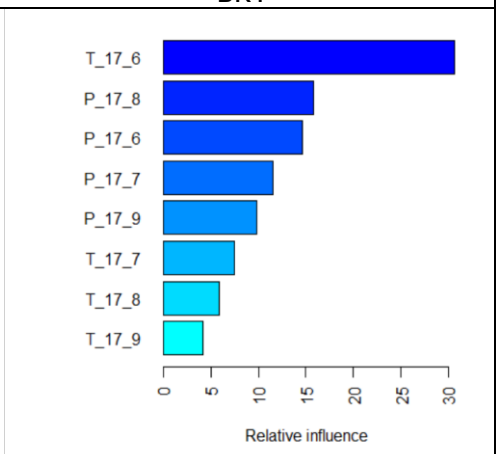
Test 20%	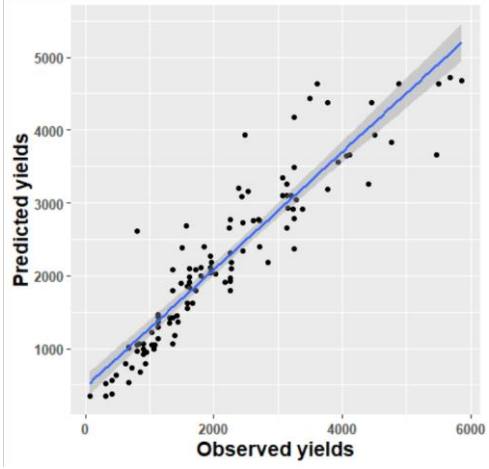	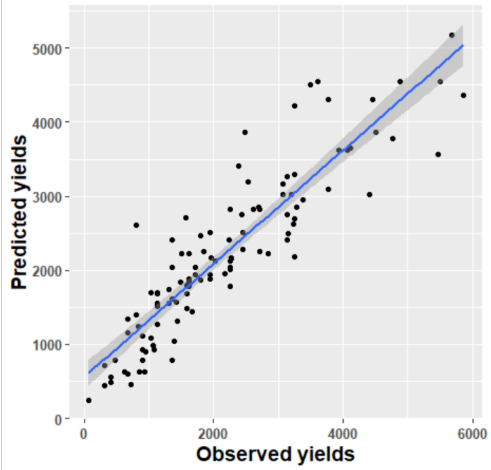
	R2 = 0.85; RMSE = 507.9247	R2 = 0.81; RMSE = 568.603
Test 2018	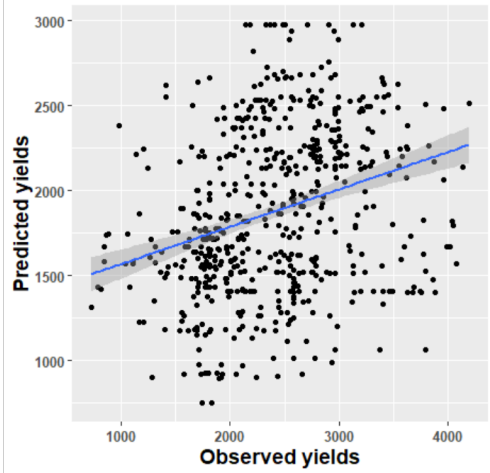	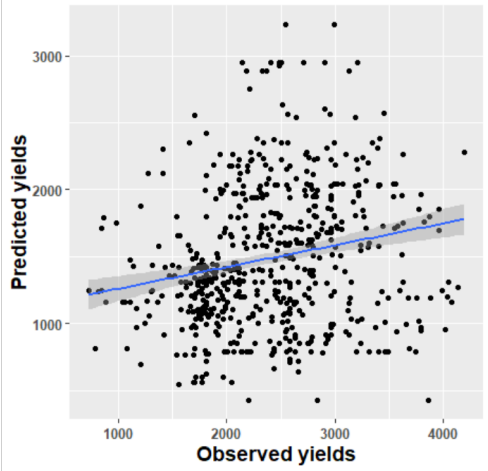
	R2 = 0.09; RMSE = 857.3202	R2 = 0.04; RMSE = 1169.335

Model 4: Vegetation Indices

Predictors	"X1706_NDVI" "X1707_NDVI" "X1708_NDVI" "X1709_NDVI" "X1706_EVI" "X1707_EVI" "X1708_EVI" "X1709_EVI" "X1706_NDWI" "X1707_NDWI" "X1708_NDWI" "X1709_NDWI"	
	RF	BRT
Variable importance	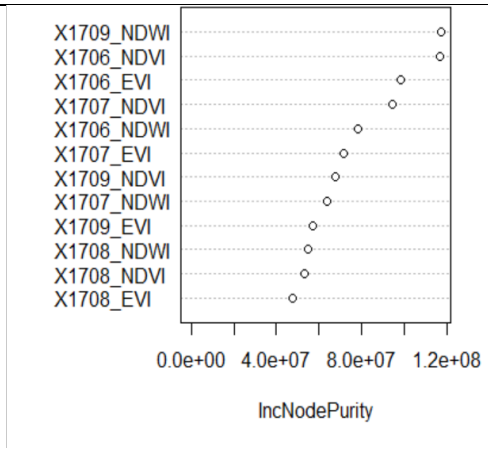	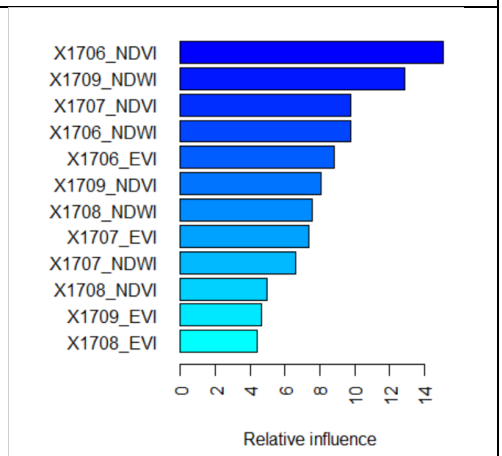
Test 20%	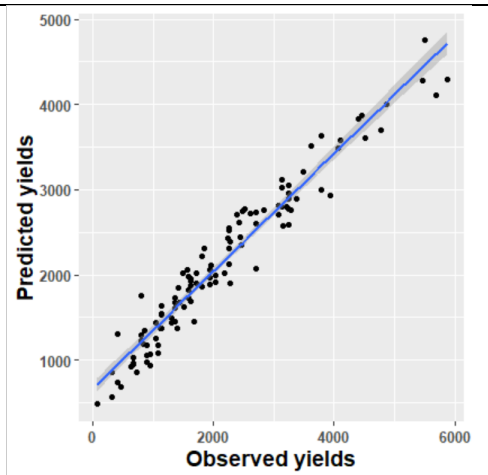	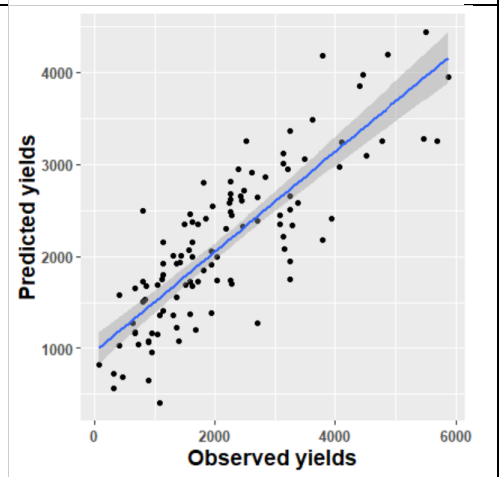
	R2 = 0.94; RMSE = 454.6128	R2 = 0.69; RMSE = 752.4256
Test 2018	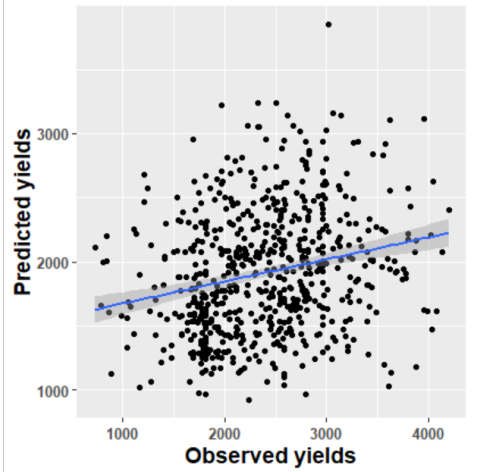	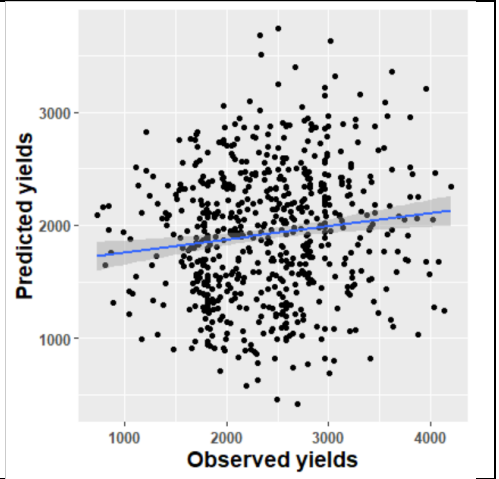
	R2 = 0.05; RMSE = 858.687	R2 = 0.02; RMSE = 938.0358

Model 5: NDVI

Predictors	"X1706_NDVI" "X1707_NDVI" "X1708_NDVI" "X1709_NDVI"	
	RF	BRT
Variable importance	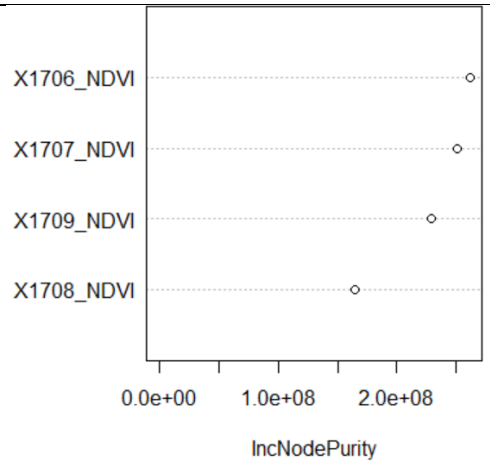	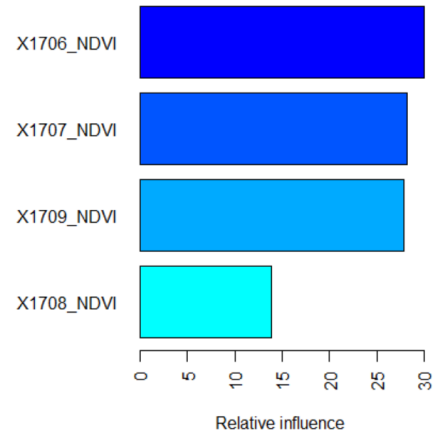
Test 20%	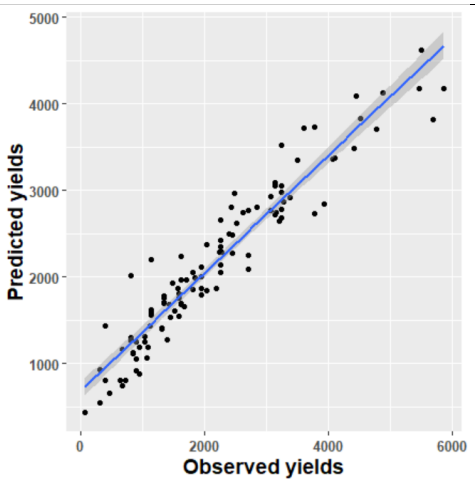	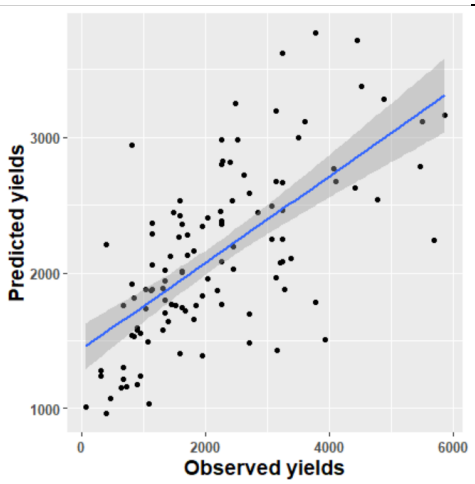
	R2 = 0.91; RMSE = 494.1756	R2 = 0.43; RMSE = 994.8818
Test 2018	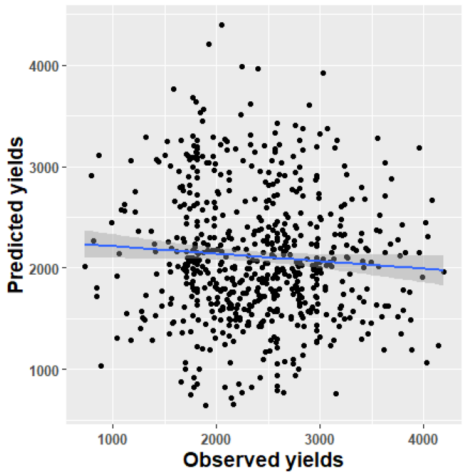	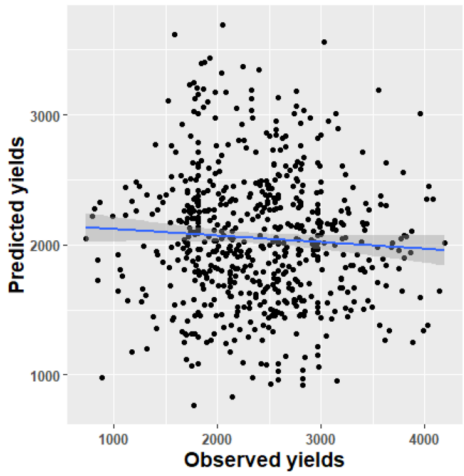
	R2 = 0.01; RMSE = 984.4545	R2 = 0.00; RMSE = 913.8685

Model 6: EVI

Predictors	"X1706_EVI" "X1707_EVI" "X1708_EVI" "X1709_EVI"	
	RF	BRT
Variable importance	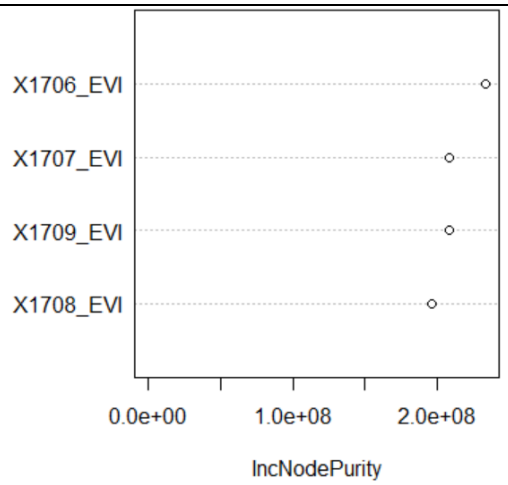	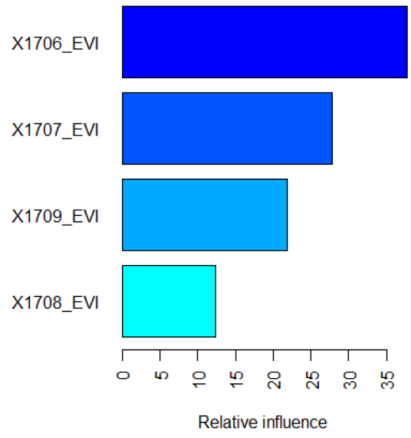
Test 20%	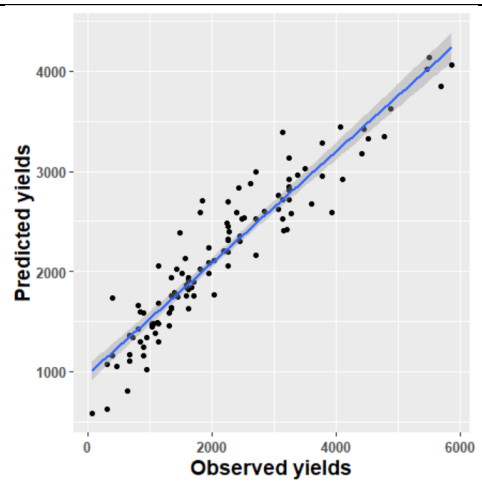	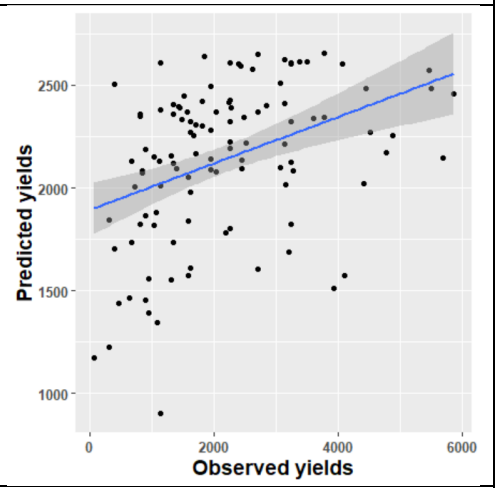
	R2 = 0.89; RMSE = 623.3155	R2 = 0.15; RMSE = 1191.621
Test 2018	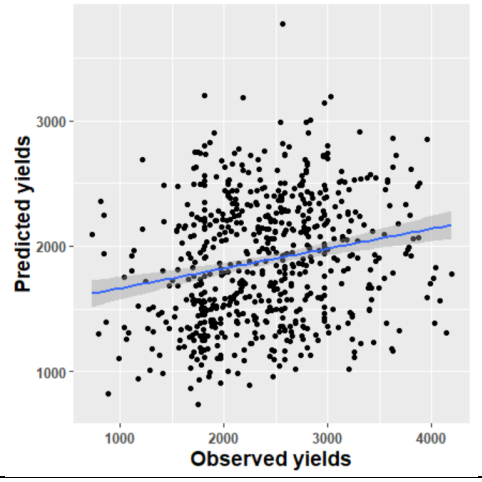	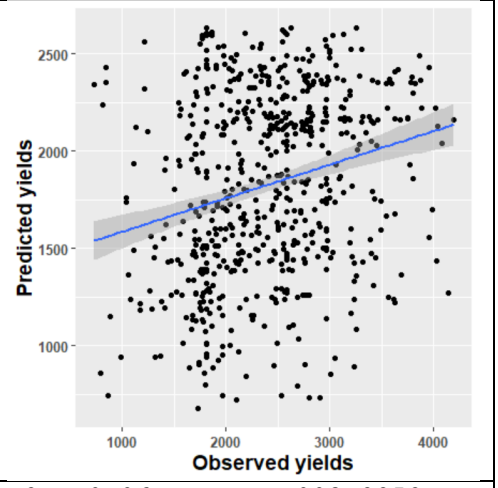
	R2 = 0.04; RMSE = 888.468	R2 = 0.06; RMSE = 903.8252

Model 7: NDWI

Predictors	"X1706_NDWI" "X1707_NDWI" "X1708_NDWI" "X1709_NDWI"	
	RF	BRT
Variable importance	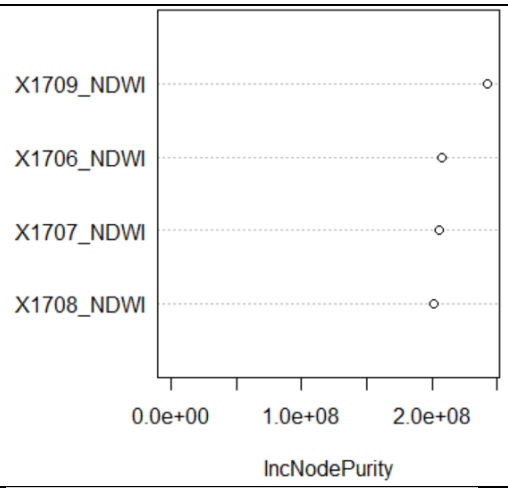	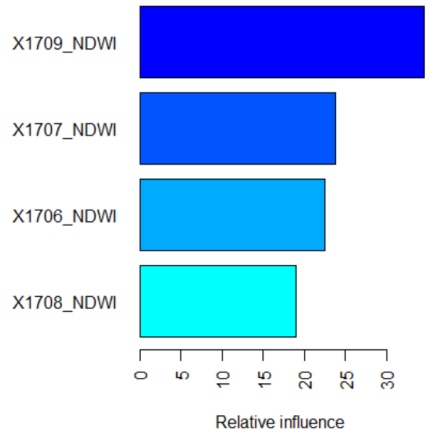
Test 20%	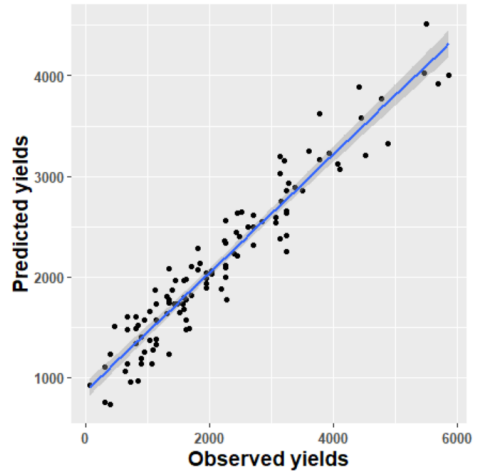	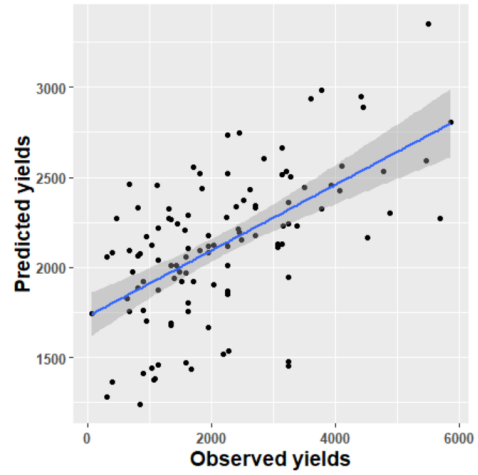
	R2 = 0.92; RMSE = 576.8203	R2 = 0.34; RMSE = 1101.683
Test 2018	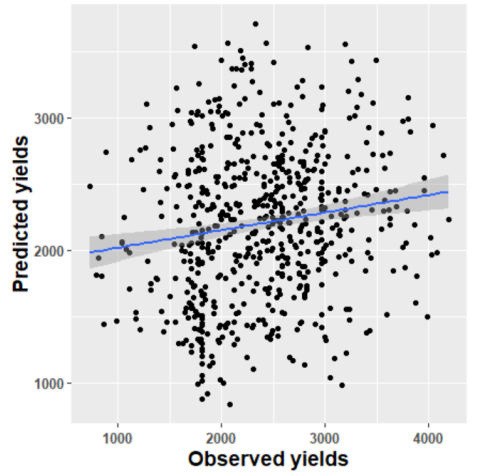	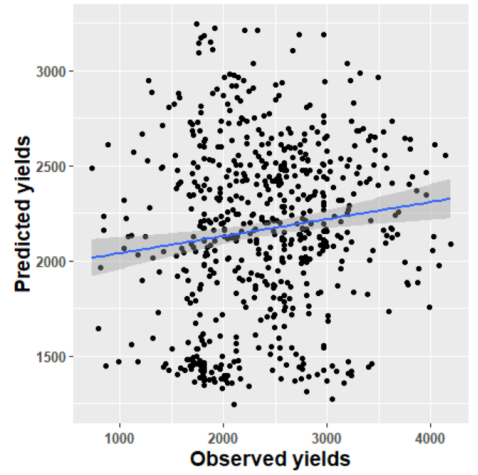
	R2 = 0.02; RMSE = 812.479	R2 = 0.02; RMSE = 774.432

5.5. References

Cai, Y., Guan, K., Lobell, D., Potgieter, A. B., Wang, S., Peng, J., Xu, T., Asseng, S., Zhang, Y., You, L., & others. (2019). Integrating satellite and climate data to predict wheat yield in Australia using machine learning approaches. Agricultural and Forest Meteorology, 274, 144–159.

Funk, C., Peterson, P., Landsfeld, M., Pedreros, D., Verdin, J., Shukla, S., Husak, G., Rowland, J., Harrison, L., Hoell, A., & Michaelsen, J. (2015). The climate hazards infrared precipitation with stations - A new environmental record for monitoring extremes. Scientific Data. https://doi.org/10.1038/sdata.2015.66

Gu, Y., Hunt, E., Wardlow, B., Basara, J. B., Brown, J. F., & Verdin, J. P. (2008). Evaluation of MODIS NDVI and NDWI for vegetation drought monitoring using Oklahoma Mesonet soil moisture data. Geophysical Research Letters. https://doi.org/10.1029/2008GL035772

Holzworth, D. P., Huth, N. I., deVoil, P. G., Zurcher, E. J., Herrmann, N. I., McLean, G., Chenu, K., van Oosterom, E. J., Snow, V., Murphy, C., Moore, A. D., Brown, H., Whish, J. P. M., Verrall, S., Fainges, J., Bell, L. W., Peake, A. S., Poulton, P. L., Hochman, Z., … Keating, B. A. (2014). APSIM - Evolution towards a new generation of agricultural systems simulation. Environmental Modelling and Software. https://doi.org/10.1016/j.envsoft.2014.07.009

Ines, A. V. M., Das, N. N., Hansen, J. W., & Njoku, E. G. (2013). Assimilation of remotely sensed soil moisture and vegetation with a crop simulation model for maize yield prediction. Remote Sensing of Environment, 138, 149–164.

Jones, J. W., Hoogenboom, G., Porter, C. H., Boote, K. J., Batchelor, W. D., Hunt, L. A., Wilkens, P. W., Singh, U., Gijsman, A. J., & Ritchie, J. T. (2003). The DSSAT cropping system model. European Journal of Agronomy. https://doi.org/10.1016/S1161-0301(02)00107-7

Kern, A., Barcza, Z., Marjanović, H., Árendás, T., Fodor, N., Bónis, P., Bognár, P., & Lichtenberger, J. (2018). Statistical modelling of crop yield in Central Europe using climate data and remote sensing vegetation indices. Agricultural and Forest Meteorology, 260–261, 300–320. https://doi.org/10.1016/j.agrformet.2018.06.009

Khaki, S., & Wang, L. (2019). Crop yield prediction using deep neural networks. Frontiers in Plant Science, 10, 621.

Leroux, L., Castets, M., Baron, C., Escorihuela, M.-J., Bégué, A., & Seen, D. Lo. (2019). Maize yield estimation in West Africa from crop process-induced combinations of multi-domain remote sensing indices. European Journal of Agronomy, 108, 11–26.

Li, A., Liang, S., Wang, A., & Qin, J. (2007). Estimating crop yield from multi-temporal satellite data using multivariate regression and neural network techniques. Photogrammetric Engineering & Remote Sensing, 73(10), 1149–1157.

Li, Y., Guan, K., Yu, A., Peng, B., Zhao, L., Li, B., & Peng, J. (2019). Toward building a transparent statistical model for improving crop yield prediction: Modeling rainfed corn in the US. Field Crops Research, 234, 55–65.

McNally, A., Arsenault, K., Kumar, S., Shukla, S., Peterson, P., Wang, S., Funk, C., Peters-Lidard, C. D., & Verdin, J. P. (2017). A land data assimilation system for sub-Saharan Africa food and water security applications. Scientific Data. https://doi.org/10.1038/sdata.2017.12

Ministère de l'agriculture. (2018). Plan de campagne agricole consolide et harmonisé 2018/2019.

Pal, M. (2005). Random forest classifier for remote sensing classification. International Journal of Remote Sensing, 26(1), 217–222. https://doi.org/10.1080/01431160412331269698

Peng, B., Guan, K., Zhou, W., Jiang, C., Frankenberg, C., Sun, Y., He, L., & Köhler, P. (2020). Assessing the benefit of satellite-based Solar-Induced Chlorophyll Fluorescence in crop yield prediction. International Journal of Applied Earth Observation and Geoinformation, 90, 102126.

Samasse, K., Hanan, N. P., Anchang, J. Y., & Diallo, Y. (2020). A high-resolution cropland map for the West African Sahel based on high-density training data, google earth engine, and locally optimized machine learning. Remote Sensing. https://doi.org/10.3390/RS12091436

Schwalbert, R. A., Amado, T., Corassa, G., Pott, L. P., Prasad, P. V. V., & Ciampitti, I. A. (2020). Satellite-based soybean yield forecast: Integrating machine learning and weather data for improving crop yield prediction in southern Brazil. Agricultural and Forest Meteorology, 284, 107886.

Thorp, K. R., Hunsaker, D. J., & French, A. N. (2010). Assimilating leaf area index estimates from remote sensing into the simulations of a cropping systems model. Transactions of the ASABE, 53(1), 251–262.

Venkatesan, M., & Pazhanivelan, S. (2018). Estimation of Maize Yield at Spatial Level Using DSSAT Crop Simulation Model. Madras Agricultural Journal, 105.

Williams, J. R., Jones, C. A., Kiniry, J. R., & Spanel, D. A. (1989). EPIC crop growth model. Transactions of the American Society of Agricultural Engineers. https://doi.org/10.13031/2013.31032

Wineman, A., Anderson, C. L., Reynolds, T. W., & Biscaye, P. (2019). Methods of crop yield measurement on multi-cropped plots: Examples from Tanzania. Food Security, 11(6), 1257–1273.

Xie, Y., Wang, P., Bai, X., Khan, J., Zhang, S., Li, L., & Wang, L. (2017). Assimilation of the leaf area index and vegetation temperature condition index for winter wheat yield estimation using Landsat imagery and the CERES-Wheat model. Agricultural and Forest Meteorology, 246, 194–206.

Yan, W., Jiang, W., Han, X., Hua, W., Yang, J., & Luo, P. (2020). Simulating and predicting crop yield and soil fertility under climate change with fertilizer management in northeast China based on the decision support system for agrotechnology transfer model. Sustainability (Switzerland). https://doi.org/10.3390/su12062194

CHAPTER 6

Conclusions and Perspectives

6.1. Conclusions

Considering the importance of agriculture for food security and livelihoods in West Africa, the development of remote sensing-based approaches to monitoring agricultural yields is critical. The accurate geolocation and area quantification of croplands is a necessary first step, as it allows an accurate extraction of variables in known cropland areas, and agricultural production is estimated using both crop area and local yield estimates. Considering that several satellite remote sensing-based land cover products which map pure and/or mixed cultivated areas exist at different spatial and temporal resolutions, this research began by analyzing the reliability of such products at West African Sahel scale for agricultural modelling (Samasse et al., 2018). The main findings of this accuracy assessment for existing land cover products across five (5) Western Sahel countries (Burkina Faso, Mali, Mauritania, Niger, and Senegal) revealed the following:

1. Crop areas predictions based on coarse spatial resolution (i.e., 300 m or greater) land cover products are overestimated. Examples of these products are ESACCI 300m series, MODIS LC, GlobCover, and GLC2000.
2. Recent higher spatial resolution datasets developed by classifying mainly Landsat time series, and using new (machine learning) approaches (GFSAD30 and GlobeLand30) have better accuracy in identifying crop areas in West African fragmented agricultural landscapes. They have, in the Sahel, an average cropland class accuracy of 68.9% and 64.2% for GlobeLand30 and GFSAD30, respectively, approaching the target accuracy of 75%. However, while more accurate than the other land cover products in this analysis, both GlobeLand30 and GFSAD30 tend to underestimate crop areas in the Sahelian region.
3. High density training datasets, derived using expert local knowledge and high resolution images (CILSS, 2016; Cotillon & Tappan, 2016), facilitate not only more accurate land use and land cover error assessments, but also open the door for the development of improved land cover datasets by associating progress in

computational power (e.g. cloud computing using Google Earth Engine), and the availability of new sensors and optimized algorithms such as machine learning techniques (Samasse et al., 2020).

As mentioned earlier, accurately identified crop locations is of paramount importance for crop monitoring applications. However, knowledge of cropland and non-cropland locations is insufficient for crop modeling since the major subsistence crops have distinct temporal characteristics (crop calendars). Thus, information on crop types is needed for crop specific yield predictions. In the present research, to compensate weaknesses identified in existing crop area products, a new cropland dataset (the 30 m WASC30), has been developed at Sahel region scale. This was followed by a crop species mapping for the country of Mali. The WASC30 cropland area product was developed through an intensive computation approach by fitting random forest classifiers for each 100 km x 100 km square across Sahelian West Africa. In this way, we reduced the influence of climate variations and regional variability in the fitting process. With an overall accuracy of 90.1% and a cropland class (rainfed and irrigated) user's accuracy of 79%, results obtained from the development of WASC30 are unprecedented in mapping cropland for Sahel region.

WASC30 was then used as an input to constrain the crop species identification for rainfed agricultural pixels. Four major cereals (maize, millet, rice, and sorghum) were mapped with an overall accuracy of 78% (Chapter 4). From both WASC30 and the crop type map, it is possible to derive agricultural statistics on cultivated areas at agroclimatic, national, subnational and village scales. Crop type fractions (the area devoted to each crop type compared to the total cultivated area), were retrieved for maize, millet, rice, and sorghum at Commune level (Administrative level 3 in Mali). A crop type fraction map indicates the climate tolerances of different crops, with local socio-cultural and economic drivers of agronomic preferences across the region. It also informs about the degree of agricultural knowledge and practices related to each crop. All these agricultural statistics are particularly important in developing countries where timely accurate georeferenced agricultural data are sometimes missing. Findings in cropland and crop type mapping also confirmed that Landsat time series, provide a critical source of information for the

important task of producing accurate statistics on cultivated areas and planting area for different crops.

The developed crop type map was used as mask to extract predictors for crop yield estimations (Chapter 5). We focused on yield analyses of maize, a staple crop highly utilized in Mali for human, livestock, and poultry feed. Ensemble machine learning techniques, as opposed to process based and statistical modeling, were explored to predict maize yield using climate (precipitation and temperature), and vegetation indices (NDVI, EVI, and NDWI) derived from Landsat 8 surface reflectance retrieved from Google Earth Engine platform. Preliminary results showed random forest algorithm outperforms boosted regression trees in predicting maize yield, and climate variables have the most important predictive power as compared to vegetation indices. During the growing season (from June to September), models showed that it is possible to predict maize yield in July, and August with an error of 378 kg/ha, and 366 kg/ha, respectively. However, while trying to predict maize yield for year 2018 which was not included in training the model, error increases quickly.

6.2. Perspectives

Methods developed in this thesis for developing cropland area, crop type datasets, and maize yield predictions are based on a single-year analysis. To become an effective tool of decision making which will support crop monitoring efforts across West African countries, one should integrate cropland locations mapping with yield modelling in a unique platform allowing development at yearly basis. For example, Google Earth Engine (GEE), provides great opportunities facilitating such an integrated application development. As a cloud computing platform, GEE implements most of classification and regression algorithms (including machine learning techniques) and gathering various geospatial datasets time series resulting from several terabytes processed satellite images, which could be used as predictors, In addition to optical bands of Landsat images used in our analyses, possibilities offered by other sensors with higher resolution (e.g. Sentinel 2) to reduce mixed pixels, different data acquisition method (e.g. Synthetic Aperture Radar (SAR) data), are freely available on GEE platform.

Regarding crop yield predictions using machine learning approaches, the results presented in this document are preliminary and leave rooms for improvements. The availability of training samples constitutes a major constraint of estimating yield in ongoing season at large scale, particularly in Sahelian countries which often lack detailed statistics on yields. Also, machine learning is a data driven method – it learns from the data and predict values based on what has been learned. That is, more the quantity of samples for training, better the process of learning. One way to reduce this constraint of training information is to couple process-based models, like DSSAT and APSIM, and machine learning. We first create simulations using different cultivars, management techniques, water management, soil, and weather data for a certain number of sampled regions to generate yield information. This yield information is used as training data for machine learning algorithms and predict yield for a larger area based on remote sensing inputs. For example, it would be valuable as future work to predict yield for all four crop types mapped in this thesis (maize, millet, rice, and sorghum) at 30 m pixel level, and carry out analysis on yield spatial variations. This yield analysis should allow us to identify where we might have some low yielding areas and the most influential factors behind spatial variability in yields for targeting on ground interventions to improve food security in the future.

Overall, classification and regression methods used to estimate crop areas and yields are reproductible. That is, they may constitute the basis of yearly improved agricultural statistics production in West Africa. Also, this reproducibility offers an opportunity to create multi-epochs crop masks. These crop masks are critical for crop conditions monitoring and early warning systems, as, in these applications, all metrics are processed based crop species locations. Also, for example, in Mali, the Ministry of Agriculture, through the Statistics and Planning Service (Cellule de Planification et de Statistiques) carries out periodic agricultural surveys (two per year). Changes capture by the dynamic crop type maps could be a critical input to guide field activities and monitor areas by crop types making more accurate agricultural production estimation. In addition, possibilities to deliver major crops yields, thus agricultural production, information one month earlier to the harvest (yield forecasting) and to analyze its variability spatially and temporally at finer administrative scale are an opportunity to early detect low yielding

areas. That is helpful for food security early warning services to plan future on-ground interventions, and required resources distribution, accordingly.

6.3. References

CILSS. (2016). Landscapes of West Africa—A window on a changing world. U.S. Geological Survey EROS: Garretson, SD, USA.

Cotillon, S. E., & Tappan, G. G. (2016). Landscapes of West Africa: A window on a changing world.

Samasse, K., Hanan, N. P., Anchang, J. Y., & Diallo, Y. (2020). A high-resolution cropland map for the West African Sahel based on high-density training data, google earth engine, and locally optimized machine learning. Remote Sensing. https://doi.org/10.3390/RS12091436

Samasse, K.; Hanan, N.P.; Tappan, G.; Diallo, Y. (2018). Assessing Cropland Area in West Africa for Agricultural Yield Analysis. Remote Sensing. https://www.mdpi.com/2072-4292/10/11/1785